

---

Theses and Dissertations

---

Fall 2010

# Radio in hydrosience: unconventional links and new sensor possibilities

James J. Niemeier  
*University of Iowa*

Copyright 2010 James J. Niemeier

This dissertation is available at Iowa Research Online: <http://ir.uiowa.edu/etd/863>

---

## Recommended Citation

Niemeier, James J.. "Radio in hydrosience: unconventional links and new sensor possibilities." PhD (Doctor of Philosophy) thesis, University of Iowa, 2010.  
<http://ir.uiowa.edu/etd/863>.

---

Follow this and additional works at: <http://ir.uiowa.edu/etd>



Part of the [Electrical and Computer Engineering Commons](#)

RADIO IN HYDROSCIENCE:  
UNCONVENTIONAL LINKS AND NEW SENSOR POSSIBILITIES

by  
James J. Niemeier

An Abstract

Of a thesis submitted in partial fulfillment  
of the requirements for the Doctor of  
Philosophy degree in Electrical and Computer Engineering  
in the Graduate College of  
The University of Iowa

December 2010

Thesis Supervisor: Associate Professor Anton Kruger

## ABSTRACT

One can use unlicensed and often very inexpensive radios for unconventional communication (underwater- and underground) links. However, one can go further, and use these radios as sensors rather than communication links. Such communication links and sensors can have important application in hydroscience. While the attenuation of RF signals is high in these mediums, by using the wireless sensor network (WSN) paradigm of multi-hop and retransmission, reliable networks can be formed underwater and underground. One no longer needs to think of RF modules as only a source of data transmission. This revelation lends itself to thinking of these modules as inexpensive RF wave generators at prescribed unlicensed frequencies. Analyzing the received signal strength indicator (RSSI) of a link over time, one can infer changes in the medium from the changes in RSSI. In this thesis, I develop a simple mathematical model to relate changes in RSSI to changes in the medium. Additionally, five experimentally validated examples demonstrate the possibility of non-traditional uses for RF modules. Demonstrated sensor possibilities include soil moisture estimation, leaf wetness measurement, and vegetation water content estimation. This thesis served to validate the use of inexpensive unlicensed RF modules as more than just communication links through air, but as links in unconventional media, and more importantly as measurement instruments.

Abstract Approved: \_\_\_\_\_  
Thesis Supervisor

\_\_\_\_\_

Title and Department

\_\_\_\_\_

Date

RADIO IN HYDROSCIENCE:  
UNCONVENTIONAL LINKS AND NEW SENSOR POSSIBILITIES

by  
James J. Niemeier

A thesis submitted in partial fulfillment  
of the requirements for the Doctor of  
Philosophy degree in Electrical and Computer Engineering  
in the Graduate College of  
The University of Iowa

December 2010

Thesis Supervisor: Associate Professor Anton Kruger

Graduate College  
The University of Iowa  
Iowa City, Iowa

CERTIFICATE OF APPROVAL

---

PH.D. THESIS

---

This is to certify that the Ph.D. thesis of

James J. Niemeier

has been approved by the Examining Committee  
for the thesis requirement for the Doctor of Philosophy  
degree in Electrical and Computer Engineering at the December 2010  
graduation.

Thesis Committee: \_\_\_\_\_  
Anton Kruger, Thesis Supervisor

\_\_\_\_\_  
Witold Krajewski

\_\_\_\_\_  
Brian Hornbuckle

\_\_\_\_\_  
Er-Wei Bai

\_\_\_\_\_  
Raghuraman Mudumbai

## ACKNOWLEDGMENTS

In addition to thanking my committee members for serving on my committee, I acknowledge the help of a number of fellow students and staff at IIHR. Nick Sitter assisted with data collection in the tethered and untethered mussel experiment and freshwater conductivity measurements. Ken Hunt and I are collaborating on the exploration of antenna design for underwater networks. Dan Ceynar helped Ken and I setup the tank and positioner for experiments related to RF propagation. I worked with Ken Hunt and Luciana Cunha on the data analysis of cellular transmissions through vegetation. Brad Barnhart is helping with the EMD analysis of RSSI of cellular communication through vegetation. Tracy Rowlandson (ISU) provided the leaf wetness data. Dan Ceynar and Radoslaw Goska provided some of the images used to illustrate the experiments in this document. Finally, I would like to thank Dr. Kruger who provided invaluable guidance in every aspect of this research and for whom this work would not have been possible.

## TABLE OF CONTENTS

LIST OF TABLES .....	v
LIST OF FIGURES .....	vi
CHAPTER I PREVIEW OF THE THESIS .....	1
Grounding .....	1
Simple Mathematical Model .....	2
Designing Links and Sensors .....	2
Engineering Considerations .....	3
Existing Research .....	5
Underwater Wireless Sensor Networks .....	6
Underground Wireless Sensor Networks .....	10
Inexpensive RF Modules as Sensors .....	12
CHAPTER II BACKGROUND .....	16
Electrical Properties and Water and Soil .....	16
Electromagnetic Wave Equation in Lossy and Conductive Media .....	19
Attenuation, Units, Power Measurement .....	22
Characteristic Impedance .....	23
Dielectrics, Conductors and Quasi Conductors .....	24
Refraction Losses .....	28
Properties of Soil .....	32
RF Modules .....	34
RF Link Background .....	37
RF Modulation .....	37
RSSI Measurements .....	41
Echo- and Streaming Server .....	47
Fresh Water Conductivity Measurements .....	48
Summary .....	52
CHAPTER III UNDERWATER NETWORKS .....	53
Application: Mussels as Biological Sensors .....	53
Laboratory Proof-of-Concept Experiments .....	57
Mussel Gape Results .....	60
Underwater Antennas for Mussels .....	60
Conclusions .....	67
CHAPTER IV UNDERGROUND NETWORKS .....	68
Feasibility of Underground Communications .....	68
A Buried Sensor Network .....	73
Results .....	77
Discussion and Conclusions .....	79
CHAPTER V SOIL MOISTURE ESTIMATION .....	81
Experimental Setup .....	82

Data Collection.....	86
Data Analysis .....	87
Conclusions .....	91
CHAPTER VI VEGETATION WATER CONTENT .....	93
An Unplanned Experiment.....	94
Simple Propagation Model.....	96
Determining Corn Water Content .....	97
Corn Water Content and RSSI .....	101
Diurnal Cycles .....	102
Fourier Spectral Analysis .....	102
Empirical Mode Decomposition.....	102
Data Stacking/Averaging .....	104
Effect of Rain on Signal Strength.....	104
Conclusions .....	106
CHAPTER VII LEAF WETNESS .....	108
Data Analysis .....	114
Discussion and Some Conclusions .....	118
CHAPTER VIII FUTURE WORK.....	120
Introduction .....	120
River Stage Measurement .....	125
TOF Measurement .....	127
Experimental Results .....	127
CHAPTER IX CONCLUSION .....	130
REFERENCES .....	134

## LIST OF TABLES

Table 1 Measured relative dielectric permittivity of freshwater at 20 °C .....	19
Table 2 Conditions for defining the state a medium .....	25
Table 3 Attenuation for some selected frequencies assuming $\sigma = 0.05$ S/m. ....	27
Table 4 Industrial Medical and Scientific (ISM) bands and GSM cellular bands.....	36
Table 5 Correlation Coefficient for attenuation of RF transect and VMC.....	89

## LIST OF FIGURES

Figure 1	Dielectric hysteresis. The top left plots shows the polarization of an initially unpolarized dielectric material as a function of an external electric field. The top right plot shows the polarization when the electric field is reduced. At point <i>b</i> , even with no external electric field, there is still some residual polarization. To remove this (point <i>c</i> ), the electric field must perform work. The bottom right plot shows the situation when the polarization has been reversed. The lower right plot shows the complete hysteresis cycle. The enclosed area determines the hysteresis losses over one cycle. ....	18
Figure 2	Ratio of $\sigma\omega\epsilon$ for some common media, including freshwater and soil, which are of interest in this thesis. The figure also shows the range of ISM and cellular communication frequencies. (from Krauss and Felisch 1999). An important conclusion from the figure is that one can consider freshwater and soil as lossy dielectrics at these frequencies. ....	26
Figure 3	The top figure depicts a linearly-polarized plane radio wave traveling in the <i>x</i> -direction in a medium with permittivity, conductivity, and permeability of $\epsilon_1, \sigma_1$ , and $\mu_1$ respectively. The corresponding intrinsic impedance of the medium is $\eta_1$ . At $x = 0$ the wave encounters a medium with permittivity, conductivity, and permeability of $\epsilon_2, \sigma_2$ , and $\mu_2$ respectively. The corresponding intrinsic impedance of the second medium is $\eta_2$ . If $\eta_1 = \eta_2$ the wave will travel unperturbed, otherwise some of the wave will be reflected back. The bottom figure shows an analogous transmission line that one can use to calculate transmitted and reflected powers. ....	29
Figure 4	The top figure shows a transmitter on a river bank transmitting to two receivers in a river. The transmitter is far enough so that one can consider the wave fronts and essentially plane and traveling nearly parallel with the water surface. At the surface, some of the radio wave energy is refracted into the water and travels distances $L_1$ and $L_2$ to the receivers. The bottom figure shows two radios underwater communication with each other. ....	30
Figure 5	Typical soil dielectric constant at about 1.1 GHz as a function of gravimetric soil moisture ( <i>mg</i> ) and volumetric soil moisture ( <i>mv</i> ) (from Barkeshli, 1985). Note that the dielectric constant show much less scatter when plotted as a function of <i>mv</i> . ....	33
Figure 6	Upper Left: Radiotronix 433 MHz receiver and transmitter pair used in underwater communication experiements. Center: Linx 315 MHz transceiver module used for underwater communication. Upper Right: Alpha receiver and transmitter pair used in underwater phase measurements. Center: Sparkfun's development board and keyfob that use Nordic 2.4 GHz radios. Lower Left: MaxStream XStream at 900 MHz and 2.4 GHz modules with quarter wave length dipole antenna. Lower Right: Enfora cell modem and antenna that operates using Global System and Mobile Communication (GSM) network. ....	35

Figure 7 Two-path multipath. The top figure shows a transmitter and receiver at heights  $A$  and  $B$  above a partially-reflecting plane, separated by a distance  $R$ . The path lengths  $d_1$  and  $d_2$  are such that the attenuation is of the same order. However, phase differences can lead to constructive and destructive interference. The middle and bottom figures are examples of such multipath effects. ....40

Figure 8 These figures show the how the variance of RSSI values decrease with a number of packets averages. Two cases are shown: one for a 900 MHz underground link, and 2.4-GHz link in a light industrial setting. The figures also show the lower bound, determined by the radio’s quantization step size. From the figures it follow that averaging more than about 300 packets (1<sup>st</sup> link) and 80 packets (2<sup>nd</sup> link) does not decrease the variance. However, it does require more power.....45

Figure 9 Echo servers are used in several experiments throughout this thesis primarily for range testing. The echo server is exactly what the name implies, all data received from the data communication equipment is sent back. The data out of the RF module is tied directly back to the data in of the module. All communications that are received and forwarded to the data out line are feed back into the data in line and transmitted.....47

Figure 10 The streaming server consists of two RF modules operating on different channels. The data in lines of both modules are connected to the data out of the opposite module. For example all data received by the module operating on channel A is transmitted out by the module operating on channel B. The channels must be selected as not to be interfering with each other. ....49

Figure 11 Left: Final dimensions of the instrument used for measuring freshwater conductivity. Two 625 cm<sup>2</sup> galvanized steel plates were mounted on plastic sheeting with a separation distance of 6 cm. Right: Final sensor used for measuring the conductivity of river water. The two plates used for the conductivity meter are made of galvanized steel, which not only resist rust, but are also submersible in water. Each plate is 10 inches by 10 inches, and therefore has a 100 square inch surface area. Brass screws hold the plates to the 11 inch by 11 inch plastic sheeting. Plastic thread all was used to hold the plates at a separation distance of 6 cm.....50

Figure 12 Left: Electronics and enclosure used for making conductivity measurements in freshwater. Right: Nick Sitter deploying the conductivity sensor into the Iowa River by the Stanley Hydraulic Laboratory in Iowa City. ....51

Figure 13 Data collected for Iowa River conductivity from May 21, 2010 until July 31, 2010. Measurements were made twice a day at 8 am and 3 pm local time. A decrease in conductivity is observed after rain events with the influx of distilled water followed increases in conductivity as this water flows downstream. Conductivity during this period ranged from 0.03 to 0.063 S/m. ....52

Figure 14 Example of bio-fouling of a sensor left in an underwater environment to collect data on water conditions. ....54

Figure 15	The left panel depicts the Hall-effect, which is the generation of a voltage across a conductor in a perpendicular magnetic field. There are Hall-effect ICs on the market that integrates a Hall sensor with an amplifier and signal conditioning. The right panel shows how we attach a Hall-effect sensor and a small magnet to monitor mussel gape. ....	55
Figure 16	The figure depicts on-going research at The University of Iowa that aims to use freshwater mussels as biological sensors. Mussels equipped with Hall-effect sensors sense mussel gape, as well as water temperature and turbidity. Computer models on remote servers interpret behavior to extract, for example, nitrogen cycle information. ....	56
Figure 17	Modified key fob with low power Hall-effect sensor. ....	58
Figure 18	The left panel shows the tethered mussel used for bio-sensing. The right panel shows a mussel with a modified key fob, Hall-effect sensor and magnet attached to the mussel. The mussel is then deployed untethered as a bio-sensor. ....	58
Figure 19	Experimental setup for collecting data of both tethered and untethered instrumented mussels. Mussel gape was sampled at five second intervals for tethered mussels. Mussel gape was sampled at 10 minute intervals for untethered mussels to conserve battery power. ....	59
Figure 20	The top panel shows mussel gape data after application of a median filter to remove impulse noise (blue), followed by 5-min zero-phase moving average-type digital filter (red). Low voltages indicate mussel's valve is open. The bottom panel is a phase comparison of mussel gape in natural light diurnal cycle (red) with mussel gape in shifted (approximately 10 hours) diurnal light cycle (green). ....	61
Figure 21:	Experimental setup for evaluating underwater antennas. The tank is filled with water with a conductivity of ( $\sigma \sim 0.034$ S/m) and the stepper motor precisely controls the distance between the transmitter and the receiving antennas with an accuracy of ( $\sim 2$ mm). The transmitting antenna was affixed to the center of the tank and the receiving antenna was attached to the stepper motor. A spectrum analyzer measured the power received by the receiving antenna as the separation distance was varied. ....	63
Figure 22	Measured received power as a function of transmitter antenna length for a separation distance of 70 cm in water. ....	65
Figure 23	The antennas tested for underwater RF mussel applications at a frequency of 433 MHz. ....	65
Figure 24	Received power vs. range for the candidate antennas along with $1/R^2$ reference. The frequency is 433-MHz. ....	66
Figure 25	Shown left is the 900-MHz radio, and shown right is the 2.4 GHz radio for the underground communication link feasibility test. ....	70
Figure 26	Experimental setup for measuring RSSI as a function of antenna depth and separation distance using XStream radio modules. Antennas were lowered in to PVC tubes that were driven in the ground. Campbell Scientific's CS616 monitored changes in soil water content. ....	71

Figure 27	The left panel depicts the principle of operation of TDR-based soil moisture sensors (see text). The right panel is a photograph of CS616 water content reflectometer.....	71
Figure 28	The top panel is RSSI data collected at 900 MHz collected for antennas buried in soil at depths of 0.5 meter in blue and depths of one meter in red for various separation distances. The model is also shown for data collected at a depth of 1 m. The bottom panel shows 2.4 GHz RSSI data collected for antennas buried in soil at depths of 0.5 and one meter for various separation distances. Lines shown are linear approximations for reference only since attenuation of collected data was high. ....	74
Figure 29	EduMote node used in field experiments and for teaching purposes at The University of Iowa. The EduMote consist of power supply, ATmega128 microcontroller, MaxStream radio, LCD, and sensor area. ....	75
Figure 30	Schematic of proof-of-concept buried WSN. Packets are routed from R0 to R4 via Path #1 as well as Path #2. Packets' payloads are the links' RSSI measures. R4 transmits the payloads to the base station above ground.....	76
Figure 31	An EduMote, which The University of Iowa uses for laboratory exercises in WSNs, inside its enclosure. I used EduMotes to build the underground WSN. Rather than burying the whole node, we only burry the antennas. Soil moisture was also monitored in between links. ....	76
Figure 32	Photographs of the experimental setup. Only the antennas were installed below the below the surface of the ground at a depth of 80 cm. The antennas were lowered into PVC tubes that were driven into the ground. Motes were sealed from the elements inside of plastic containers. CS616 soil moisture probes monitored soil conditions between links. Data consisted of RSSI and soil moisture between all links. All data was routed and stored at the base station that consisted of custom data logger designed for this experiment. ....	77
Figure 33	RSSI for a three meter link (blue) and a shorter alternative path (red) are shown for a three day period. As the soil was manually moistened, the longer link began to drop packet and only the alternative route was available for packet routing. Packets were transmitted every two minutes and the dark lines are the five minute moving average of RSSI.....	78
Figure 34	Time-series of RSSI data for link R2 – R3 in Path 1 in the prototype WSN. The soil was wetted with ~5 gallons of water shortly after the start of the test. As the water seeps into the soil, the link's attenuation increases (RSSI decreases) and then slowly increases as the soil dries out. ....	78
Figure 35	Layout of experimental setup for testing signal attenuation and soil moisture. The antennas for 12 motes operating at 900 MHz were lowered into the ground to a depth of 60 cm around the perimeter of a three meter diameter circle. Each mote was given a unique ID consisting of a hexadecimal value between 0→B. Seven CS616 soil moisture probe paired with temperature probes and installed inside the circle of radios. Each CS616 and accompanying temperature probe was given a unique address for identification. The CS616 sensors were installed into the top 30 cm of soil and temperature sensor in the top 8 cm of soil. ....	83

Figure 36	Components used to validate RSSI measurements in making soil moisture measurements. Top: the custom data-logger with cell modem used to collect soil moisture and soil temperature to be transmitted back to The University of Iowa. Lower left: is pair of XStream RF modules with support electronics used for measuring RSSI. Lower right: TDR probe with support electronics used in making VWC estimations. ....	84
Figure 37	Experimental setup for comparing changes in soil moisture to changes in RF signal attenuation at 900 MHz as depicted in Figure 35. Seven soil moisture-soil temperature probes were installed inside a ring of 12 buried radio antennas. Data was transmitted to The University of Iowa by cellular transmission. ....	85
Figure 38	Normalized time series of underground link RSSI (red) and soil moisture data (blue), collected over a nine day period in mid-September 2010. Soil moisture probes were installed to measure water content in the top 30 cm of soil. Radio antennas were buried at a depth of 60 cm. During this period there were four rain events that altered soil moisture content. As the water content of soil moisture increased the attenuation of the RF signal also increased. ....	87
Figure 39	Measured RSSI for all possible links at four fixed distances at near a constant volumetric water content of soil of 52→55%. The data follows the simple model with $\alpha = -18.78$ dB/m. ....	90
Figure 40	Measured RSSI for links of distance 2.6 m for various VWC. The data follows the model $e^{-2\alpha R}/R^n$ for fixed distance R and $\alpha$ is a function of VWC. ....	91
Figure 41	The top panel shows the experimental site at Ames, Iowa, and the bottom panel shows the dual tipping platform that houses a cell modem for relaying data. We observed variations in the cell modem RSSI, which inspired the techniques outlined in this chapter. ....	95
Figure 42	Gauges NRG01, NRG02 and NRG03 are in the flat part of the field with unobstructed views of the cell tower. Gauges NRG04, NRG05 and NRG06 were located on the opposite side of a hill from the tower and NRG07 is located in a depression in the southeast corner of the field. The topography between the deployment field and cell tower was relatively flat. ....	96
Figure 43	The top plot shows RSSI time series for Station 7. One can clearly observe a long-term decrease, and then a gradual increase in the received radio signal. On the day the corn was harvested, the average RSSI jumped 10 dBm. Other stations showed similar behavior. The bottom plot is an exploded view of time series plot that suggests that a diurnal cycle in the RSSI signal may be present as well (red line, drawn in by hand). ....	98
Figure 44	Cell modems in the rain gauge network at the experimental site in Ames transmitted through a combination of corn and air. Antennas are located in the lower one fourth of the mature plant height. ....	98
Figure 45	Drying corn plants to determine plant water content. Sample plants were harvested from the field, weight, dried and reweighed to calculate the water contained in the plant. We performed this 6 times over the summer of 2007. ....	99

Figure 46	The top plot is a contour plot of interpolated plant water content (by weight), for the whole plant. The uniformity indicated here is representative of the water content at other times and individual parts of the plants. Dots indicate collection locations. The plant water content was uniform with respect to weight, so we averaged all values for a day. The bottom plot shows the results. ....	99
Figure 47	The top plot shows RSSI as a function of plant water content for Station 5. The bottom plot shows normalized linear fits for all stations. Surprisingly, Station 7, which transmits through the longest path of corn, shows the least variation of plant water content.....	100
Figure 48	Average (for all stations) power spectral density of RSSI. One can clearly observe a spike at 1 cycle/day, indicating a diurnal cycle in the RSSI. This is consistent with results from Empirical Mode Decomposition (EMD) and Data Stacking, see below.....	101
Figure 49	Empirical mode decomposition for RSSI data from Station 3. EMDs for other stations are very similar. ....	103
Figure 50	Zoomed in plot of the daily periodic mode, showing a clear diurnal cycle.....	104
Figure 51	An “average day” RSSI obtained using data stacking. The left plot is for stations that transmit through the corn, while the right plot is for stations that have a clear view to the cell tower.....	105
Figure 52	Scatter plot of cell modem RSSI vs. rainfall rate. The data suggest that there appears to be no correlation between rainfall and RSSI of the cell modem. ....	105
Figure 53	Schematic of experimental concept. Small, low power radios are placed inside a corn field and transmit to a base station outside of the field. Leaf wetness modulates the attenuation through the canopy. The base station records the received signal strength indicator (RSSI) and allows one to infer leaf wetness. ....	108
Figure 54	Locations of six RF nodes and base station collocated with rain gauge and leaf wetness sensors in the field in Ames. Node ES02 was used as a control and had an unobstructed view of the base station, all other nodes were located within the canopy. ....	110
Figure 55	The top panel is an example of a resistive leaf wetness sensor. In a resistive leaf wetness sensor, a change in resistance occurs at the wet-dry transition. The change in resistance is in the range of 50 kΩ to 200 kΩ. The bottom panel is an example of a dielectric leaf wetness sensor. A change in the dielectric constant occurs as the sensor wets and dries. The manufacturer claims the sensor can detect trace amounts of water/ice on the sensor. Both of these types of leaf wetness sensors merely model the leaf of a plant.....	111
Figure 56	The radio antennas were installed in the center of the cornrows at about half of canopy height. Leaf wetness sensors were installed at one third and two-thirds canopy height. 2.4 GHz RF modules provided the links for making RSSI measurements. ....	113

Figure 57	Time-series of RSSI from ES3, voltage from leaf wetness sensor, and rain rate. One can observe long-term increase in RSSI as the corn dries out, as well as high-frequency fluctuations. Our hypothesis is that these high frequency fluctuations are related to leaf wetness. The bottom plot is a zoomed-in section of the time-series showing how rain changes the leaf wetness and attenuation, while the RSSI of the reference link is essentially unaffected by rain. ....	115
Figure 58	The left plot shows original RSSI data for site ES3 sampled at 2-minute intervals. The right plot is the detrended data averaged to 15-min intervals, and normalized to 0-dBm attenuation. ....	115
Figure 59	RSSI for links ES3, ES4, and ES5 were averaged for comparison with leaf wetness sensor data. The reference link outside the corn shows much less variation, supporting the hypothesis that the plant moisture modulates RSSI. ....	116
Figure 60	The plot shows an “average day” leaf wetness and RSSI for both canopy nodes and the reference link. ....	116
Figure 61	The plot shows an “average day” leaf wetness and RSSI for both canopy nodes and the reference link. However, rather than the whole 50-day period, this plot corresponds to a three-week no-rain period. ....	117
Figure 62	Scatter plot of leaf wetness sensor output voltage versus normalized attenuation of the averaged RF signal for links ES3, ES4, and ES5. A correlation coefficient of $R^2 = 0.83$ was calculated. ....	118
Figure 63	Top is the possible implementation of measuring TOF using a streaming server. Latency is a function of the fixed overhead of the radios and ....	122
Figure 64	The figure depicts the concept behind round-trip TOF measurements to estimate river stage. A transmitter on the bank transmits on 433-MHz to a streaming server on the bottom of the river. The streaming server echoes back on 315 MHz. The river stage modulates the phase difference between the 433-MHz and 315-MHz signals on the bank. One can easily measure the phase difference and estimate the river stage. ....	124
Figure 65	EM waves propagate at $\sim 30$ ns/m in water. The delay between received- and transmitted pulse trains are $t_1 + 30 \times \text{Depth}$ (ns), where $t_1$ represents the latencies of the radios, time-of flight through air, electronics, etc. ....	126
Figure 66	The top panel shows the operation of an XOR gate as a phase detector. The inputs to the XOR gate are square waves at the same frequency $f_i$ , but not at the same phase. The output of the XOR gate is a series of pulses at frequency $f_i$ , but the duty cycle is a function of the phase difference between inputs. Low-pass filtering the pulses extracts the average value, giving an output voltage linear with phase difference, as shown in the lower pane. ....	128
Figure 67	Results from the phase measurement experiment. The data suggest that it is possible to measure water depth by measuring the TOF. Unfortunately results were skewed by the functionality of very off-shelf modules depicted in the thesis. ....	128

## CHAPTER I

### PREVIEW OF THE THESIS

The central assertion in this thesis is the following: one can use unlicensed and often very inexpensive radios for unconventional communication (underwater- and underground) links. However, one can go further, and use these radios as sensors rather than communication links. The communication links and sensors can have important application in hydroscience. In this thesis, I validate this assertion by

- Providing physics-based arguments for the proposed links and sensors
- Providing a simple mathematical model that explains measured values
- Showing that one can use the model to design links and sensors
- Considering important engineering considerations (cost, robustness) and showing that the proposed links and sensors have advantages compared to some existing technologies
- Providing five examples that I have validated experimentally, namely
  - Underwater communication links using industrial scientific medical (ISM) radios
  - Underground communication links using ISM radios
  - Soil moisture estimation using ISM radios
  - Vegetation water content using cell modems
  - Leaf wetness measurements using ISM radios

#### Grounding

We begin with Maxwell's equations, the keystones of electromagnetic theory. From there we derive the wave equation in a conductive medium. I will proceed to show that the RF modules I use operate at frequencies where one can consider freshwater and some soils as dielectric media. While the attenuation of RF signals is high in these mediums, by using wireless sensor network (WSN) paradigm of multi-hop and retransmission, reliable networks can be formed underwater and underground. In this thesis, "underwater" is taken to be in freshwater applications.

I will also show that one no longer needs to think of RF modules as only a source of data transmission. This revelation lends itself to thinking of these modules as inexpensive RF wave generators at prescribed unlicensed frequencies. Analyzing the received signal strength indicator (RSSI) of a link over time, one can infer changes in the medium from the changes in RSSI. I will show that a simple mathematical model can be used for the analysis and give five experimentally validated examples demonstrating the possibility of non-traditional uses for RF modules that are so prolific today.

### Simple Mathematical Model

In this thesis I show that the following mathematic model

$$P_r = \frac{P_o e^{-2\alpha R}}{R^n}$$

where  $P_r$  is the received power,  $P_o$  is the power transmitted,  $R$  is the distance between transmitter and receiver,  $n$  is the path loss exponent, and  $\alpha$  is the attenuation constant is adequate to describe the links and sensors mentioned above. For the experiments shown in this work, the distance between transmitter and receiver,  $R$  remained constant. The transmitted power of the module is known and the received power can be measured. The value  $n$  depends on the environment:  $n = 2$  in free space but it can take on different values in case of multipath. Observed changes in RSSI are related to changes in the propagation medium which are quantified by  $\alpha$ . For example, in the soil moisture experiments (Chapter V), the distance  $R$  remains constant and  $\alpha$  is a function of soil type and water contained within the soil. The soil type between antennas remains constant between successive measurements. Changes in observed signal strength can largely be attributed to changes in the amount of water contained in the soil. The permittivity of soil does change with soil temperature and be corrected for if soil temperature is known.

### Designing Links and Sensors

To design an underground link, one would need to estimate bounds or variance in  $\alpha$ . This would then provide bounds on RSSI and would drive maximum separation distances of nodes. Alternatively one could estimate link reliability for nodes that are separated by a specific distance for varying soil moisture conditions. As a result, network throughput could be calculated for various network configurations. These bounds would also dictate antenna placement when using the module as a sensor.

### Engineering Considerations

In this thesis, I argue that the proposed links and sensors can have clear advantages when compared to standard methodologies. Consider for example soil moisture measurement. A very popular sensor is the so-called time domain reflectometry (TDR) probe. Chapter V shows that it is possible to make soil moisture measurement using small, inexpensive, unlicensed radios. The soil moisture measurements are along a line between two radios buried in the soil. A change in soil moisture modulates the attenuation of the RF signals between the two radios and provides a distributed/integrated measurement of the soil moisture. The experimental data collected using RSSI for soil moisture estimations was validated using the well known TDR sensors. Since the TDR sensors only provide a point measurement several were used in validating the RF link measurements.

Advantages of using RF links to measure soil moisture are that the soil is not disrupted where you want to make a measurement. Many of the point source measuring techniques require burial in the soil to make a measurement, disrupting the very area around where you're making the measurement possibly contaminating the data you are attempting to collect. The major advantage of point measurements is that one knows exactly what is being measured. The volume of the RF link distributed measurement may be largely unknown. Another distinct advantage is that the RF links typically will be an easier installation. The radios are installed outside of the measurement area by driving small PVC pipes into the soil and lowering the antennas into the

soil. Both ends are capped to prevent water from infiltrating the pipe. The RSSI measurement provides a water content measurement over the entire link as opposed to the point measurement of the TDR probe. This is a significant benefit because integrated measurements are less sensitive to a local anomaly in the soil. The RSSI measurements on most RF modules are straightforward and quick to make and can be made with limited additional electronics. The distributed measurement allows one to make measurements that would be very hard to make otherwise. For example, it now could be possible to make measurements through root balls of trees by placing a ring of radios around the tree. One exiting advantage is the following: Since there is a communication link in place and power consumption is low, one could bury the sensors and keep them in an agricultural field over the course of a season. With the presence of the RF link it is also possible to send diagnostic data on the health of the nodes. This data could include battery voltage, link reliability and operating temperature. It may even be possible to incorporate inductive coupling to remotely charge low batteries eliminating the need to dig up buried sensors.

Some of my early research was in the development for monitoring soil moisture at The Iowa Validation Site near Ames, Iowa (Niemeier 2007). That research was in the development of a network to collect soil moisture and soil temperature measurements at eleven locations throughout a 1 km<sup>2</sup> field. Each location consisted of multiple point soil moisture and multiple point soil temperature measurements. This experiment used TDR probes to obtain soil moisture measurements and a custom fabricated/calibrated temperature sensor to obtain soil temperature measurements. One of the difficulties of this experiment was in removal of nearly 200 sensors from the field twice a year, once to plant the crop in the field in spring and once again to harvest the crop in fall. From this experience of developing a real world network, I gained knowledge in the effects of environmental fouling of equipment, temperature effects of electronics and the difficulties in passing wires in a harsh environment. One usually would not think of a corn or bean field in Iowa as a harsh environment. Snow, rain, flooding, heat and wire chewing animals all add to the difficulties in maintaining a network. A well designed RF network for monitoring

soil moisture could be designed to be completely self-contained with no external wiring, thus making environmental sealing simpler and more cost effective. Also, if installed deep enough there would be no need to remove the equipment during crop harvest or planting, eliminating needless man hours and soil disruption during installation and removal of sensors.

The cost of a pair of radios to create a single link, with antennas and additional electronics for measuring RSSI is equivalent to two TDR probes. Both systems would require additional data loggers to record the measurements. Disadvantages to RSSI measurements are that the technique depends on the soil type. However, the same is true for conventional TDR probes, which require calibration to the soil to get a proper measurement. In this work I show similar validation arguments for using the RF links in vegetation water content measurements and leaf wetness measurements along with using the modules in untraditional environments.

### Existing Research

The following is a brief look at research by others in the area of using RF modules in hydroscience. Following the trend of Moore's law, radios have become smaller, faster and more power efficient. Unlicensed radios, operating in the Industrial, Scientific and Medical (ISM) bands are now ubiquitous due to their small size and inexpensive cost. Short-range radio links are now found in most homes in devices such as Wii® (Nintendo 2010) game controllers. The controller communicates wirelessly with the console via short-range Bluetooth radio (Bluetooth 2010), with which it is possible to operate up to four controllers as far as 10 m (~30 ft) away from the console. The popularity of such devices with the public has provided engineers with a plethora of radio modules to choose for design of wireless networks. There are many advantages to wireless networks over a wired network. One large benefit is a reduction in the network cost due to interconnection devices using traditional copper wire. Also, wireless networks permit users to dynamically join and leave networks, forming ad hoc networks and creating a communication link for as long as necessary.

The scope of this document is to convince the reader that radios are useful for more than just conventional uses of transmitting data from source  $A$  to sink  $B$  through the typical medium of air. The low cost of modules along with the use of wireless sensor networks (WSN) paradigm, make it attractive to use radios in unconventional manners. **My thesis is that one can and indeed should consider these low cost modules as more than communication devices. One should think of them as cost-effective source of electromagnetic (EM) waves at prescribed unlicensed frequencies.** By looking at changes in the transmission characteristics through a medium with time, one can infer changes in the medium. This now leads to thinking of the radio module as a *sensor* rather than a communication link. The data transmitted over the link may or may not even be relevant, since it is now the *observed changes* in the transmission that are of interest. There are many potential advantages to this approach. One example is the following. Such measurements will provide a *distributed measurement* over the entire link, as opposed to point measurements made by a single sensor. The distributed link measurement could help in the reduction of uncertainty found in-situ point measurements. The scope of this document looks at possible ways to use of off-the-shelf radios in new, unconventional manners.

In this thesis, I explore two ideas. The first of these are that one can use radios to transmit data in unconventional settings such as underwater and underground. The second idea is that one can use changes in received signal strength to infer changes in the attenuation of the medium between the transmitter and the receiver. One can in turn use this to infer changes about in the intervening medium.

### Underwater Wireless Sensor Networks

A survey of the literature reveals that some of the previously mentioned ideas, while not mainstream, have been around for many years. There are well-developed theories and methodologies in place. An example here is underwater communication in the sea. The motivation for undersea communication comes from the military and the need for communication with submarines (Turner 1959, Chesnoy 1996). This communication may consist

of ultrasonic, infrared radiation (IR) and radio frequency (RF). Of these, ultra-sonic has proven to be a reliable, long range form of underwater communication, although its robustness in deep sea communication doesn't lend itself to large scale, low power wireless sensor networks. Heidemann et al. (2006) considers the difficulties in constructing an underwater sensor networks and states first, radio is not suitable for underwater usage because of extremely limited propagation and states current mote radios transmit 50–100 cm. There are several sections related to RF transmission in water in this thesis that prove differently. While acoustic telemetry is a promising form of underwater communication, off-the-shelf acoustic modems are not suitable for underwater sensor-nets with hundreds of nodes: their power draws, ranges, and price points are all designed for sparse, long-range, expensive systems rather than small, dense, and economical sensor-nets. Second, the shift from RF to acoustics changes the physics of communication from the speed of light in a vacuum ( $3 \times 10^8$  m/s) to the speed of sound in water (around  $1.5 \times 10^3$  m/s) a difference of five orders of magnitude. While propagation delay is negligible for short-range RF, it is a central fact of underwater acoustic networks. Kong et al. 2005 considers the challenges in overcoming the limited bandwidth of ultrasonic communications created from the slow propagation velocity of sound in water.

Like RF, IR communication suffers from high signal attenuation in water, but benefits from high bandwidth, lower power, smaller size, and long life. Anguita et al. 2009 discuss how available radio modules such as Bluetooth or Wireless LAN (IEEE 802.11), which operate in the gigahertz range (around 2.4 GHz), cannot be used underwater but IR may be applicable for short range communication. Anguita et al. 2009 showed in experimental tests, the best IR wavelength is around 420 nm (blue-violet wavelengths) and that this value changes in the presence of turbidity. During preliminary test, a transmission at a distance of 1.8 m was achieved at 100 Kbit/sec, with a light impulse of 5 ms; the increase of the distance between the LED and the photodiode in the tank causes an increase in the bit error rate and the impossibility to have a connection beyond 1.8 m. I investigated a similar technique, using IR LEDs to measure water turbidity on floating data loggers with RF links (Davies et al. 2008). Meihong et al. 2009 looks

at various modulation techniques in underwater IR communication. Through modeling and simulation, it was demonstrated that pulse position modulation (PPM) is better suited for low powered undersea systems and phase shift keying (PSK) yields the best performance in terms of bandwidth and error performance with poor power efficiency. The simulation results showed that red light has better transmission characteristics in waters with higher chlorophyll concentration.

A common mantra in underwater communication papers is how RF is not applicable in underwater communication (Anguita et al. 2009, Meihong et al. 2009, Heidemann et al. 2006). While RF is not well suited for underwater communication, there are several advantages of underwater RF communication. RF waves can cross the air to water interface and is discussed in Chapter II. RF signals are tolerant of water turbulence, as opposed to acoustic and optical signals. RF is not as susceptible to environmental fouling and can work in stained water conditions, which limits optical. Like optical, RF provides an increased bandwidth range over acoustical waves. Hybrid networks that use both acoustic and RF communication have been proposed. *TurtleNet* is a design proposed in Ali et al. 2008, and uses both acoustic and RF communication to route data. In that design, nodes would use acoustic waves for long range underwater communication and a piston would then raise the node out of the water to then route data wirelessly through the air.

By far, the most common approaches for underwater communication is to use low frequencies in the range of 80 Hz, and very high power (Moore 1967). The aim is to establish long-range communication: several hundred miles. The interest in undersea communication has led to a fair amount of research on the conductivity of seawater and antenna designs for undersea communication (Rivera 2001).

In recent years, there has been some interest in the propagation of EM waves at high frequencies. For example, Al-Shamma'a et al., 2004 explored the propagation of EM waves in seawater in the range of 100 kHz to 20 MHz. They performed a number of laboratory experiments in tanks filled with saline solution. They tested several antennas including a loop

and a dipole antenna. They reported signal attenuations that range between 55 dB/m and 80 dB/m. For conventional radio links, such attenuation would be intolerable. However, in recent years the concept of underwater wireless sensor networks (UWSNs) has emerged. In Well et al. 2009 link reliability is simulated for RF communication in seawater at a carrier frequency of 3 kHz. They investigated link reliability for five different possible node topologies. These nodes are to eventually be placed on the sea floor to monitor coastal erosion beneath the sea surface. In the WSN paradigm, a communication network consists of multiple small, inexpensive, and low power nodes that cooperate in sensing their environment and deliver data. With this view, an attenuation of 50 dB/m, while large, will still allow reliable communication over 2 m with many off-the-shelf radios on the market. Zang et al. 2004, describes the design and construction of an underwater sensor actuator network to detect extreme temperature gradients, motivated by the fact that regions of sharp temperature change (thermoclines) are a breeding ground for certain marine microorganisms. Four sensors were equipped with temperature probes and 433-MHz radios with resulting transmission distances limited to 30 cm. The system was tested and could reliably detect a thermocline in a tank filled with saline solution.

While the majority of the work has been dedicated toward communication in sea water some work has looked at fresh water communication. Hafez et al. 1979 looked at RF attenuation between 33 and 363 MHz. Their findings indicated that attenuation around 100 MHz is dominated by conductivity and is relatively independent of frequency below 100 MHz, while increasing the frequency above 100 MHz results in a rapid increase in attenuation. For water conductivity of 0.01 S/m, the attenuation rate at 100 MHz is surprisingly low (2.5 dB/m) and near 10 dB/m at 300 MHz. Along this same lines Lindsay et al. 1977, used 164 MHz RF modules for tracking spawning fish. At that time, the FCC had allocated that frequency for wildlife telemetry tracking. RF modules with half-wave dipole antenna were attached to the fish. The antenna length was corrected for use in water since the effective length is 1/9 the length in free-space. In 2004 the FCC allocated frequency bands 40.66–40.70 MHz and 216–220 MHz to

be used for the tracking of, and the telemetry of scientific data from, ocean buoys and animal wildlife (BIRDNET 2010). Sitter et al. 2009 and Hunt et al. 2010 describe work that I have been involved with in designing underwater wireless sensor networks using RF communication for bio-sensing communication. This application and development of this work is described in detail later in this document.

### Underground Wireless Sensor Networks

Setting WSNs aside for a moment, there are several telemetry applications that will operate under a 50 dB/m constraint. An excellent example is the work done in the development of the *Soil Scout* (Tiusanen 2005, 2006, 2007, 2009) for monitoring soil moisture. The Soil Scout is a small wireless sensor that operates at 869 MHz, which is a European license free band. Data collected by the Soil Scout sensors are transmitted to an above ground base station. The sensors are buried below the soil surface at depths up to 40 cm for sensors close to the base station and shallower depths for more remote sensors. Soil Scouts are 42 × 90 mm digital instruments equipped with an innovative underground single-ended monopole antenna (USEMA) on the printed circuit board. Data consists of soil moisture and soil temperature measurements transmitted every 10 minutes over a five month period in real conditions. Sensors were deployed in an oat field before planting crops and left in the field during harvest.

Current work from this group is in a signal attenuation model to predict long periods of lost signals when soil moisture and on-soil vegetation conditions change. The model includes three attenuating mechanisms: (1) dielectric loss in soil; (2) reflection from the surface; and (3) angular defocusing of the intensity due to refraction. The most significant model input parameters are frequency, out-coming angle, and both real and imaginary soil permittivity, which are both dependent on frequency, moisture and soil texture. Further work will focus on increasing transmission power and improving knowledge of the effect of vegetation. Difficulties encountered consist of development of an antenna that will operate efficiently as the soil

conditions change with water content and sealing of the sensor. A significant number of sensors didn't survive the experiment due to improper sealing.

The attenuation of RF communications in of underground sensors will have to take into consideration the changes in soil water content. Peplinski et al. 1995, Hipp 1974 and Curtis 2001 all look at the affects of soil electromagnetic parameters as a function of frequency. The real part of the complex dielectric constant and the normalized phase velocity are both very strong functions of volumetric moisture. While there is a strong relationship between permittivity and moisture content, there is no simple relationship between moisture content and power attenuation.

There are other factors involved in the loss parameters besides just the amount of water in the sample. Soil type and non-soil contents, such as salts, may have an effect on soil conductivity. There is a group of sensors which use a technique called time domain reflectometry (TDR) that use this strong dependence of dielectric permittivity on the volumetric moisture of a sample soil. Campbell Scientific's CS616 is one such probe (CS616 2010). The operation of the CS616 is described in later chapters.

In the study of soil moisture, there are several advantages to completely wireless nodes (Niemeier et al. 2008), as opposed to wired sensor stations (Niemeier et al. 2006). There are several problems created in wired networks in an agricultural setting. During periods of field work, such as cultivating, planting and harvest, all instruments above ground need to be removed from the field. In Niemeier et al. 2008, I explored the possibility of using 100 mW RF links underground, at common off-the-shelf frequencies of 900 MHz and 2.4 GHz. That experiment is covered in detail later in this document. It was found that reliable underground links could be obtained at distances of up to three meters for sensor buried at depths of one meter for the 900 MHz link and links of less than a meter at 2.4 GHz. The link reliability was found to be dependent on soil moisture content. For the standard soil moisture sensor deployment used in Niemeier et al. 2006, the distances achieved using the 900 MHz radio would be more than adequate. Stuntebeck et al. 2006 also looked at the possibility of using telemetry based

communication from below ground sensors to above ground base station. They used the Crossbow MicaZ mote that is operated at 2.4 GHz in moderately wet clay soil. Wet clay soils produce the most attenuation of an electromagnetic wave, while dry sandy soils produce the least. Transmitters were buried in the ground while receivers were located above ground. Reliable communication between an underground and a surface node was only achievable over a range of 7 m, even with the underground node placed at a relatively shallow depth of 6 cm. It was concluded that 2.4 GHz radios were not appropriate for underground sensor networks.

Another application of underground telemetry is seen in Trinchero et al. 2009. Here underground RF communication at 750 MHz was used in measuring water pressure and tracking water conduit underground at depths of 5 to 250 cm. The electronics equipment with a pressure transducer and RF module were sealed and placed in plastic pipes located underground. Reliable communication was observed in water pipes of 20 cm in diameter at a depth of 250 cm below the earth's surface. A detailed investigation into underground wireless sensor networks is provided in Akyildiz et al. 2006. They explore the challenges of designing underground wireless networks. This investigation includes a look at applications, power consumption considerations, selection of node placement, node size and frequency. They also talk about effects of soil properties such as water content, particle size, density, and temperature on the underground channel.

There is an interest in underground RF sensor networks for applications in the mining industry. Most of these applications are either for long range at frequencies of a few hertz (Stolarczyk et al. 1991) or for dense networks that transmit through air links in the tunnels (Wang et al. 2009). These systems were devised for tracking miner locations within the mine.

#### Inexpensive RF Modules as Sensors

There has been a significant amount of work done in modeling of the attenuation of signals in the ISM band (Richter et al. 2003, Hashim et al. 2006 and Dal Bello et al. 1998) from the effects of vegetation. Movement of vegetation structures introduces an adverse environment

for high frequency radio wave propagation. Particularly when the prevailing weather conditions are windy, the movement of this vegetation is observed to cause severe fading in RF channels. These effects are a function of leaf size versus wavelength. As the wind increases the scatter in signal strength also increases. While attenuation of signal strength due to vegetation is considered an annoyance in most RF communications there are applications where the attenuation is a useful measurement.

With respect to using changes in RSSI to infer changes in the medium, there is much less in the literature. However, preliminary results from several experiments (Hunt et al. 2008, and J. Giacomini et al. 2007), suggest that one may be able to quantify plant moisture content and dew on plants. In Hunt et al. in press, my involvement was to assist in the investigation of the relationship between cellular communication attenuation and corn plant water content. Seven nodes containing cell modems were used to transmit data collected from rain gauge platforms. Three of these nodes were located on the edge of the corn field with a clear view of the cell tower and four nodes were located within the corn field. The RSSI was observed over the entire life cycle of the corn plants for nodes located in a corn field located near Ames, Iowa. RSSI decreased as the corn plants grew to heights well above the antennas for nodes located in the field. As the plants begin to senesce the signal strength became stronger for nodes located in a corn field. A daily cycle was also observed in the collected data which would lead to the implementation of an experiment to investigate the relationship of dew on the corn plants with respect to signal strength (Niemeier et al. 2009). Both experiments are examined later in this document. Giacomini et al. 2007, also investigates the attenuation of RF signals through corn. The experiment used 1 mW radios at 916-MHz in a corn field located in Brazil to measure corn plant water content. The sensor nodes were at 1.5 m high and at 10 m distant from each other. All the antennas were at vertical position. In each sequence, 100 RSSI measurements were taken for each sensor node pair. The experiment demonstrated that changes in plant water content (gravimetric moisture) forces a proportional changing in microwave power loss. In effect, as

gravimetric moisture decreased from 80% to 60%, the power loss decreased from 65.4 dB to 61.8 dB.

The importance of these works is for scientists who are interested in validating remotely-sensed soil moisture estimates. Hornbuckle and England (2003) asks the question “Dew: invisible at 1.4 GHz?” This paper concluded that observations and modeling results support the hypothesis that water on the canopy in the form of dew did effect the brightness measurements at 1.4 GHz. Dew had the net effect of decreasing the measured brightness for both antenna polarizations. The offset of the measurement created by dew may lead to error in satellite remotely sensed soil moisture estimations. Two examples are the Soil Moisture and Ocean Salinity (SMOS) mission of the European Space Agency (SMOS 2010) and the upcoming Soil Moisture Active and Passive (SMAP) mission of the National Aeronautics and Space Agency (SMAP 2010), which use terrestrial microwave emissions to monitor soil moisture. The effect of dew on 2.4 GHz links (Niemeier et al. 2009) is considered later in this document.

Others have looked at the use of cellular network signal strength for monitoring near surface water vapor (David et al. 2007) and in rainfall estimation (Leijnse et al. 2007, Messer 2006, Messer 2007, Messer et al. 2008). For all these studies cellular communication links are at frequency ranges of 17 GHz to 38 GHz. David et al. 2007 compared inter-daily variations in the absolute moisture which were calculated from RSSI data obtained from the 22 GHz wireless communication network, as compared to in-situ measurements, over a month in Israel. The results show a very good match between in-situ measurements and the proposed method, the correlation coefficient between the time series in the two presented cases were 0.9 and 0.82. In typical conditions of 1,013 hPa pressure, temperature of 15 °C and water vapor density of 7.5 g/m<sup>3</sup>, the attenuation caused to a microwave beam interacting with the water vapor molecules at a frequency of 22 GHz is roughly around 0.2 dB/km.

Leijnse et al. 2007 analyze data collected using two 38 GHz commercial cellular links during eight rainfall events over a 2 month period during the fall of 2003 in the Netherlands. Comparisons of these cellular rainfall intensities estimations to those measured by a nearby rain

gauge and by two C band weather radars have yielded promising results. A statistical analysis shows that in relatively uniform rain, the links compare better to the gauge, whereas in variable rain the comparison between the links and the radar is better. Cellular signal attenuation due to rain at frequency in the range of 17 GHz to 23 GHz was explored in Messer 2006, Messer 2007 and Messer et al. 2008. It was stated that cellular radio links for mobile operation at frequencies of 1 to 2 GHz are weakly sensitive to rainfall. The test network consisted of 22 fixed line-of-sight microwave links and six high resolution rain gauges deployed in an area of 15 km<sup>2</sup> in Israel. A correlation coefficient of 0.8 was observed when comparing cellular estimated rainfall with rain gauge measurements. It was noted in these papers that before signals measured by cellular communication links can be used to estimate rainfall operationally, several improvements need to be implemented. The reference signal level needs to be known, so that the attenuation can be determined from the deviation of the signal from this level. The very coarse power resolution of the signals that have been used in these papers may cause large rounding errors, especially in long and low-intensity events. Sampling errors in events that are highly variable in time can easily be overcome by increasing the temporal sampling rate of the links. Finally, the antennas either need to be calibrated for wet antenna attenuation or they need to be shielded from rain.

Finally, distance measurement using phase measurements (Wei Zhou et al. 2007) using ultrasonic waves (Gueuning et al. 1996), optical wave lengths (Perchet et al. 1997) and RF (Belostotski et al. 2001) is not a new idea. Chapter IX of this document looks at an application of this technique at RF for water stage measurement (Kruger et al. 2009).

## CHAPTER II

### BACKGROUND

#### Electrical Properties and Water and Soil

The work in this thesis is predicated on radio wave propagation through soil and water. Thus, it is appropriate to consider properties of these media at the ISM and cellular communication frequencies. In this section, I pull together relevant equations, facts, and derivations from standard electromagnetic text.

Pure water is a very poor conductor. However, water disassociates readily, and the ions carry charge. Textbooks normally list the conductivity of freshwater as (nominally) 0.005–0.05 S/m and that of seawater as 4 S/m. We measured (see section Fresh Water Conductivity Measurements) the DC conductivity of Iowa City tap water to be about 0.03 S/m and that of the Iowa River at the Burlington Street bridge as about 0.05 S/m. Rain, runoff, and so on will modulate the conductivity, but we were surprised how little the conductivity of the Iowa River changed over a season (see Figure 13). Water is non-magnetic so one can take the magnetic permeability as that of vacuum. In vacuum, radio waves are not attenuated, except for purely geometric weakening as wave spread out from a source. For example, the received power from a point source is inversely proportional to the square of the distance  $P_r \propto P_0/R^2$ , where  $P_r$  is the received power,  $P_0$  is the transmitted power, and  $R$  is the distance between transmitter and receiver.

Water and soil attenuate radio waves. Attenuation can be through pure conduction (i.e., ohmic losses) resulting from the medium's finite conductivity. However, even a dielectric with zero conductivity can exhibit *dielectric hysteresis*, which leads to losses. Consider a dielectric, non-magnetic material, composed of polar molecules. An example is distilled water. Initially the polar water molecules are randomly oriented. When one applies an external electric field, the polar water molecules orient themselves in the field. As one increases the electric field, the orientation or polarization of the molecules increases, but at high electric fields, an additional increase does

not result in more polarization. The path  $o \rightarrow a$  in Figure 1 (top left plot) indicates this. Now, if one reduces the electric field, the molecules retain some of their polarization, and when the external field is zero, there is some residue of polarization left as is indicated by the path  $a \rightarrow b$  in Figure 1 (top right plot). When one now reverses the electric field, it must perform work to remove this residual polarization. Then the electric field will polarize the water molecules in the other direction. The path  $b \rightarrow c \rightarrow d$  in Figure 1 (bottom left plot) indicates this. Finally, the path  $d \rightarrow e \rightarrow f \rightarrow a$  in Figure 1 (bottom right plot) shows how the polarization of the water molecules change as the field is reversed again.

The enclosed area represents the work the external electric field performs as it reorients the molecules over one cycle. The work the electric field performs manifests as a conversion to heat. A dielectric material with a larger hysteresis area will result in more heat generation, and will attenuate radio wave more than those materials with smaller hysteresis area.

Another view is the following. Water molecules are polar that tend to rotate in the presence of an alternating electric field. There is a phase delay between the application of an electric field and the response of water molecules. As the molecules collide, they incur energy loss. One models the phase delay by adding an imaginary part to the dielectric permittivity. Proper choice of the imaginary part's sign captures the energy loss.

The relative permittivity  $\epsilon_r$  of water is (nominally) 80 at DC. At higher frequencies, the relative permittivity is complex, expressed as  $\epsilon = \epsilon' - j\epsilon''$ . The imaginary part, associated with the dielectric hysteresis, is small, but result in additional loss, which quickly increases with frequency. It turns out that the frequency of the radio wave plays a crucial role in determining what losses dominate. Below some transition frequency, conduction losses dominate, and above this frequency, dielectric hysteresis losses dominate. The following table summarizes the electrical properties of freshwater at ISM frequencies.

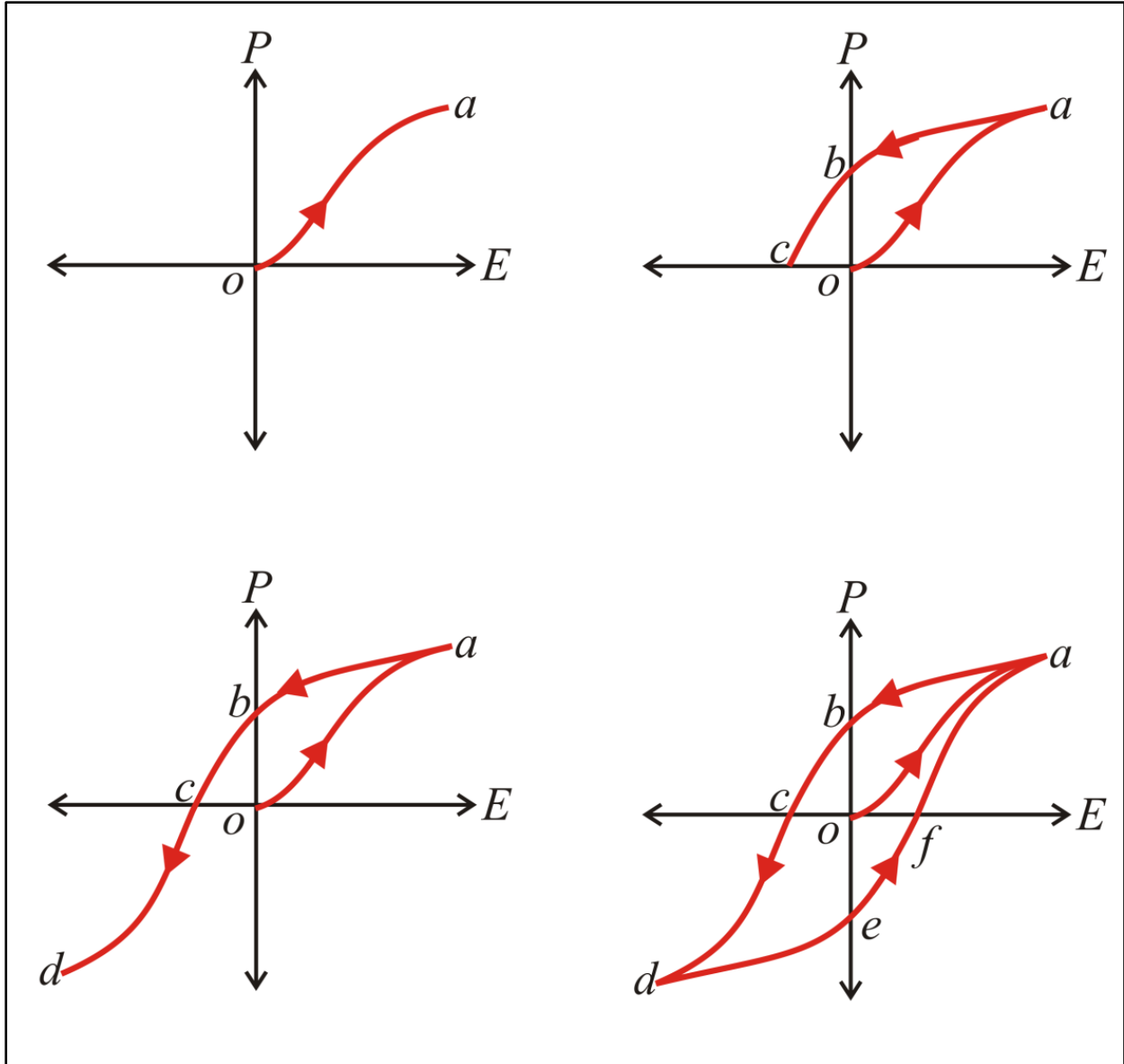


Figure 1 Dielectric hysteresis. The top left plots shows the polarization of an initially unpolarized dielectric material as a function of an external electric field. The top right plot shows the polarization when the electric field is reduced. At point  $b$ , even with no external electric field, there is still some residual polarization. To remove this (point  $c$ ), the electric field must perform work. The bottom right plot shows the situation when the polarization has been reversed. The lower right plot shows the complete hysteresis cycle. The enclosed area determines the hysteresis losses over one cycle.

Table 1 Measured relative dielectric permittivity of freshwater at 20 °C.

Frequency (Hz)	Real part of $\epsilon_r$	Imaginary Part of $\epsilon_r$
100 MHz	80.22	0.445
200 MHz	80.21	0.889
300 MHz	80.2	1.333
315 MHz	80.19	1.400
400 MHz	80.18	1.777
433 MHz	80.17	1.924
500 MHz	80.15	2.221
900 MHz	80.01	3.990
1 GHz	79.96	4.430
2.4 GHz	78.72	10.46
25 GHz	28.89	34.54
100 GHz	7.675	12.7
200 GHz	5.733	7.01

Table 1 shows the measured  $\epsilon_r$  for water at several frequencies (Meissner and Wentz 2004). Dielectric hysteresis, represented with a complex dielectric permittivity, can have a significant effect on the attenuation  $\alpha$ .

#### Electromagnetic Wave Equation in Lossy and Conductive Media

Undergraduate texts in electromagnetic theory normally treat wave propagation in lossless, charge-free media. Propagation in good conductors (metals) is explained in terms of the so-called skin-depths, and students are left with the impression that radio waves do not penetrate conductors, so that radio communication in conductive media is not feasible. These texts may

have sections on propagation in lossy dielectric, but instructors will often skip these sections. Below we briefly derive the wave equation in a conductive, dielectric medium (fresh water), and draw some important conclusions.

Consider Maxwell's curl equation

$$\nabla \times \mathbf{H} = \mathbf{J} + \frac{\partial \mathbf{D}}{\partial t}$$

where  $\mathbf{H}$  is the magnetic field ( $\text{A m}^{-1}$ ),  $\mathbf{J}$  is the current density ( $\text{A m}^{-2}$ ) and  $\mathbf{D}$  is the electric flux density ( $\text{C m}^{-2}$ ).  $\mathbf{H}$ ,  $\mathbf{J}$ , and  $\mathbf{D}$  are vector quantities. The conductivity  $\sigma$  ( $\text{S m}^{-1}$ ) relates the current density to the electric field  $\mathbf{E}$  ( $\text{V m}^{-1}$ ), through

$$\mathbf{J} = \sigma \mathbf{E}$$

This equation is the generalized form of Ohm's law. Combining these equations result in.

$$\nabla \times \mathbf{H} = \sigma \mathbf{E} + \frac{\partial \mathbf{D}}{\partial t}$$

Consider a linearly polarized wave traveling in the  $x$  direction with the electric field in the  $y$  direction. The vector curl equation above then reduces to the scalar equation

$$-\frac{\partial H_z}{\partial x} = \sigma E_y + \epsilon \frac{\partial E_y}{\partial t}$$

Here  $\epsilon$  is the *dielectric permittivity* ( $\text{F m}^{-1}$ ) of the material.

Next, consider Maxwell's other curl equation

$$\nabla \times \mathbf{E} = -\mu \frac{\partial \mathbf{H}}{\partial t}$$

where  $\mu$  is the magnetic permeability ( $\text{H m}^{-1}$ ). For a linearly polarized wave traveling in the  $x$  direction with the electric field in the  $y$  direction, vector curl equation above then reduces to the scalar equation

$$-\frac{\partial E_y}{\partial x} = -\mu \frac{\partial H_z}{\partial t}$$

Expressing the wave in phasor form  $E_y = E_0 e^{j\omega t}$ , and substituting in the scalar equations for the wave gives

$$\frac{\partial H_z}{\partial x} = -(\sigma + j\omega\epsilon)E_y$$

$$\frac{\partial E_y}{\partial x} = -j\omega\mu H_z$$

Here  $\omega$  is the radian frequency of the wave. Differentiating the second equation with respect to  $x$  and substituting  $\partial H_z/\partial x$  into the first equation gives

$$\frac{\partial^2 E_y}{\partial x^2} = (j\omega\mu\sigma - \omega^2\mu\epsilon)E_y = \gamma^2 E_y$$

This is the wave equation for a linearly-polarized (electric field in the  $y$  direction) in a conducting medium, and  $\gamma$  is the *wave number* or *propagation constant*. The wave is traveling in the  $x$  direction. If the conductivity  $\sigma$  is finite, the wave will experience attenuation. In general, the medium may also have dielectric- and magnetic hysteresis so that  $\epsilon$  and  $\mu$  are complex:

$$\epsilon = \epsilon' - j\epsilon'', \quad \mu = \mu' - j\mu''$$

The imaginary parts of these quantities, when multiplied by  $j$  in the various expressions, become negative real terms and becomes attenuation terms. In most materials (certainly in water and in soil)  $\mu'' \approx 0$ , and  $\mu = \mu' = \mu_0 = 4\pi \times 10^{-7} \text{ H m}^{-1}$

A solution to the wave equation, namely

$$\frac{\partial^2 E_y}{\partial x^2} = (j\omega\mu\sigma - \omega^2\mu\epsilon)E_y = \gamma E_y$$

is given by

$$E_y = E_0 e^{-\gamma x}$$

One can easily verify this by substituting into the wave equation. The wave number  $\gamma$  has a real and an imaginary part, since

$$\begin{aligned}\gamma^2 &= j\omega\mu\sigma - \omega^2\mu\epsilon \\ &= j\omega\mu\sigma - \omega^2\mu(\epsilon' - j\epsilon'')\end{aligned}$$

Let  $\gamma = \alpha + j\beta$ , then a solution to the wave equation is

$$E_y = E_0 e^{-\alpha x} e^{-j\beta x}$$

This shows that  $\alpha$  is associated with the attenuation of the wave as it propagates in the  $x$  direction through the medium and  $\beta$  is associated with the phase of the wave. The attenuation is measured in nepers per meter. If  $\alpha = 1$  the amplitude of the wave will decrease to  $e^{-1} \approx 0.37$  of its original value after 1 m.

$$\gamma^2 = j\omega\mu\sigma - \omega^2\mu\epsilon$$

Using  $\sigma = 0.05 \text{ S m}^{-1}$  and a nominal value of  $\epsilon_r = 80$  at 433 MHz gives

$$\gamma = \alpha + j\beta = 1.05 + j81.2$$

This corresponds to an attenuation of about 1 Np/m. However, using the measured value, namely  $\epsilon_r = 80.17 - j1.824$  at 433 MHz gives

$$\gamma = \alpha + j\beta = 2.03 + j81.26$$

This corresponds to an attenuation of 2.03 Np/m at 433 MHz. This shows that seemingly small imaginary part of the dielectric constant dramatically affects the attenuation.

#### Attenuation, Units, Power Measurement

The real part ( $\alpha$ ) of the propagation constant ( $\gamma$ ) is the attenuation constant measured in Neper/m. However, one will often encounter attenuation values specified in decibel/m. The conversion between Neper/m and decibel/m is a source of confusion. Further, the RSSI values

the ratios that are the topic of this thesis, are values of received power. The purpose of this section is to clarify some of the confusion.

By definition, decibel is 10 times the logarithm of the ratio of two *powers*. Thus, the ratio of two *powers*  $P_1$  and  $P_2$ , expressed in decibel is

$$\text{Ratio of } P_1 \text{ to } P_2 \text{ in dB} = 10 \log_{10} \frac{P_1}{P_2}$$

In electrical circuits, one will often measure voltages rather than powers. For example, consider an amplifier with input resistance  $R_i$  and output resistance  $R_o$ . One will then measure the input voltage  $V_i$  and output voltage  $V_o$  and determine the gain

$$\text{Power Gain} = 10 \log_{10} \left( \frac{P_o}{P_i} \right) = 10 \log_{10} \left( \frac{V_o^2 / R_o}{V_i^2 / R_i} \right) = 10 \log_{10} \left( \frac{V_o^2 R_i}{V_i^2 R_o} \right)$$

If (and only if)  $R_i = R_o$  then

$$\text{Power Gain} = 10 \log_{10} \left( \frac{V_o^2}{V_i^2} \right) = 20 \log_{10} \left( \frac{V_o}{V_i} \right)$$

Thus, when dealing with voltages, the multiplier “20” is used instead of “10”, but this only applies if the resistances/impedances are equal.

Thus far, we considered the electric field or the radio wave, and the attenuation  $\alpha$  relates to the attenuation of the electric field:

$$E_y = E_0 e^{-\alpha x} e^{-j\beta x}$$

However, one can derive an equivalent expression for the magnetic field

$$H_z = H_0 e^{-\alpha x} e^{-j\beta x}$$

The power follows from the Pointing theorem (from Krauss and Felisch 1999):

$$P = E_y \times H_z^*$$

where  $H_z^*$  denotes the complex conjugate. This shows that the power decays as

$$P(x) = P_0 e^{-2\alpha x}$$

The power attenuation expressed in decibel/m follows from

$$\text{Attenuation} = -10 \log_{10} \left( \frac{P(x=1)}{P_0} \right) = -10 \log_{10} \frac{P_0 e^{-2\alpha}}{P_0} = 20\alpha \log_{10} e = 8.686\alpha$$

Thus, to convert between attenuation in Neper/m (defined for either the electric and magnetic component of the radio wave) to the power attenuation in dB/m (what one will measure with a radio's RSSI), use

$$1 \text{ Neper/m} \leftrightarrow 8.686 \text{ dB/m}$$

### Characteristic Impedance

The characteristic impedance  $Z_0$  of a medium related the ratio of the electric- to magnetic fields of a radio wave in the medium. One can easily show that

$$\eta = \sqrt{\frac{j\omega\mu}{\sigma + j\omega\epsilon}}$$

In freshwater one would use the general (complex) expression for  $\epsilon$  and use  $\mu = \mu_0$ . The characteristic impedance of freshwater at 433 MHz,  $\epsilon_r = 80.17 - j1.824$ , and assuming  $\sigma = 0.05 \text{ S m}^{-1}$

$$\eta_{\text{water}} = 42.1 + j1.05 \Omega$$

The characteristic impedance of air ( $\sigma = 0$ )

$$\eta_{\text{air}} = \sqrt{\frac{j\omega\mu}{\sigma + j\omega\epsilon}} = \sqrt{\frac{\mu_0}{\epsilon_r \epsilon_0}} \cong \sqrt{\frac{\mu_0}{\epsilon_0}} = \frac{4\pi \times 10^{-7}}{8.85 \times 10^{-12}} = 377 \Omega$$

### Dielectrics, Conductors and Quasi Conductors

Consider the propagation constant

$$\gamma^2 = j\omega\mu\sigma - \omega^2\mu\epsilon$$

As noted above,  $\epsilon$  is in general complex, but for simplicity it is not explicitly shown here. One may define three conditions, shown below in Table 2.

Table 2 Conditions for defining the state a medium

Condition 1	$\omega\epsilon \gg \sigma$	$\frac{\sigma}{\omega\epsilon} < \frac{1}{100}$	Dielectric
Condition 2	$\omega\epsilon \ll \sigma$	$\frac{\sigma}{\omega\epsilon} > 100$	Conductor
Condition 3	$\omega\epsilon \approx \sigma$	$\frac{1}{100} < \frac{\sigma}{\omega\epsilon} < 100$	Quasi conductor

**Condition 1** corresponds to the case where the material behaves primarily as a dielectric. The material's finite conductivity and the possibly complex dielectric constant result in losses or attenuation of radio waves that propagate through the medium.

**Condition 2** corresponds to the case where the material behaves primarily as a conductor. Dielectric hysteresis losses may be present, but these are much smaller than conduction losses. Since  $\sigma \gg \omega\epsilon$ , the propagation constant becomes

$$\gamma^2 \approx j\omega\mu\sigma$$

$$\gamma = (1 + j)\sqrt{\frac{\omega\mu\sigma}{2}}$$

Recalling that  $\gamma = \alpha + j\beta$ , we get

$$\alpha = \sqrt{\frac{\omega\mu\sigma}{2}} \text{ Neper m}^{-1}, \quad \beta = \sqrt{\frac{\omega\mu\sigma}{2}} \text{ rad m}^{-1}$$

**Condition 3** corresponds to the case where conduction- and hysteresis losses are the same order of magnitude. The material is a quasi conductor/dielectric.

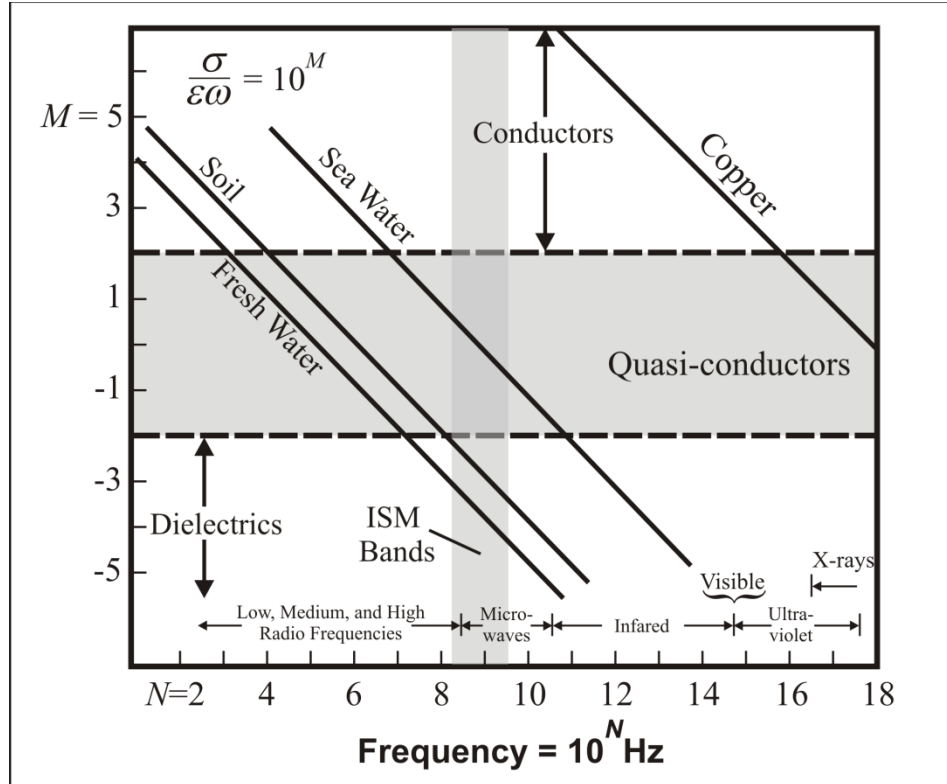


Figure 2 Ratio of  $\sigma/(\omega\epsilon)$  for some common media, including freshwater and soil, which are of interest in this thesis. The figure also shows the range of ISM and cellular communication frequencies. (from Krauss and Felisch 1999). An important conclusion from the figure is that one can consider freshwater and soil as lossy dielectrics at these frequencies.

Clearly, the frequency determines whether a material satisfies which condition. A material that behaves as a dielectric at one frequency may be a conductor at another frequency. An interesting way to present the interplay between  $\sigma$ ,  $\omega$  and  $\epsilon$  is to plot  $\sigma/(\omega\epsilon)$  in a log-log fashion (Krauss and Felisch 1999) as seen in Figure 2.

From the figures it is clear that one should consider water and soil as (albeit lossy) dielectrics at the frequencies of interest in this thesis. This has important implication for the work presented in this thesis. These are

1. One can treat radio propagation as electromagnetic propagation in a lossy dielectric. This means that one's intuition and knowledge about radio wave propagation in air largely

applies. For example, with simple conceptual models one can estimate refraction losses from a transmitter on a riverbank to a receiver underwater.

2. One can largely ignore direct conduction between transmitters and receivers. Thus, for example, from a radio wave propagation perspective, it is not crucial if the antennas are bare wire or insulated.
3. A straightforward mathematical model is adequate to describe the power of a radio wave as it propagates through the medium. Specifically

$$P_r \propto \frac{P_t e^{-2\alpha R}}{R^n}$$

Here,  $P_r$  and  $P_t$  are the received and transmitted powers,  $R$  is the separation between the transmitter and receiver,  $n$  is a path attenuation constant, and  $\alpha$  is the attenuation constant of for the medium.

Calculated values for both attenuation and intrinsic impedance for water at the ISM frequencies used in the thesis are given in Table 3. The values were calculated using the equations derived in this text assuming  $\sigma = 0.05 \text{ S m}^{-1}$ .

Table 3 Attenuation for some selected frequencies assuming  $\sigma = 0.05 \text{ S m}^{-1}$ .

Frequency	Attenuation (dB/m)	Intrinsic Impedance $\Omega$
315 MHz	13.6	$42.0 + j1.1$
433 MHz	17.6	$42.1 + j1.1$
900 MHz	45.7	$42.1 + j1.3$
2.4 GHz	266	$42.2 + j2.9$

### Refraction Losses

The air-water, air-soil interface reflect and refract radio waves and leads to loss of the radio signal at the receiver. In this section, we estimate the magnitude of these losses. First, consider a radio wave with normal incidence on a water surface. The intrinsic impedances of the water and air differ, so the interface will reflect some of the energy back. Figure 3 shows the situation as well as a transmission-line equivalent circuit. By using transmission-line concepts, one can calculate a voltage reflection coefficient

$$\Gamma = \frac{\eta_w - \eta_{air}}{\eta_w + \eta_{air}}$$

The corresponding power reflection coefficient is  $|\Gamma^2|$ . Above, we calculated the values for air and freshwater at 433 MHz as  $377 \Omega$  and  $42.1 + j1.05 \Omega$  respectively. Thus

$$\Gamma = \frac{377 - 42.1 - j1.05}{377 + 42.1 + j1.05} = 0.799 - j0.005$$

$$|\Gamma^2| = 0.63$$

This means 37% of the incident power crosses into the water, while 63% is reflected back. This represents a refraction loss of 4.5 dB.

Normal incidence represents the best-case scenario for transmitting radio wave from air to water. One would have this situation when the receiver is in a river directly below a transmitter mounted on a bridge. The worst case is when the transmitter is located on the bank of the river some distance back. In this instance, the radio waves travel nearly parallel with the water surface. In this case, the refraction-loss ratio, which is the ratio of the intrinsic impedance of the water and air is important

$$\frac{\eta_w}{\eta_{air}} = 0.1115 + j0.0028$$

Power attenuation is

$$\left| \frac{\eta_w}{\eta_{air}} \right|^2 = 0.012$$

This represents a loss of about 9.5 dB at the air/water interface.

At the frequencies we are interested in the relative permittivity  $\epsilon'_r$  is roughly 81, so the phase constant  $\beta$  is about 9 times that in air. The wavelength is given by  $\lambda = 2\pi/\beta$ , so the wavelength is approximately 1/9 that in air. The speed of light/radio waves in a medium is given by  $c = 1/\sqrt{\mu\epsilon'}$  and is 1/9 that in air. Finally the intrinsic impedance is 1/9 that in air.

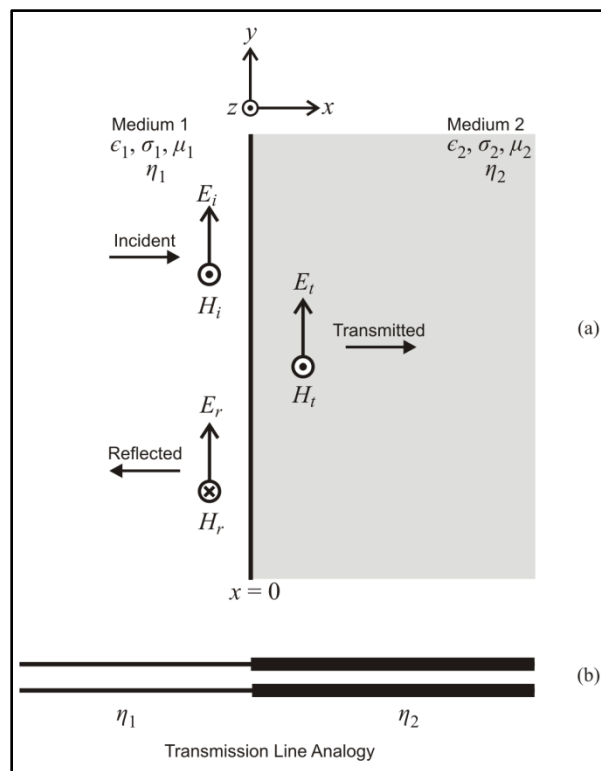


Figure 3 The top figure depicts a linearly-polarized plane radio wave traveling in the  $x$ -direction in a medium with permittivity, conductivity, and permeability of  $\epsilon_1, \sigma_1$ , and  $\mu_1$  respectively. The corresponding intrinsic impedance of the medium is  $\eta_1$ . At  $x = 0$  the wave encounters a medium with permittivity, conductivity, and permeability of  $\epsilon_2, \sigma_2$ , and  $\mu_2$  respectively. The corresponding intrinsic impedance of the second medium is  $\eta_2$ . If  $\eta_1 = \eta_2$  the wave will travel unperturbed, otherwise some of the wave will be reflected back. The bottom figure shows an analogous transmission line that one can use to calculate transmitted and reflected powers.

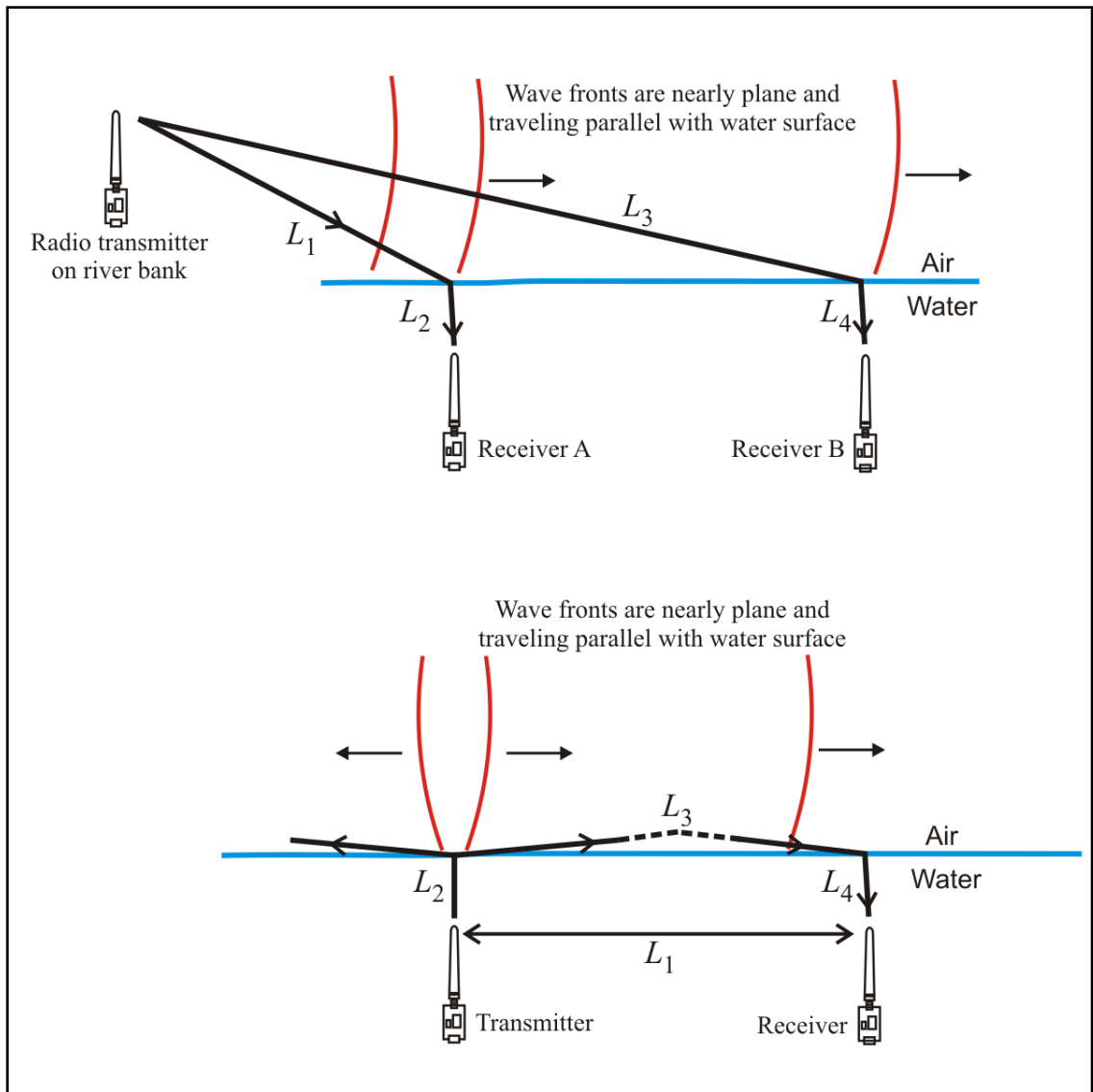


Figure 4 The top figure shows a transmitter on a river bank transmitting to two receivers in a river. The transmitter is far enough so that one can consider the wave fronts and essentially plane and traveling nearly parallel with the water surface. At the surface, some of the radio wave energy is refracted into the water and travels distances  $L_1$  and  $L_2$  to the receivers. The bottom figure shows two radios underwater communication with each other.

The upper figure in Figure 4 shown a transmitter situated on a river bank transmitting to a receiver on the bottom of the river. The radio wave power decays as the waves travel from the transmitter. The attenuation in air at the frequencies of interest in this thesis is essentially from

geometric weakening. At the water surface the waves is refracted and there is a refraction loss. Then the wave is attenuated as it travels through the water (paths  $L_2$  and  $L_4$ ) according to  $e^{-2\alpha R}/R^2$ .

Expressing all the quantities in logarithmic (i.e., dBm and dB) we have

$$P_r = P_t - \text{Loss in Air} - \text{Refraction Loss} - \text{Attenuation In Water}$$

where  $P_r$  and  $P_t$  are the transmitted and receiver power, respectively. Consider a 100 mW (= 20 dBm), link at 433 MHz. Assume 2 dB/m attenuation through the air (mostly from geometric weakening), a refraction loss of 10 dB, and an attenuation of 17.6 dB/m in water at 433 MHz.

$$P_r = 20 \text{ dBm} - 2L_1 - 10 - 17.6 L_2$$

If  $L_1 = 20$  m and  $L = 2.5$  m, then

$$P_r = 20 \text{ dBm} - (2 \times 20) - 10 - (17.6 \times 2.5) = -74 \text{ dBm}$$

Since most ISM modules have a sensitivity of up to -100 dBm, this is well within the sensitivity of the ISM radios considered in this thesis.

The second link illustrated in the Figure 4 is between two radios, both underwater. Ignoring reflections from the bottom and water-air interface, there are two paths, namely the underwater link  $L_1$  and then the  $L_2 \rightarrow L_3 \rightarrow L_4$  path. One can estimate the attenuation of the underwater link  $L_1$  from Table 3. The figure show that waves that reach the surface above the transmitter are heavily refracted. This is a direct result from the low speed ( $c/9$ ) of radio waves in water. The refracted waves travel nearly parallel with the water surface with little attenuation. However, there is some attenuation, resulting from “leaking” of the energy into the water. Some of this energy reaches the receiver at through the link  $L_4$ . The  $L_2 \rightarrow L_3 \rightarrow L_4$  may in fact exhibit less attenuation than the direct path. Denoting  $\alpha'$  as the attenuation of the wave as it travels across the water, then the  $L_2 \rightarrow L_3 \rightarrow L_4$  path will be advantageous when

$$\alpha_w L_2 + \alpha' L_3 + \alpha_w L_4 \leq \alpha_w L_1$$

$$\Rightarrow L_1 \leq L_2 + L_4 + \frac{\alpha'}{\alpha_w} L_3$$

Intuitively, when the radios are in shallow water,  $L_2 \rightarrow L_3 \rightarrow L_4$  path is advantages, since they transmit through less water than the  $L_1$  path. When  $\alpha_w \gg \alpha'$  as in the case with seawater, then this simplifies to

$$L_1 \leq L_2 + L_4$$

### Properties of Soil

Two of the possible applications I describe in this thesis, namely underground networks and soil moisture estimation, use ISM radios buried underground. Thus, it is appropriate to consider radio wave propagation in soil. Clearly, soil is a complex medium and its properties will affect in-situ measurements. For example, refraction of radio waves by the different soil layers is of major concern in, for example, GPR, but in this thesis, the distances small, and I ignore refraction. In this thesis, I use a simple model of soil, namely a matrix of dielectric material (sand, rock, some organic material) with voids. The relative dielectric constant of the soil matrix is around 2 to 8. However, the voids can hold water, and this dramatically changes the relative dielectric permittivity.

Consider a dry soil with a representative dielectric permittivity of  $\epsilon_r = 5 - j0.01$ . A representative value for water is  $\epsilon_r = 80 - j0.01$  (see Table 1). Thus, in mixture of soil and water, clearly the electrical permittivity dominates. The electrical conductivity of soil results from salts that form ions when in solution with water. In agricultural settings, fertilizer compounds elevate the soil conductivity. Soil conductivity ranges from  $0.02 \text{ S m}^{-1}$  to  $0.15 \text{ S m}^{-1}$  while freshwater's conductivity ranges from  $0.005 \text{ S m}^{-1}$  to  $0.05 \text{ S m}^{-1}$ . Thus soil and freshwater's conductivity is comparable and the dielectric permittivity of moist soil is dominated by water in the matrix voids. One can conclude that at the ISM frequencies, one can treat soil as a lossy dielectric. This is shown in Figure 2.

Further, one would expect a direct relationship between soil moisture and dielectric permittivity. One can define soil moisture content as *gravimetric water content* (% water by weight) or as *volumetric water content* (% water by volume). It is the number of polarized dipole molecules that determine the dielectric permittivity, so the volumetric water content is appropriate for electrical measurements of soil water content. Also, as Barkeshli (1985), points

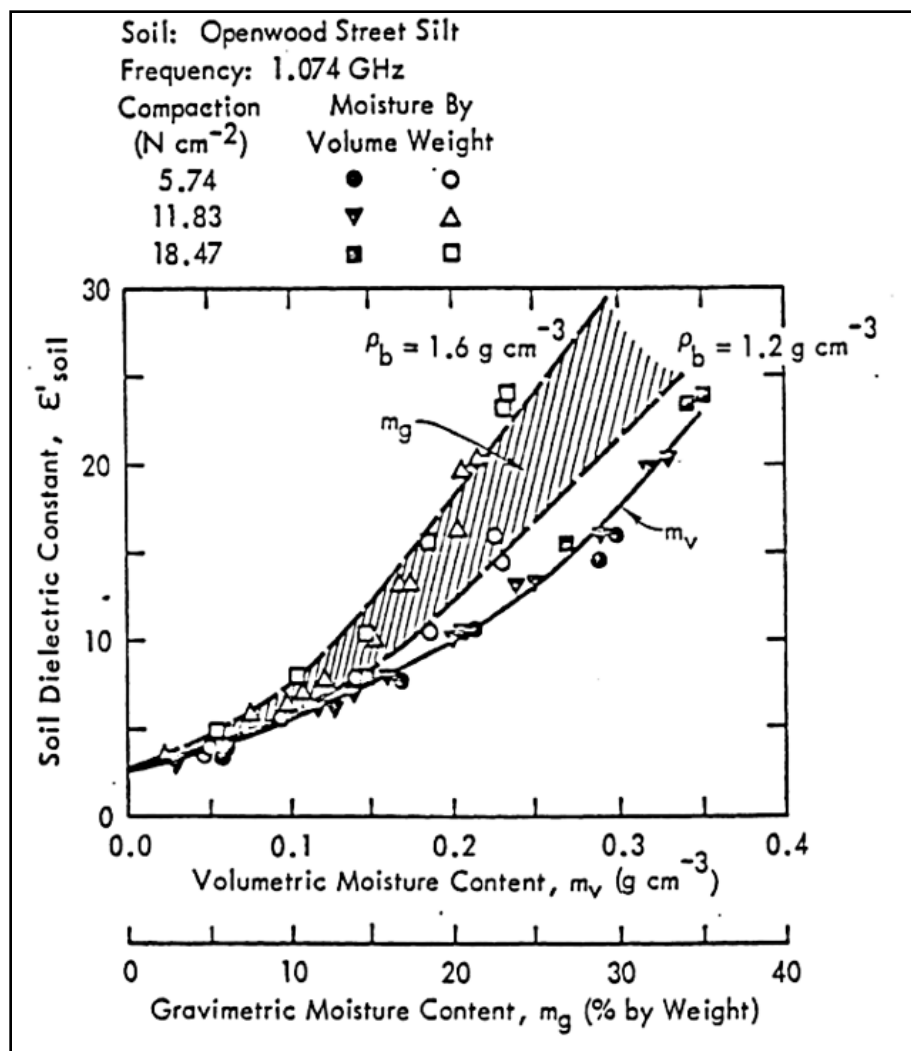


Figure 5 Typical soil dielectric constant at about 1.1 GHz as a function of gravimetric soil moisture ( $m_g$ ) and volumetric soil moisture ( $m_v$ ) (from Barkeshli, 1985). Note that the dielectric constant show much less scatter when plotted as a function of  $m_v$ .

out,  $\epsilon_r$  for soil show much less scatter when plotted as a function of volumetric water content rather than gravimetric water content as seen in Figure 5. Finally, note that the way I treat soil in this thesis corresponds to how other in-situ instruments treat soil. For example, capacitance and TDR soil moisture probes (see Chapter IV and V) take this approach. For proper measurements one should calibrate such instruments for the soil they are used in.

### RF Modules

The ISM radio bands were originally reserved internationally for the use of RF energy for industrial, scientific and medical purposes other than communication. Because communication devices using the ISM bands must tolerate any interference from ISM equipment, these bands are typically given over to uses intended for unlicensed operation, since unlicensed operation typically needs to be tolerant of interference from other devices anyway. Figure 6 shows the various radio modules and cell modems that were used throughout this thesis. These modules range in price from a couple US dollars to a few hundred US dollars. The higher end modules are equipped with a microcontroller that allows the modules to be re-configured for different modes of operation. This also allows for error checking, formation of data into packets, automatic retransmissions, low power modes and many more possibilities.

Table 4 summarizes the assigned ISM frequency bands and cellular communication bands in the U.S. However, for a variety of reasons, some ISM bands are more popular than others. Consequently, there are many small, inexpensive, 433.92-MHz radio modules available on the market. On the other hand, we could not find any standalone 5.800 GHz modules. These frequencies are heavily-used in Wi-Fi network applications, but radios are tightly-integrated into routers and so on. In this thesis, “ISM” is implied to be bands indicated with asterisks in the table. Still, the table shows that in principle, there are a wide range of frequencies available.

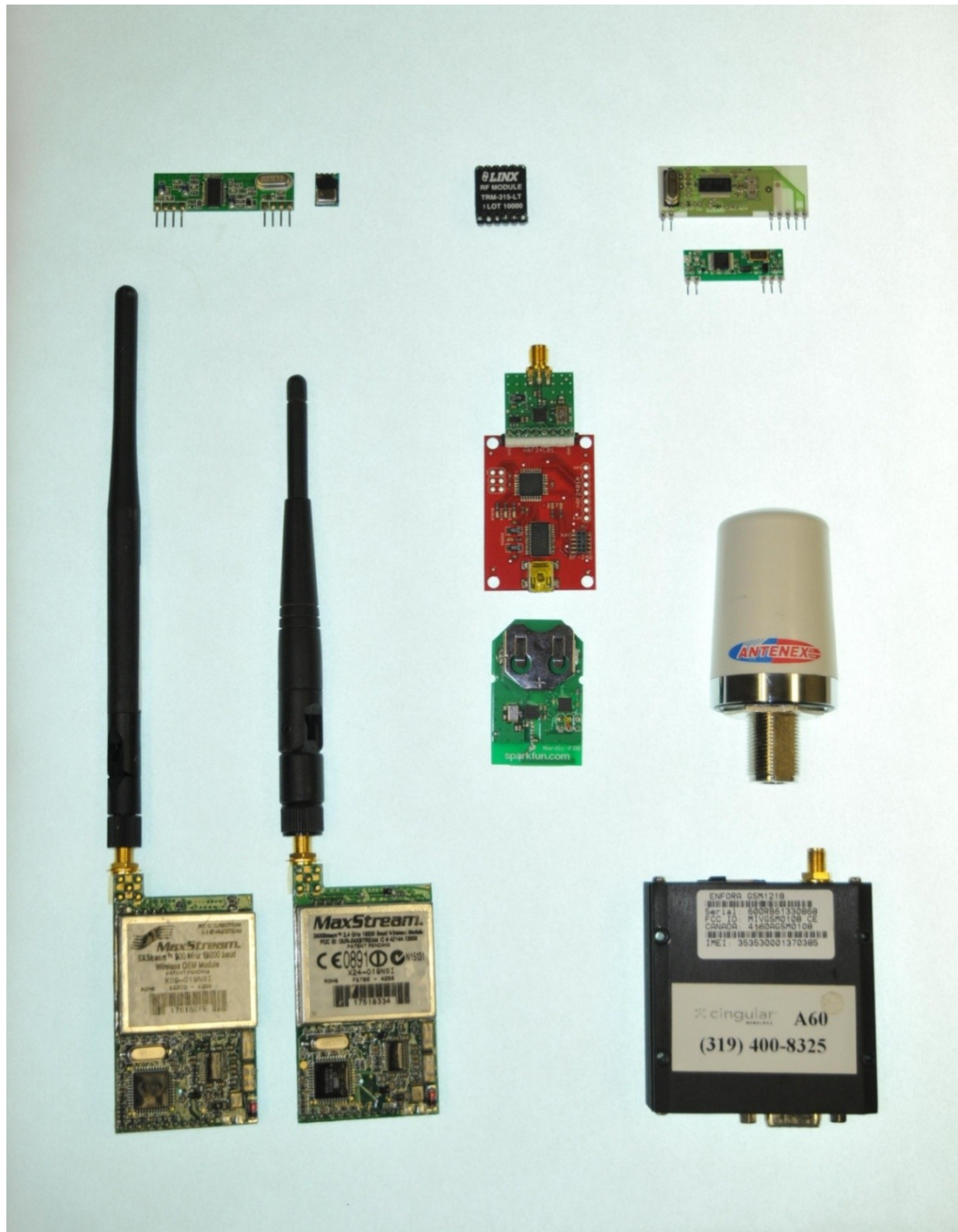


Figure 6 Upper Left: Radiotronics 433 MHz receiver and transmitter pair used in underwater communication experiments. Center: Linx 315 MHz transceiver module used for underwater communication. Upper Right: Alpha receiver and transmitter pair used in underwater phase measurements. Center: Sparkfun's development board and keyfob that use Nordic 2.4 GHz radios. Lower Left: MaxStream XStream at 900 MHz and 2.4 GHz modules with quarter wave length dipole antenna. Lower Right: Enfora cell modem and antenna that operates using Global System and Mobile Communication (GSM) network.

Table 4 Industrial Medical and Scientific (ISM) bands and GSM cellular bands.

Frequency Range (Hz)	Center Frequency (Hz)	Band
6.765-6.795 MHz	6.780 MHz	ISM
13.553 -13.567 MHz	13.560 MHz	ISM
26.957-27.283 MHz	27.120 MHz	ISM
40.66-40.70 MHz	40.68 MHz	ISM
433.05-434.79 MHz	433.92 MHz*	ISM
902-928 MHz	915 MHz*	ISM
2.400-2.500 GHz	2.450 GHz*	ISM
5.725-5.875 GHz	5.800 GHz	ISM
24-24.25 GHz	24.125 GHz	ISM
61-61.5 GHz	61.25 GHz	ISM
122-123 GHz	122.5 GHz	ISM
244-246 GHz	245 GHz	ISM
824-849 MHz uplink 869-894 MHz downlink	836.5 MHz uplink* 881.5 MHz downlink*	GSM-850 United States and Canada
1850-1910 MHz uplink 1930-1990 MHz downlink	1880 MHz uplink* 1960 MHz downlink*	GSM-1900 United States and Canada

Higher-end radios as well as the cell-modems used in the experiments described in this thesis are equipped with a microcontroller that is between the radio and the data source. The controller forms data packets and controls modulation schemes, channels, hopping sequence (see RF Modulation below), and radio power levels. Assuming the radio has been properly configured, the controller is transparent and passes data on to the radio, and data the radio received on to the rest of the system. The so-called AT-command mechanism allows one to configure the radio over the same channel, and it works as follows. When the microcontroller sees a certain sequence of characters separated with a specific delay time, it switches from

transparent, pass-through mode to command mode. Once in command mode, a user can send configuration command to the radio to set, for example, the transmit power level or poll RSSI. When ready to transmit, one sends the proper command, and the controller switches back to pass-through mode. Subsequent characters are transmitted as data. The sequence is shown below:

Data  
 Data  
**Delay**  
 +++  
**Delay**  
 ATRS  
 ATCN  
 Data  
 Data

The delay, three-character sequence “+++”, followed by another delay/silence is the signal to the radio’s controller to switch from pass-thru mode, to command mode. The “ATRS” is an instruction to the controller to provide the RSSI value from the previous reception, and the “ATCN” is an instruction to the controller to switch back to pass-thru mode.

### RF Link Background

#### RF Modulation

The different RF modules referred to in this document use several standard forms for data transmission. The modules range from very simple modules to more sophisticated modules. I refer to simple modules as modules that transmit the data without extra information. The more sophisticated modules may incorporate information to packet network routing, error checking, wake-up commands, acknowledgements and retransmission. With this extra level to sophistication comes add cost in the overall price of the modules. One advantage of the simple

modules is that they have a fixed overhead in data transmission, while the more sophisticated modules may have a variable latency. For many applications variable latency has no effect in the desired performance of the module. The modules used operate using various RF modulation techniques.

On-off keying (OOK) is a simple form of amplitude-shift keying (ASK), where data is encoded by the presence or absence of the carrier signal. The presence of the carrier for a specific timeframe represents one state while the absence of the carrier for a specific time frame represents the other state. One can view OOK as amplitude modulation (AM), where only two levels are allowed:  $0 \rightarrow$  "OFF" and  $1 \rightarrow$  "ON". This basic form of communication is used in many cost effective RF modules and can be purchased for only a couple of US dollars. The Linx and Radiotronix modules referenced in this document use this form of modulation. These modules ranged from a few dollars each up to \$20 USD. Several of the simple RF modules used in this thesis employed frequency modulation (FM) where the data shifts the carrier frequency. This is analogous to OOK where two different frequencies represent the two possible levels: frequency **A**  $\rightarrow$  "OFF" and frequency **B**  $\rightarrow$  "ON".

Some ISM radios use spread spectrum (Proakis and Salehi, 2002) communication links. As the name implies, in spread spectrum communication, the channel bandwidth is much larger than the bandwidth of the underlying data. This may be somewhat counterintuitive, but such an approach has potential advantages. Spread Spectrum transmissions utilize the bandwidth more efficiently since transmissions can share a frequency band with many types of conventional transmissions with minimal interference. There are two broad classes of spread spectrum, namely frequency hopping spread spectrum, or FHSS, and Code Division Multiple Access (CDMA) spread spectrum. FHSS is the easiest to explain, and the most relevant to this thesis, because some the radios I used, can be programmed to employ FHSS. Briefly, in FHSS the transmitter dwells for some time at one carrier frequency and transmits data. The transmitter then switches (i.e. hops) to a different frequency, dwells there for some time, and transmits some additional data. An obvious application is that unless one knows the hopping sequence and the

dwelt time is short, the transmission will be scrambled or even invisible to a receiver listening on a single frequency. Thus, spread spectrum communication is often used to ensure secure communication. However, frequency-hopping has other advantages as well. One is that it tends to provide more noise immunity than fixed-channel communication. For example, if there is a noise source that pollutes a narrow band of the frequency spectrum, this may severely impact a fixed-channel radio link. However, with a FHSS system that dwells in that channel only briefly, the effect is much less. FHSS communication is also less sensitive to multipath effects. The MaxStream radios used in many of these validation experiments employ FHSS.

Whenever a change in medium is encountered, the signal is absorbed, attenuated, refracted, or reflected. Refraction and reflection cause the signals to change direction of propagation. This change in path directions often results in a convergence of the direct path signal with one or more of the reflected signals. When the receiving antenna is the point of convergence for these multi-path signals, the consequences are generally not favorable.

Multipath is a propagation phenomenon that results in RF signals reaching the receiver antenna by two or more paths, this is shown in the top panel of Figure 7. The transmitter is at a fixed frequency in this example. Multipath interference can be created by atmospheric dust, ionosphere reflection and refraction, and reflection from water bodies and terrestrial objects such as mountains and buildings. The effect of multipath can be constructive or destructive interference, and phase shifting of the signal. The top figure shows a transmitter and receiver at heights  $A$  and  $B$  above a partially-reflecting plane, separated by a distance  $R$ . The path lengths  $d_1$  and  $d_2$  are such that the attenuation is of the same order. However, phase differences can lead to constructive and destructive interference. The middle and bottom figures are examples of such multipath effects at 900 MHz ( $\lambda = 33.3$  cm) and 350 MHz ( $\lambda = 85.7$  cm) respectively. By altering the transmitting frequency as in FHSS the effects of multipath can be lessened. A null in signal strength created from multipath effects at a specific distance at one fixed frequency, may not be present at that same distance at slightly shifted frequency.

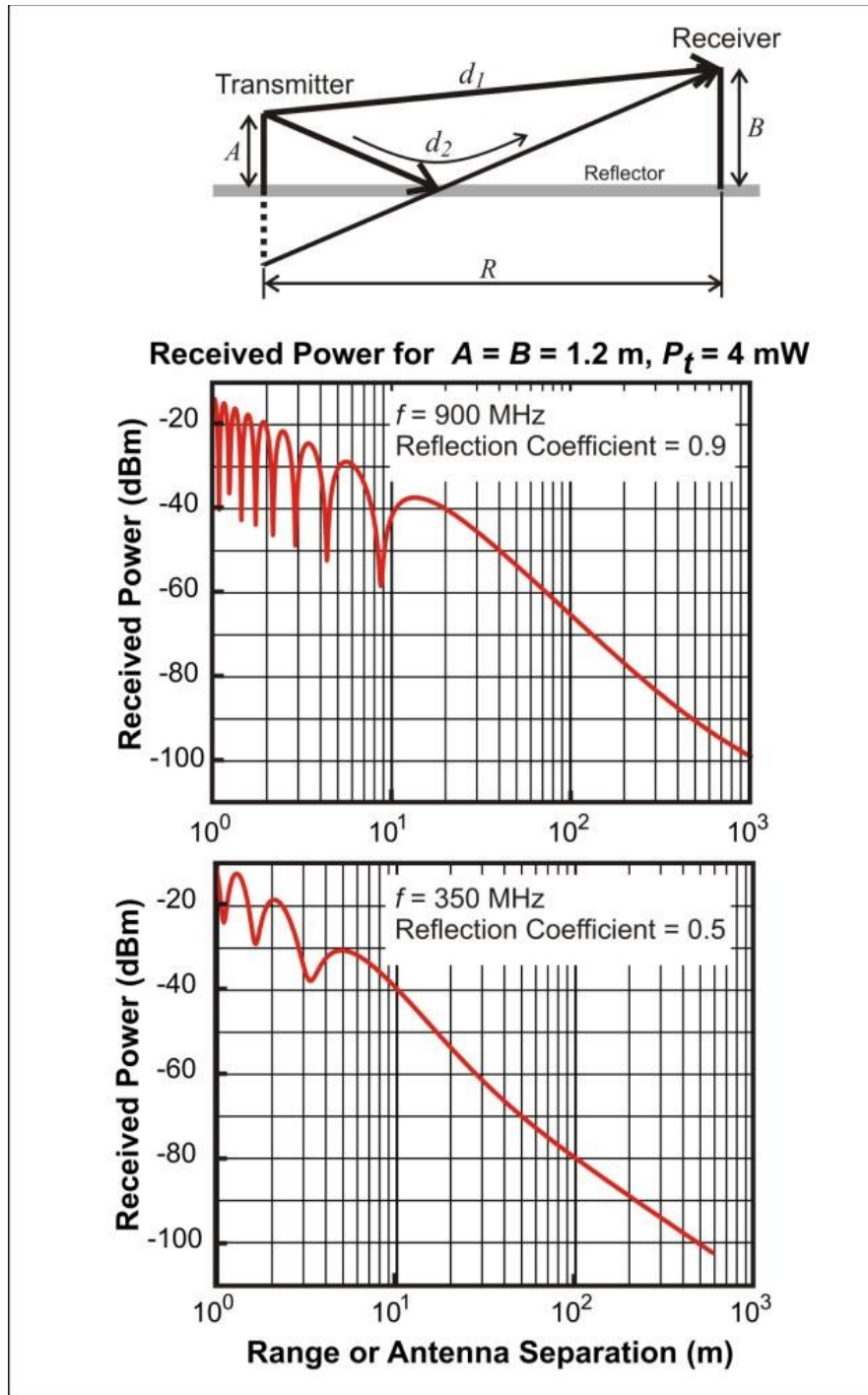


Figure 7 Two-path multipath. The top figure shows a transmitter and receiver at heights  $A$  and  $B$  above a partially-reflecting plane, separated by a distance  $R$ . The path lengths  $d_1$  and  $d_2$  are such that the attenuation is of the same order. However, phase differences can lead to constructive and destructive interference. The middle and bottom figures are examples of such multipath effects.

CDMA is a completely different approach to spread spectrum communications to allow multiple transmitters to send information over a single communication channel. Transmitters are assigned a code to allow multiple users to be multiplexed over the same physical channel. CDMA is a form of spread spectrum since the modulated coded signal has a much higher data bandwidth than the data being communicated. CDMA is analogous to a room full of people talking in different languages while the communication may be heard by everyone in the room, only the people who speak the same language understand a specific conversation. In a similar manner in CDMA only the people with the same code can decode the transmission and all other communication is perceived as background noise. However, it achieves the same goal as FHSS, namely spread the information over a wide bandwidth, and has the same advantages: good channel utilization, security, and good multipath properties. CDMA was developed by Qualcomm and is widely used for cellular communications. However, the cell modems I used in this thesis (see Chapter V) are part of the global system for mobile communication (GSM) network and do not use CDMA.

Global system for mobile communication (GSM) is the most popular standard for mobile telephony systems in the world. Currently it is used by over 1.5 billion people around the world. In 1997 the standard added packet data capabilities by means of General Packet Radio Service (GPRS). The modulation used in GSM is Gaussian minimum-shift keying (GMSK), a kind of continuous frequency shift keying. The signal to be modulated onto the carrier is first smoothed by a Gaussian low-pass filter prior to being fed to a frequency modulator, which reduces the interference to neighboring channels.

### RSSI Measurements

RSSI is typically used as a diagnostic to look at link quality for most RF communication. As shown earlier, there has been significant research modeling the effect of RF waves in cities and through vegetation to name but a few areas. Time scale of the processes we are interested in is on the order of minutes to hours to days. This is different from “fading” in communication

systems. For antennas at fix distances we will be observing changes in RSSI to infer changes in the medium.

There are numerous schemes for measuring RSSI of different RF modules. RSSI measurement for modules used in experiments described later in this document consists of three techniques. Sending AT commands to poll the module for the RSSI of the last received packet. AT commands are used in controlling modules to do their specified functions. Some of the modules used output a voltage that is proportional to the incoming packet signal strength. Finally the MaxStream's XStream radio modules offers a pulse width modulated (PWM) signal that is proportional to the incoming packet signal strength. This allows the user to measure RSSI while receiving communication. It is also possible to poll the XStream modules for the RSSI of the last received packet by sending the module the appropriate AT command. To do this the module needs to be switched from communication mode to command mode by sending a series of three plus signs on the data input line. Once in command mode the request can be sent to poll the RSSI of the last packet the module received. Once in command mode the module can no longer receive incoming packets and all RF communication to the module is lost. This limits the data throughput of the RF link and increases the time need to average over several transmissions if a more stable RSSI measurement is desired. The XStream family of modules uses FHSS with seven hopping sequences sharing 25 frequencies. While the hopping of frequencies aids in link communication reliability it produces unstable RSSI measurements between consecutive packets. Each frequency in the hopping sequence may see different effects in multipath and therefore have different signal strength. Each packet may be transmitted using several different hopping frequencies with variation in signal strength.

There are several possibilities for stabilizing RSSI measurements of the XStream modules. By increasing the packet size it is possible to incorporate more frequency hops in a single transmission. A stable RSSI measurement can be calculated by taking the average of several packets that encompasses all the possible frequency hopping sequences multiple times.

RSSI measurements in inexpensive radios are typically performed as follows. Circuitry in the radio extracts the carrier, and generates a current that is proportional to its amplitude. This current is passed through a semiconductor diode, for which

$$I_D = I_s e^{V_D/V_T}$$

Here  $I_D$  is the diode current and  $V_D$  is the diode voltage. In these equations,  $V_T$  is the thermal voltage (about 26 mV at 25°C) and  $I_s$  is a constant. Rewriting

$$V_D = V_T \ln\left(\frac{I_D}{I_s}\right)$$

This performs the basic carrier-amplitude  $\rightarrow$  logarithm (needed for dB) conversion. In the case of low-end, very inexpensive radios, an analog amplifier then scales the voltage to correspond to the RSSI measured in dBm. In the case of radios that have microcontrollers, the microcontrollers' built-in analog-to-digital converters are used to digitize the RSSI. These digitizers are typically 8-bit, but with only 6 bits are used. Thus, the RSSI is quantized to  $2^6 = 64$  levels. Consider a radio that is designed to operate over a range of -40 dBm to -110 dBm and assume the 70 dB range is quantized as described above. This results in a quantization step of about 1.1 dB. An examination of Maxstream's XStream modules reveals quantization steps of 1.46 dB when RSSI is polled in command mode and 1.75 dB when using the PWM output.

A experiment was devised to explore how many packets were need to obtain a stable RSSI measurement using the PWM output of the XStream radio modules operating at 2.4 GHz. Since the XStream modules are sophisticated modules, the size of the payload is a small portion of the overall total transmission. Packets consist of a RF initializer, header, payload and cyclical redundancy check (CRC) to verify data integrity. For this experiment the payload size was selected to be eight bytes. The XStream modules can be configured to handle payloads up to 100 bytes. The PWM output offers a resolution of RSSI measurements to 1.75 dBm. The RSSI was averaged for a predefined number of packets sent through a link in an industrial setting.

Three motes were used to investigate RSSI stabilization. Motes are nodes in wireless sensor networks that are capable of performing some processing, gathering sensory information and communicating with other connected notes in the network. The main components of a mote consist of a microcontroller, transceiver, external memory, power source and one or more sensors. While the motes described throughout this thesis have the capabilities to attach sensors, the mote itself is now considered the sensor.

The three motes consisted of a base station that controls and records all data flow, mote **A** that transmits the specified number of packets and mote **B** that measures the RSSI of transmissions from mote **A**. The base station begins by sending a request to mote **A** to transmit a specified number of packets. Mote **A** transmits the specified number of packets to mote **B**. Once all of packets have been transmitted by **A** the base station sends a request for **B** to send the measured average RSSI from all transmission received from mote **A**. The base station is connected through a serial link to a PC running Secure CRT. The data is then recorded in a text file using Secure CRT's capture input function. The number of packets sent by mote **A** can be varied by the base station from three packets up to 950 packets. It takes approximately 15 minutes for the base station to step through and record all possible number of packet transmissions. Once the number of transmissions reached 950 the process was repeated starting at three transmissions again. The system collected data in a light industrial setting for 24 hours until 100 samples were made for each transmission size using XStream modules operating at 2.4 GHz. The data collection process was repeated using XStream modules operating at 900 MHz with the antennas lowered into 2.54 cm PVC tubes driven into the ground to a depth of 70 cm and separation distance of 2 m. Soil moisture content was estimated to be near 30% during the experiment and the system collected 20 samples for each packet size. In Figure 8, the horizontal axis represents the number of RSSI values sampled, and the vertical axis represents the standard deviation of the RSSI values from the mean, calculated as follows

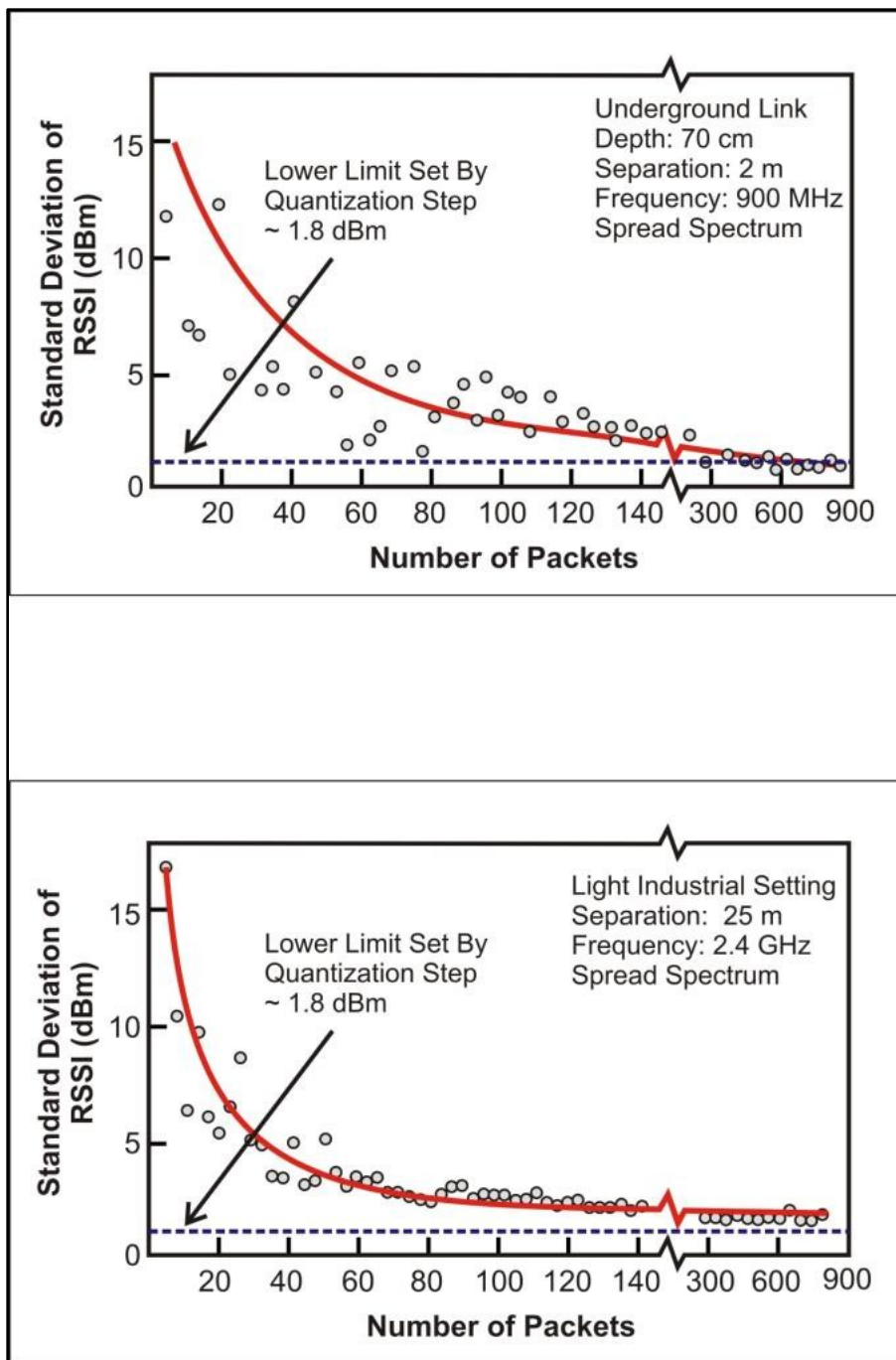


Figure 8 These figures show the how the variance of RSSI values decrease with a number of packets averages. Two cases are shown: one for a 900 MHz underground link, and 2.4-GHz link in a light industrial setting. The figures also show the lower bound, determined by the radio's quantization step size. From the figures it follow that averaging more than about 300 packets (1<sup>st</sup> link) and 80 packets (2<sup>nd</sup> link) does not decrease the variance. However, it does require more power.

$$\sigma = \sqrt{\frac{1}{N} \sum_{i=1}^N (x_i - \mu)^2}$$

where  $x_i$  is the measured RSSI values,  $\mu$  is the mean of the samples, and  $N$  is the number of samples. Figure 8 top shows the data collected in the underground link and in the industrial setting bottom. The distances between antennas were fixed in both experiments. The quantization step size for XStream modules is also indicated in Figure 8. From the plot it is clear that there are diminishing returns in averaging the RSSI for more than 300 packets. There are significant savings in power by transmitting as few of packets as possible to make an accurate RSSI measurement.

In the various experiments I perform in this thesis, there is a tradeoff between the number of samples and the variance of the resulting data. For example, Figure 8 suggests that if one uses 300 averages, one would be close to the limit determined by the radios' quantization step. However, RSSI measurements consume power, and take time. For example the XStream modules operate at 5 VDC and consume 140 mA when transmitting and 50 mA in receive mode. Typically in networks with sparse communication most of the power consumption can be attributed to active listening (i.e. the power consumed listening for incoming transmissions). XStream modules have a power saving mode that consumes only 26 uA when powered down or in sleep mode. The radio can then be programmed to periodically wake and briefly listen for communication before reentering power down mode. A user specified time can be pre-programmed into the module for keeping the module active once communication has been detected and before entering sleep mode again. By implementing sleep modes the total power consumption will be dominated by the number of transmissions made by the module. Thus, in my experiments I average RSSI measurements over 120 packets in air and 200 packets for underground transmission to increase battery life.

## Echo- and Streaming Server

A reoccurring theme in the text will be to use radios modules to receive data and then send it back to the original sender or forward the data with no interference of signals. There are two techniques used to accomplish these tasks. Only RF modules are need to accomplish both task with no need for additional electronics. An *echo server* is an arrangement where a transceiver feeds its output directly back to its transmitter. Thus, everything received, is transmitted/echoed verbatim to the originator. Echo servers are very useful for performing range tests, and measuring latencies, and so on. Figure 9 depicts an echo server created by using a loop back connector which ties the data out line to the data in line of the RF module.

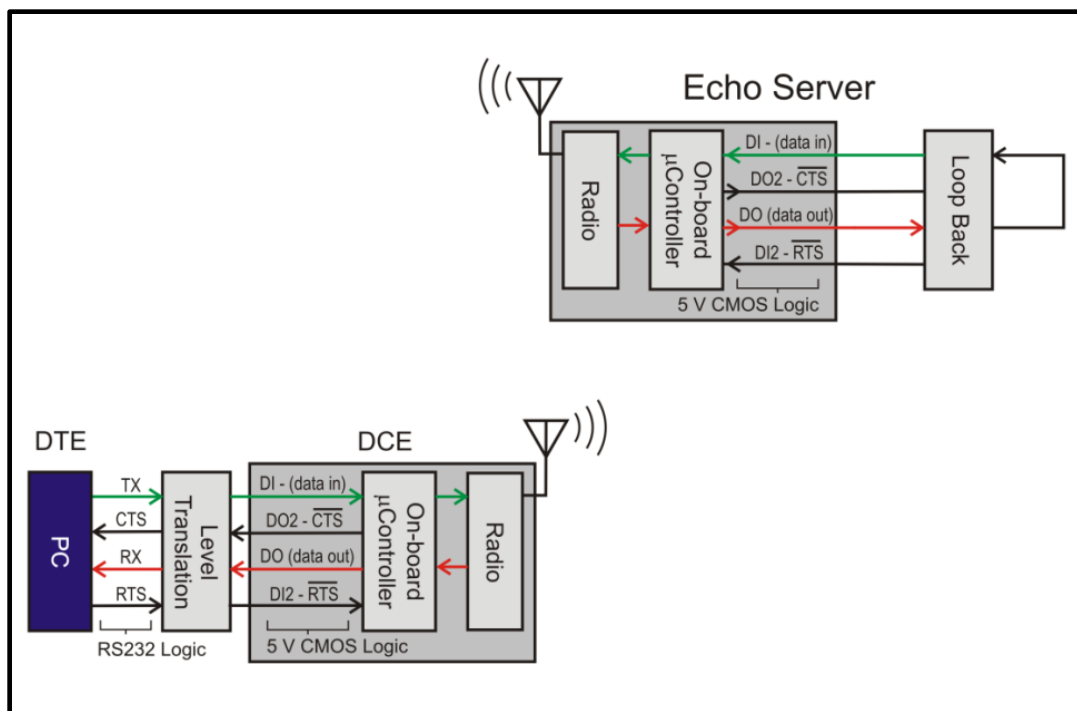


Figure 9 Echo servers are used in several experiments throughout this thesis primarily for range testing. The echo server is exactly what the name implies, all data received from the data communication equipment is sent back. The data out of the RF module is tied directly back to the data in of the module. All communications that are received and forwarded to the data out line are feed back into the data in line and transmitted.

The computer which here is considered data terminal equipment (DTE) is connected to the RF module which in this case is considered data communication equipment (DCE). All transmissions sent by the DTE are forwarded back by the echo server. DTE is an end device that converts user information in signals or reconverts received signals. A DTE communicates with the DCE. Usually the DTE is a computer and the DCE is a modem or another carrier-owned device.

In the case of interconnecting devices of the same type DTE-DTE or DCE-DCE require the use of crossover cables or Null modems. *Streaming servers* consists of a pair of RF modules operating on non-interfering channels. An example of non-interfering channels could consist of RF modules operating at different frequencies or at the same frequency by at different non-interfering hopping sequences. In a streaming server a signal transmitted on frequency  $A$  is received by a remote module operating on frequency  $A$ , the data out line of module

A null modem can be used to create a streaming server. The null modem connects the data out of each module to the data in of the other module. Thus everything received by one module is forwarded by the other module. The null module also connects the request to send (RTS) of both modems to the clear to send (CTS) lines of the other modem. Figure 10 depicts two RF modules connected by a Null modem to create a streaming server. The CTS and RTS lines are used for flow control on the modules.

### Fresh Water Conductivity Measurements

As previously stated, there is a wealth of knowledge available about properties of seawater but little interest has been shown in the area of freshwater in streams and rivers. The conductivity of water can have a significant impact on underwater radio communication, making it very important to have some way of measuring it accurately. A simple approach is to use two parallel plates separated by a fixed distance, and measure the resistance between them.

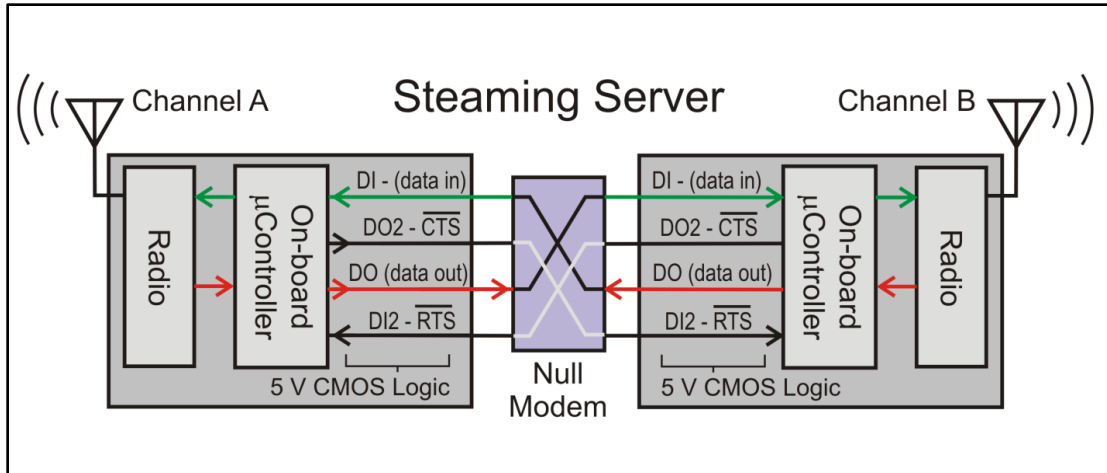


Figure 10 The streaming server consists of two RF modules operating on different channels. The data in lines of both modules are connected to the data out of the opposite module. For example all data received by the module operating on channel A is transmitted out by the module operating on channel B. The channels must be selected as not to be interfering with each other.

Conductivity is the measure of a material's ability to conduct current and is the inverse of resistivity. This relationship is shown in,

$$\sigma = \frac{1}{\rho}$$

where  $\sigma$  is conductivity and  $\rho$  is resistivity.

Resistance is a measure of an object's opposition to the passage of a steady current. The resistance of a conductor of uniform cross section  $R$  will be proportional to the resistivity of the material  $\rho$  and the length of the conductor  $L$ , and inversely proportional to the cross-sectional area  $A$ .

$$R = \rho \frac{L}{A}$$

The resistance between the two plates can be measured by attaching a signal generator with known output resistance and voltage in series with the plates. In order for this approach to work, the charge across the plates must be discharged periodically,

which requires the voltage source to be AC. By measuring the voltage drop across the plates and manipulating the simple voltage divider, the resistance between the two plates,  $R_x$ , can be calculated.

$$R_x = \frac{V_x}{V_s - V_x} R_s$$

Both the source's output resistance  $R_s$  and output voltage  $V_s$  are known and the voltage across the two plates  $V_x$  can be measured using an oscilloscope.

The two plates used for the conductivity meter are made of galvanized steel which is rust resistant for prolonged submersion in water. Each plate is 25 cm by 25 cm, and therefore has a  $625 \text{ cm}^2$  surface area. These dimensions are shown below in Figure 11 left. The plates are mounted on a 28 cm by 28 cm piece of plastic, which are separated by a plastic standoff in each corner. The final product is shown in Figure 11, brass screws in the corners of the metal plates attach it to the plastic sheeting; these screws also allow wires to easily attach to the plates.



Figure 11 Left: Final dimensions of the instrument used for measuring freshwater conductivity. Two  $625 \text{ cm}^2$  galvanized steel plates were mounted on plastic sheeting with a separation distance of 6 cm. Right: Final sensor used for measuring the conductivity of river water. The two plates used for the conductivity meter are made of galvanized steel, which not only resist rust, but are also submersible in water. Each plate is 10 inches by 10 inches, and therefore has a 100 square inch surface area. Brass screws hold the plates to the 11 inch by 11 inch plastic sheeting. Plastic thread all was used to hold the plates at a separation distance of 6 cm.

To simplify measurements and to make the system more portable, a signal generator was designed which outputs an 8 V peak-to-peak square wave at three frequencies 100 Hz, 1 kHz, or 10 kHz. These three frequencies allowed us to see if there was a variation in freshwater conductivity at low frequencies. The output signal is used to measure the voltage drop across the plates, which is then used to calculate the resistance and conductivity. A rotary switch is used to select between the 100 Hz, 1 kHz, and 10 kHz square waves. The signal generator has an output resistance of about 300 Ohms, which was chosen to provide a suitable range for conductivity measurements. The overall system draws about 14 mA when running at any of three frequencies and is shown in Figure 12 Left. Figure 12 right shows the conductivity sensor with two 15 foot wires attached being deployed in the Iowa River in Iowa City. Conductivity measurements were made twice a day at 8 am and 3 pm local time over a period starting on May 21, 2010 and ending July 31, 2010 and shown in Figure 13. The collected data show a decrease in conductivity following rain events with the influx of distilled water. The conductivity increased as the rain water flowed down stream. Conductivity of Iowa River water during that period varied from 0.03 to 0.063 S/m. Looking back at Figure 2 this measured range places the conductivity for Iowa River water in the dielectric region for ISM frequency RF modules.



Figure 12 Left: Electronics and enclosure used for making conductivity measurements in freshwater. Right: Nick Sitter deploying the conductivity sensor into the Iowa River by the Stanley Hydraulic Laboratory in Iowa City.

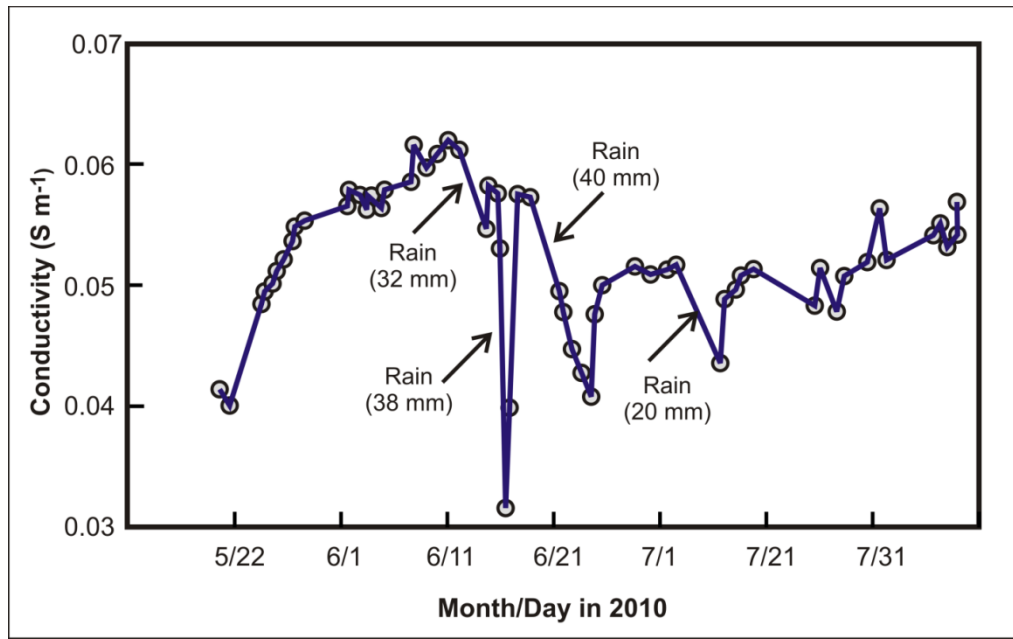


Figure 13 Data collected for Iowa River conductivity from May 21, 2010 until July 31, 2010. Measurements were made twice a day at 8 am and 3 pm local time. A decrease in conductivity is observed after rain events with the influx of distilled water followed increases in conductivity as this water flows downstream. Conductivity during this period ranged from 0.03 to 0.063 S/m.

### Summary

For the preceding material it is clear that RF modules operating in the ISM band are capable of more than transmission through the air. I will show two example of transmission through unconventional media. This thesis then continues to look at the possibility of using RF modules for more than a form of communication but as inexpensive RF generators at unlicensed frequencies. Three applications will be looked at in subsequent sections soil moisture, vegetation water content and leaf wetness measurement. A recurring theme will be that many of these traditional techniques for measuring the quantity of interest is in the deployment of point measurement sensors. Such point measurements may be enhanced when made in conjunction with distributed measurements over the entire RF link.

## CHAPTER III

### UNDERWATER NETWORKS

As I mentioned in the *Introduction* and other places in the manuscript, most people assume that one cannot operate radios underwater (Anguita et al. 2009, Meihong et al. 2009, Heidemann et al. 2006), but this view is not entirely true. Yes, water attenuates radio waves, so long-range underwater radio communication is not feasible, except at very low frequencies, using long antennas, and high power (Moore 1967). On the other hand, modern radio receivers are sensitive enough so that one can establish communication underwater over several feet to perhaps several meters in freshwater. This view is supported by calculations and measurements documented previously in this manuscript, and by others (Lindsay et al. 1977, Zang et al. 2004). Rather than a curiosity, one can use this fact to establish reliable and useful underwater wireless networks. A WSN consist of multiple nodes that make short-range transmissions and cooperate in data delivery. In the rest of this chapter, I describe one novel underwater wireless application, namely, an underwater WSN that uses mussels as sensors. My work in this on-going research effort at The University of Iowa is on providing the physical communication link between nodes in the network. I also describe preliminary investigations into effective underwater antennas. Other forms of underwater communication such as ultrasonic and IR also offers opportunities for underwater communication. One can go to any number of electronics suppliers and get low power RF modules, while it is difficult if not impossible to get comparably sized ultrasonic or IF module.

#### Application: Mussels as Biological Sensors

Bio-fouling is a difficult problem to solve when working in underwater environments. Figure 14 shows an expensive water-quality sensor that was placed in an underwater environment to collect data. The effects of bio-fouling can be slowed or perhaps even eliminated by using biological sensors that are inherently clean. Researchers are working on using

freshwater mussels as biological sensors. We are designing a system using freshwater mussels as biological sensors Hunt et al. 2010 and Sitter et al. 2009.



Figure 14 Example of bio-fouling of a sensor left in an underwater environment to collect data on water conditions.

The goal is to instrument mussels with Hall-effect sensors and magnets. The Hall-effect is the generation of a voltage across a conductor in a perpendicular magnetic field. Figure 15 left illustrates the operation and placement of a Hall-effect sensor on the mussel. The sensors detect the rhythmic opening and closing of the mussels called the mussel gape (Figure 15 right). As the mussel opens to feed the gape increases and the distance between the magnet and Hall-effect sensor increases. As distance increases magnetic field intensity seen at the Hall-effect sensor decreases.

Changes in the mussel gape can indicate environmental stress, changes in mussels' food supply, or may serve as a proxy for turbidity. Additionally, mussels collectively have the potential to significantly affect dissolved oxygen content and nitrate levels in river reaches. There are several examples of tethered mussel biological sensors (Bril et al. 2009, De Zwart et al. 1995, Kelly 1994, Morgan 1981 et al. 1981).

The goal of the researchers at The University of Iowa is to instrument mussels and place them back in their natural environment, but untethered. We plan to attach gape sensors, microcontrollers, and radios to mussels and place them back in their natural environment, see Figure 16. Small, inexpensive radios operating in the ISM bands will provide the physical link of an underwater WSN. Despite the attenuation radio waves experience in water, the low cost of these radios should allow us to deploy enough to set up a reliable communications network. Gape data collected by each mussel will route through the network of radio instrumented mussels to a central base station. The data collected from one, or perhaps several base stations, will be routed back to The University of Iowa through cellular transmission and ingested into the database. Additionally, there may be opportunities for power harvesting using piezoelectricity power harvesters. Piezoelectricity is a charge which accumulates in certain solid materials in response to applied mechanical strain. The word piezoelectricity means electricity resulting from pressure. It may be possible to harvest energy using piezoelectric generated by the flow of water in the stream bed the mussels are located in.

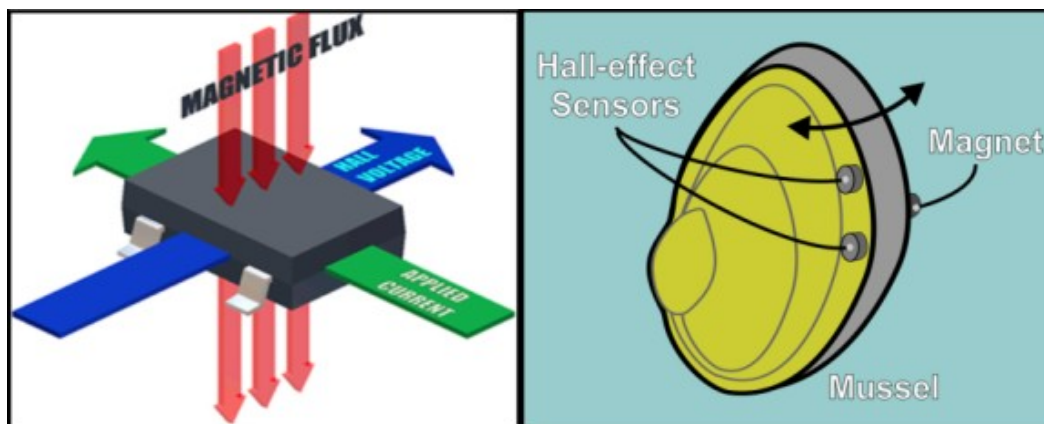


Figure 15 The left panel depicts the Hall-effect, which is the generation of a voltage across a conductor in a perpendicular magnetic field. There are Hall-effect ICs on the market that integrates a Hall sensor with an amplifier and signal conditioning. The right panel shows how we attach a Hall-effect sensor and a small magnet to monitor mussel gape.

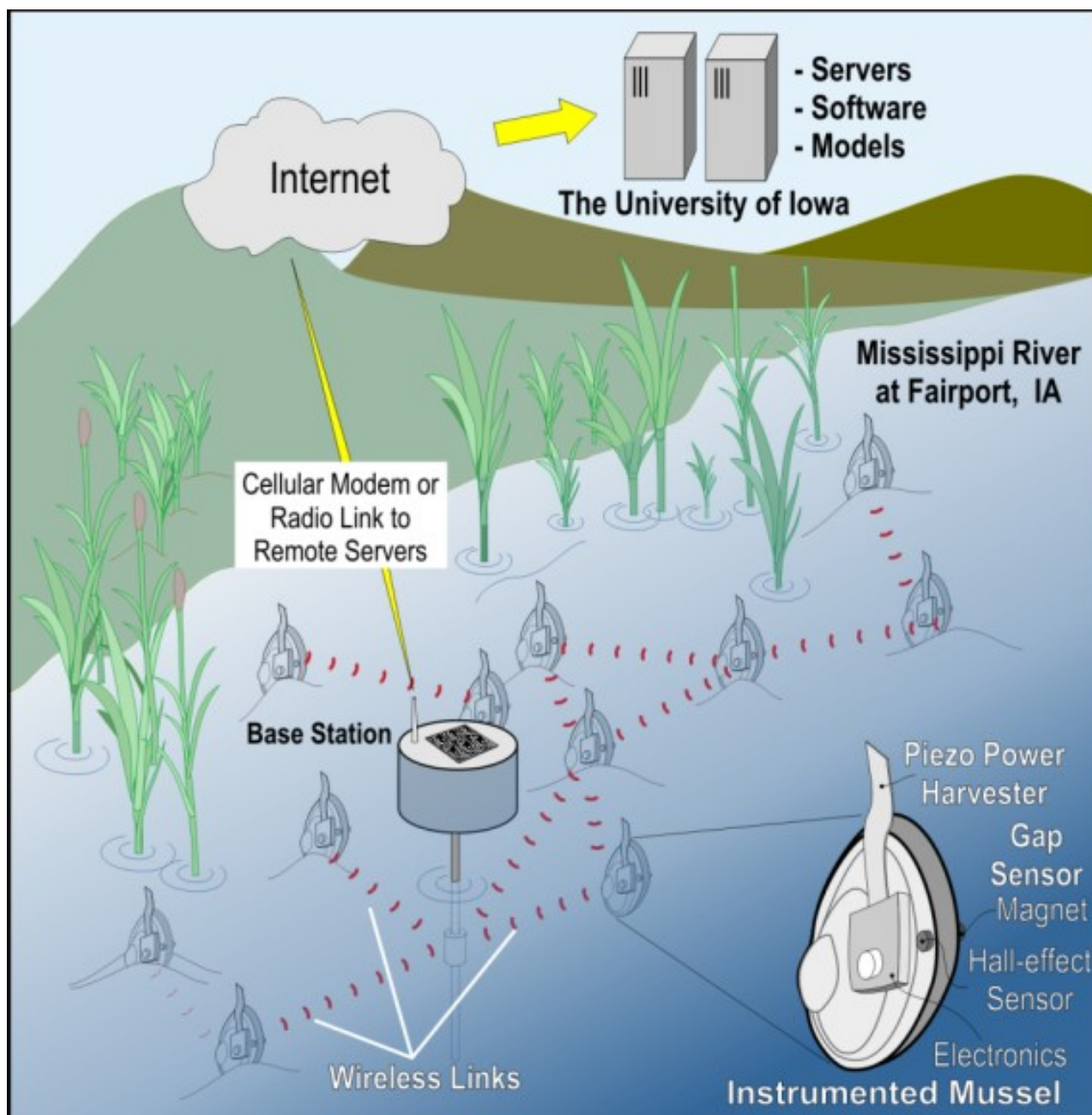


Figure 16 The figure depicts on-going research at The University of Iowa that aims to use freshwater mussels as biological sensors. Mussels equipped with Hall-effect sensors sense mussel gape, as well as water temperature and turbidity. Computer models on remote servers interpret behavior to extract, for example, nitrogen cycle information.

### Laboratory Proof-of-Concept Experiments

As a proof of concept, we instrumented mussels with both tethered and untethered data acquisition systems. The Hall-effect sensors of the tethered mussels were attached to several meters of wire. The data logger for the tethered mussel consisted of a microcontroller with a 12-bit analog to digital converter for measuring the output voltage of the Hall-effect sensor. Data is retrieved and stored in a laptop connected to the data logger via serial communication.

The untethered mussel was also instrumented with a Hall-effect sensor/magnet, microcontroller and RF link. We modified a commercially available key fob for the underwater wireless link, see Figure 17. This device was chosen for its size and functionality. It contains all the basic elements needed for this experiment, namely a power supply, programmable microcontroller and radio, all in a small package. This nicely-packaged key fob contains a Nordic nRF24L01+ radio and an ATtiny24 microcontroller. A 20mm, 3V coin cell supplies power. The Nordic nRF24L01+ radio operates at 2.4 GHz. As shown in Table 3, at this frequency fresh water has an attenuation of 266 dB/m. However, since the tank's dimensions were less than 1 m and water depth was about 0.5 m, this high attenuation was not a concern.

I modified the key fob slightly for addition of the Hall-effect sensor, and the addition of a step-up voltage regulator to maintain a constant voltage of 3.3 V as the battery discharged. The ATtiny24 has an on-chip 8-bit ADC. I programmed the controller to sample and transmit the Hall-effect sensor voltage every 10 minutes to a receiver located outside of the tank. A 10-minute sample interval with the 250 mAh coin cell provided 40 days of runtime. To prevent water intrusion the entire system was sealed in thermally conductive epoxy produced by MG Chemicals model 832C. This epoxy was chosen since it has a low dielectric constant of three at 2.4 GHz. Figure 18 shows examples of tethered and untethered mussels used as bio-sensors. The equipment was attached to the mussels using an environmentally friendly two part epoxy as not to harm the mussels or contaminate their living environment.



Figure 17 Off-the-shelf modified key fob with low power Hall-effect sensor that was attached to mussel.

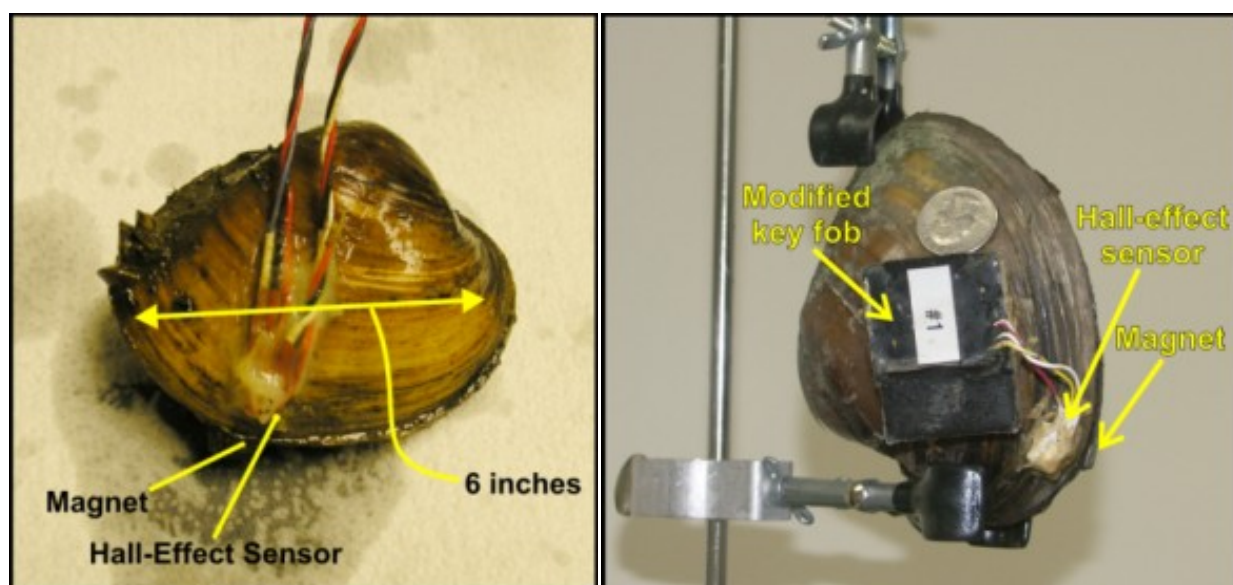


Figure 18 The left panel shows the tethered mussel used for bio-sensing. The right panel shows a mussel with a modified key fob, Hall-effect sensor and magnet attached to the mussel. The mussel is then deployed untethered as a bio-sensor.

Data was received by a Nordic Serial Interface Board produced by Sparkfun Electronics which contained a RF module nRF24L01+ and an ATmega164V microcontroller. A serial link connected the Nordic Serial Interface Board to the laptop computer running a custom MATLAB program where all the data was stored. The experimental setup used for the tethered and untethered mussel experiment is shown in Figure 19. Mussels are filter feeders and were fed by replacing their water with water from the Iowa River.

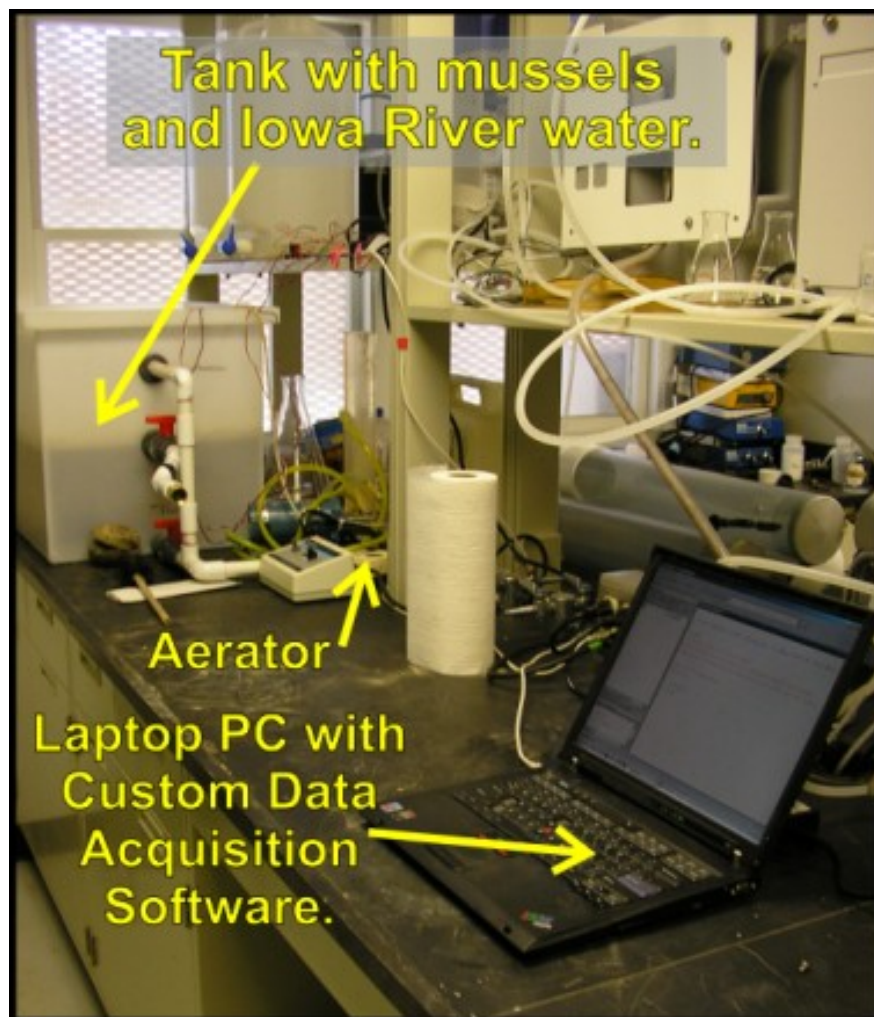


Figure 19 Experimental setup for collecting data of both tethered and untethered instrumented mussels. Mussel gape was sampled at five second intervals for tethered mussels. Mussel gape was sampled at 10 minute intervals for untethered mussels to conserve battery power.

### Mussel Gape Results

The untethered link provided very reliable communication over the 40-day period. Only a small percentage of packets were dropped, excluding a three day period of time when the laptop was accidentally unplugged. No attempts were made to retransmit dropped packets. The nRF24L01+ radio provides data packetization with built-in error checking of received data and has built-in capabilities for auto-retransmission. All high-level communication functionality was disabled to provide a better view of true link reliability. With the implementation of retransmission, link reliability could approach 100% for this set up. Alternatively, link reliability could be improved substantially by using a lower frequency radio that has less attenuation in water (see Table 3).

Figure 20 shows some of the data collected for the mussel experiment. There is a clear cycle of the mussel opening and closing on a daily basis. For a period of time after the data acquisition failure the natural light cycle of the tank was shifted. The tank was covered to block out all natural light. An incandescent bulb was used to provide an alternative light source 180 degrees out of phase with natural light source. The mussels also shifted their daily cycle by 180 degrees to match the artificial lighting as evident in Figure 20 bottom.

The data strongly suggest that the mussel adjusted its gape to the externally imposed light cycle. The importance for our study is that one can use a mussel's gape as a sensor—light patterns in this instance. This may have application in monitoring turbidity in rivers, which are used as a proxy for water quality.

### Underwater Antennas for Mussels

Our experiments clearly show that one can use commercially available radios and key fobs underwater with waterproofing. However, the antennas designed for use in air are unsuitable for use in water, because of the different electromagnetic properties of water and air. While not the main thrust of my research, I am helping design effective antennas for underwater applications, particularly antennas that one could attach to mussels (Hunt et al. 2010).

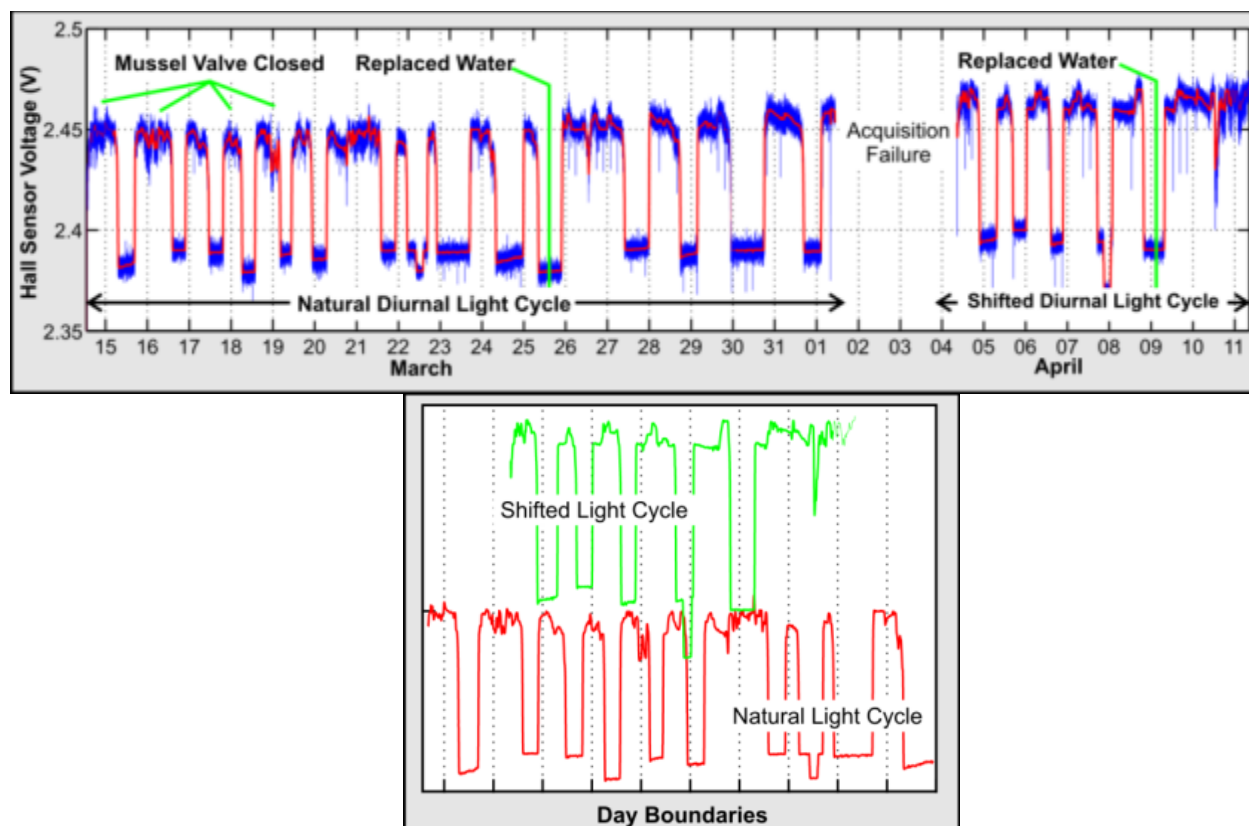


Figure 20 The top panel shows mussel gape data after application of a median filter to remove impulse noise (blue), followed by 5-min zero-phase moving average-type digital filter (red). Low voltages indicate mussel's valve is open. The bottom panel is a phase comparison of mussel gape in natural light diurnal cycle (red) with mussel gape in shifted (approximately 10 hours) diurnal light cycle (green).

An effective antenna for this application must meet a number of requirements. Primarily, the antenna must be small enough so that one can glue the antenna to a mussel. Mussel sizes vary with age and species—we currently focus on mussels that are about 8 cm long and 5 cm wide. One wants the antennas not much larger than 50% of these dimensions, namely  $4 \times 2.5$  cm. We do not make assumptions regarding mussel orientation, so an isotropic antenna is desirable. Mussels may burry themselves in the mud layer in a river when seeking protection. Thus, the antenna must operate in river water, or partially- and even completely buried in sediment. These different environments have different conductivities and dielectric constants, and these impact wavelengths of RF waves.

Furthermore, the electrical conductivity varies in rivers with time so that an antenna radiates into a non-stationary propagation environment. This implies that a broadband antenna is preferable to a highly tuned, narrowband antenna. Also, as we outlined previously, river water presents a significantly different environment to an antenna and attached radio than does the air. The water affects the radiation pattern and antenna impedance, and thus the overall efficiency of the transmitter. The input impedance of an antenna is the impedance at its input terminals, both the real and imaginary part. The maximum power is delivered to the antenna when the antenna and transmitter are matched, that is the input impedance of the antenna equals the complex conjugate of the output impedance of the transmitter. The maximum power is delivered to a receiver when the receiver and antenna are matched.

Because of the difference in wavelength, the physical dimensions of an antenna in water would be about 1/9 of the dimensions of an equivalent antenna in air. Because of the difference in intrinsic impedance, the input impedance of an antenna in water would be about 1/9 of the input impedance of the equivalent antenna in air. Still, our goal is to use very simple, inexpensive antennas, and avoid impedance matching networks. We want to identify antennas that will allow non-electrical engineering researchers to easily construct underwater biological sensor networks. Finally, antennas in water are prone to corrosion and fouling. An insulated antenna is preferred to one made of bare metal.

We investigated the performance of three common antennas, namely the dipole, loop, and folded dipole as follows. We designed these antennas as if they would operate in air, but reduced the dimensions by a factor of 9 to account for the wavelength shortening that occurs in water.

Figure 21 shows the experimental setup, which consists of a circular plastic tank 2.5 meters in diameter and 2.1 meters tall, filled with water ( $\sigma \sim 0.034$  S/m). Drinkable water typically ranges from 0.0005 to 0.05 S/m, and salt water is typically 3.4 S/m. A length of PVC pipe extends vertically from the center of the bottom of the tank. On top of this lower pipe, we placed a module containing a Radiotronix RCT-433-AS(B) transmitter sealed in epoxy. The RCT-433-

AS(B) transmitter has an output impedance of 50 ohms and contains a simple network to match antenna impedances close to 50 ohms to the transmitter. A computer-controlled  $x$ - $y$  positioner is located on top of the tank. Another PVC pipe extends vertically down into the tank from the positioner. A spectrum analyzer measured the power received by the receiving antenna as the separation distance was varied.

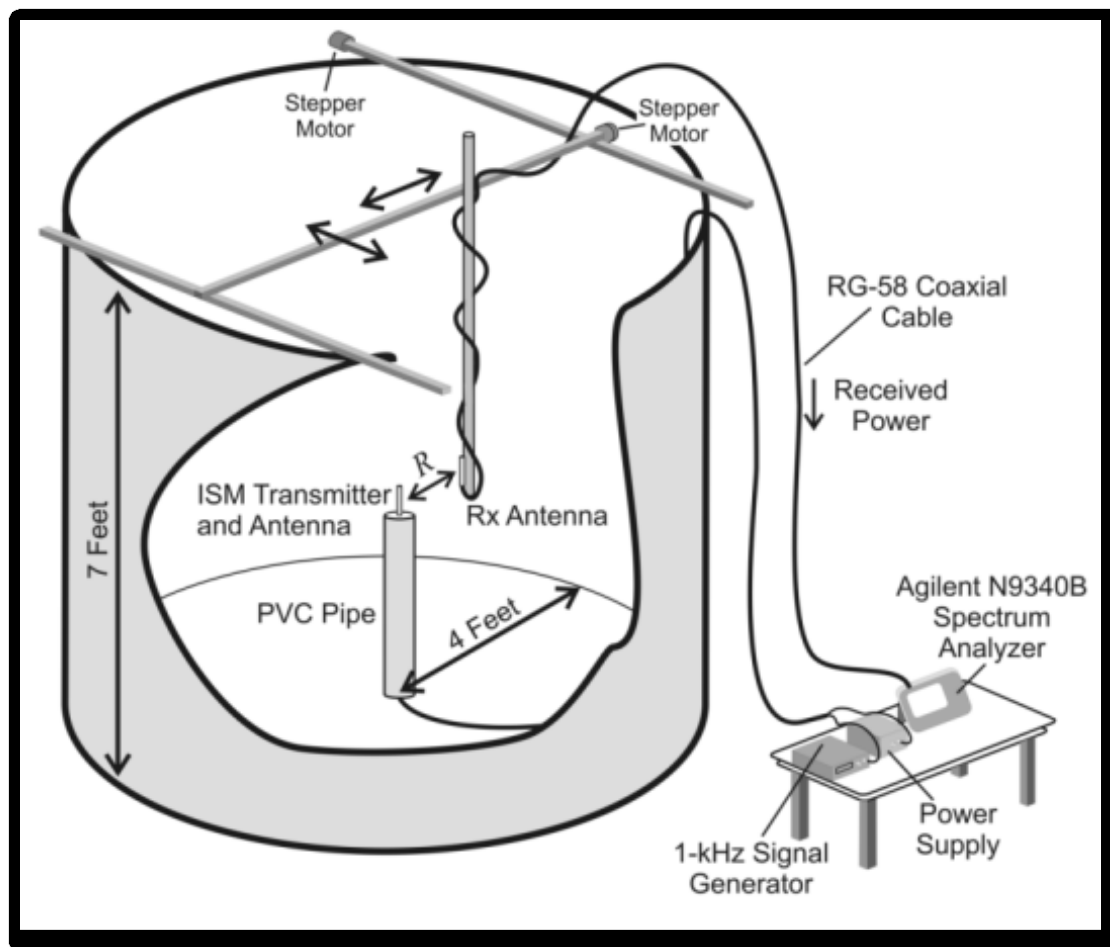


Figure 21 Experimental setup for evaluating underwater antennas. The tank is filled with water with a conductivity of ( $\sigma \sim 0.034$  S/m) and the stepper motor precisely controls the distance between the transmitter and the receiving antennas with an accuracy of ( $\sim 2$  mm). The transmitting antenna was affixed to the center of the tank and the receiving antenna was attached to the stepper motor. A spectrum analyzer measured the power received by the receiving antenna as the separation distance was varied.

The experimental setup allows one to position the receiving antenna accurately ( $\sim 2$  mm) with excellent repeatability. Attached to the upper pipe was a receiving antenna consisting of a small insulated dipole with a total length of 1.59 cm ( $0.2\lambda$ ). This receiving antenna was at the same depth as the transmitter. A five meter RG58 cable connects the receiving antenna to an Agilent N9340B spectrum analyzer. The antenna to be evaluated is attached to the transmitter and the positioner moves the receiving antenna in small increments.

At each increment, we measured and recorded the received channel power. We set the channel power to 150-kHz, centered on the transmitter's 433-MHz carrier frequency. The transmitter was modulated with a 1-kHz square wave. To reduce random noise, we configured the spectrum analyzer to average 50 power measurements. With a sweep time of 126 ms, this corresponds to averaging for about 6.3 s. To eliminate ground loops and unintended coupling between the transmitter (via its power supply and/or the 1-kHz signal generator) we operated the spectrum analyzer off its internal battery power supply.

Since dipole antennas are simple to construct, and widely-used, we started our investigation with dipole antennas as follows. We constructed a 5-wavelength (38 cm) antenna and measured the received power at a maximum separation of 70 cm. We reduced the dipole length in half-wavelength steps and measured the channel power at each step. Figure 22 summarizes the results and indicates that a  $1\lambda$  dipole radiates efficiently. There were several antenna lengths that appeared not to radiate energy for this transmitter. One possible reason for this is that the datasheet states that this transmitter will not operate if there is a major mismatch between antenna impedance and module impedance. Signals were received from this group of antenna when the transmitter was located in the air above the water while the receiving antenna was located in water. No signals were received from this group of transmitter antennas even when located directly next to the receiver in the water. We made detailed power vs. range measurements for  $1\lambda$  dipole and  $5\lambda$  dipole antennas in water.

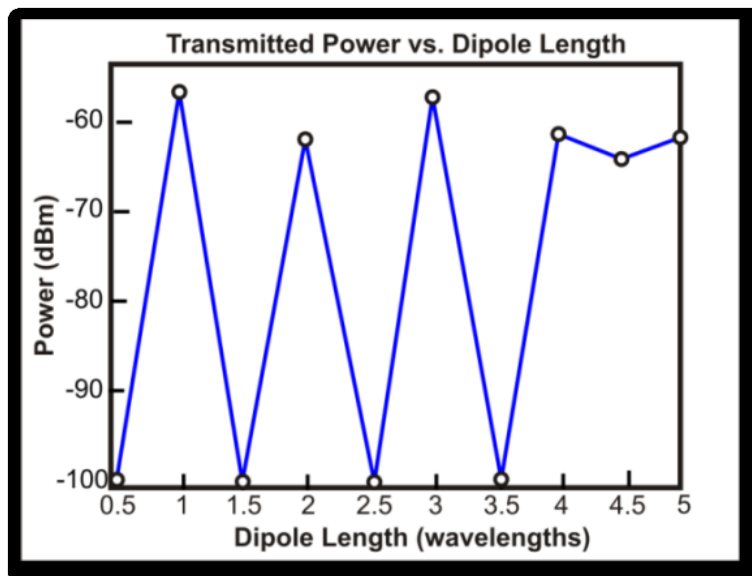


Figure 22 Measured received power as a function of transmitter antenna length for a separation distance of 70 cm in water.

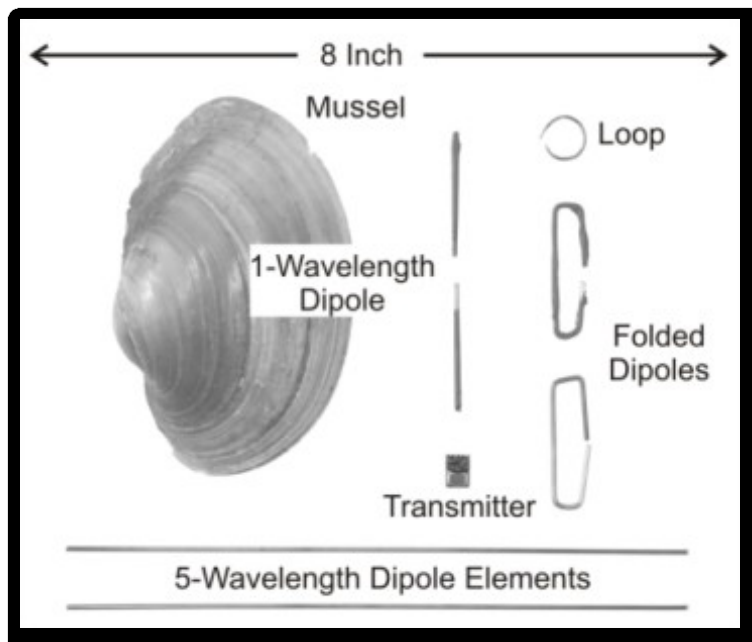


Figure 23 The antennas tested for underwater RF mussel applications at a frequency of 433 MHz.

Another popular, compact antenna is a folded dipole, which is the next antenna that we explored. We also explored a half-wavelength (circumference) loop antenna. Additionally, we explored the effect of constructing antennas from bare vs. insulated copper. Figure 23 shows the antennas that were used in this trial along with a mussel and transmitter.

Figure 24 summarizes the results for the different antennas. The calculated near-field for the antennas is about 5 cm, and the far field is about 15 cm, also indicated in the figure. For reference, the figure also shows a  $1/R^2$  response, which is what one would in a non-conducting medium. The insulated 1-wavelength dipole performed the best. Over the entire range of measurements, its received power was about 5 dBm greater than any other antenna. Small oscillations in the received power are evident when the range is about 43 cm. Both folded dipoles performed very well, with the insulated folded dipole performing a little better than the uninsulated folded dipole. As with the dipole, oscillations in the received power are evident

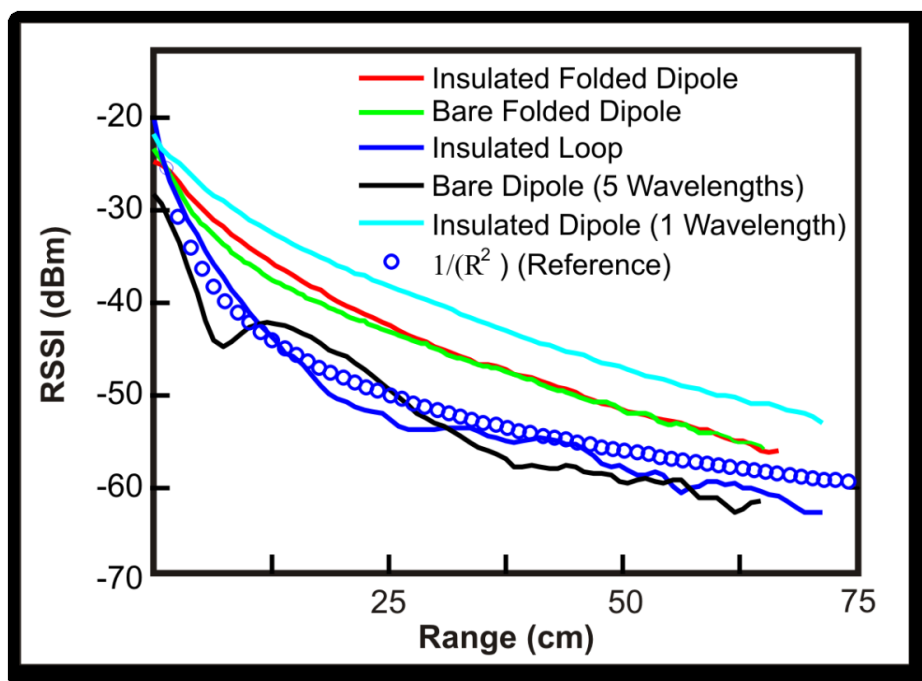


Figure 24 Received power vs. range for the candidate antennas along with  $1/R^2$  reference. The frequency is 433-MHz.

close to the tank wall. These oscillations suggest reflections and multipath. Closer examination reveals that the maxima and minima are spaced 3.8 cm or  $0.5\lambda$  apart, which supports the notion of reflections off the tank wall. In the very near field, the insulated loop performs better than any other antenna, but the received power falls off very rapidly. The power of the insulated loop shows significant variation at greater distances.

Our results show that a simple, insulated dipole outperforms the other candidate antennas, and meets the other important requirement, namely is small enough to be attached to a freshwater mussel. However, there are other factors which we have not yet explored. The close proximity of the mussel and the river bottom may affect transmitted power, as could interference by reflections from the water free surface. Furthermore, we have not yet measured the radiation patterns of the antennas to see which is most isotropic.

### Conclusions

Even though water severely attenuates radio waves, especially at higher ISM frequencies, it is possible to obtain reliable communication over small distances. Rather than using traditional telemetry, one can build an underwater WSN where nodes cooperate. In this case, the short range is not a problem, and may in fact be beneficial. Researchers at The University of Iowa want to use freshwater mussels as biological sensors, measuring their gape using Hall-effect sensors.

I helped perform laboratory-based experiments with wired and tethered mussels, as well as mussels equipped with small radio transmitters. The radio link worked very well over a period of several weeks, thus establishing the proof-of-concept. The electronics to implement such links are inexpensive and widely-available (I modified a commercial key fob). We also explored different antennas that may be appropriate for using on mussels (Hunt et al. 2010). An exciting, albeit preliminary, result is simple dipole and folded dipole antennas perform well, and at 433-MHz, the frequency that we explored, are small enough to attach to mussels.

## CHAPTER IV

### UNDERGROUND NETWORKS

Conventional thinking holds that underground- and underwater radio communications are not possible, except at very low frequencies, using very long antennas and high transmit power. The main reason is that water and soil (especially wet soil) severely attenuates radio waves. Another complication is that “ground” is a complex propagation medium consisting of topsoil, various clay and rock layers, the water table, and so on. Each of these has a different dielectric constant so that radio waves are reflected and refracted in addition to being attenuated. One should note however, that with sufficient power, radio waves can penetrate significant distances into the ground. Ground-Penetrating Radars or GPR (Daniels, 2004) have long exploited this fact, using frequencies that range from 20 MHz for deep penetration (10’s of meters), to 150 MHz (typical), to 300–500 MHz for shallower depths.

GPR aside, in this chapter I argue that using inexpensive radios it is in fact possible to achieve reliable underground radio *communication* over distances of several meters. While these distances are small when compared with what one could achieve with traditional radio telemetry, this does allow for creating underground WSNs. In this chapter, I document a proof-of-concept underground radio network. Nodes in the underground WSN measuring soil moisture content are buried over an  $6 \times 6$  meter area (up to 1 meter deep). The nodes organize themselves into a WSN, reconfigure routes as radio link quality waxes and wanes, and cooperate in routing data packets to a surface base station, and so on. While investigating underground WSN, I learned of other researchers that have been developing such networks (Akyildiz et al. 2006, Tiusanen 2009).

#### Feasibility of Underground Communications

I performed a feasibility test to investigate the possibility of underground networks. The aim of this test was to investigate the maximum transmission distance of reliable links. Similar work has been done where links transmit directly to a base station located above ground

(Stuntebeck et al. 2006). For my feasibility test, transmissions were between nodes located below the surface. The investigation looks at two popular ISM frequencies, namely 900 MHz and 2.4 GHz. The RF modules I used are manufactured by Maxstream and are models 9XStream and 24XStream; and operate at 900 MHz and 2.4 GHz respectively. Figure 25 Shown left is the 900-MHz radio, and shown right is the 2.4 GHz radio for the underground communication link feasibility test.. MaxStream's 9XStream radio can detect signal strength to -110 dBm, while the 24XStream has a receiver sensitivity of -105 dBm. The transmission output power is 20 dBm and 17 dBm for the 900 MHz and 2.4 GHz modules respectively. Both models use frequency-hopping spread spectrum (FHSS). I selected frequency-hopping radios to combat multi-path effects.

I used the X-CTU software provided with MaxStream radios, for testing signal attenuation. This software has a range testing function built in for use with a remote echo server. The remote echo server consist of a Maxstream radio operating at the same RF carrier frequency and hopping sequence with the module's data received output tied to the data transmit input with a loop back connector see Figure 9. All data received by the remote echo server is transmitted back to the sending radio. A test packet is sent by the X-CTU software over a radio attached to the computer to the remote echo server. As the packet returns from the remote echo server the software calculates and displays the receive signal strength in dBm.

To prevent disruption of the soil and possibly altering the results of the experiment, only the antennas would be lowered in the ground. It was decided that measurements would be made at antenna depths in the soil of 0.5 and one meter and separation distances in 0.3 meter increments. Hollow 3.8 cm diameter PVC tubs one meter in length were driven into the ground in 0.3 meter increments to serve as the test platform. The PVC tubes allowed the antennas to be easily lowered to various depths without disturbing the soil to bury the antennas. For this experiment no attempt was made to calibrate the antenna for soil types.

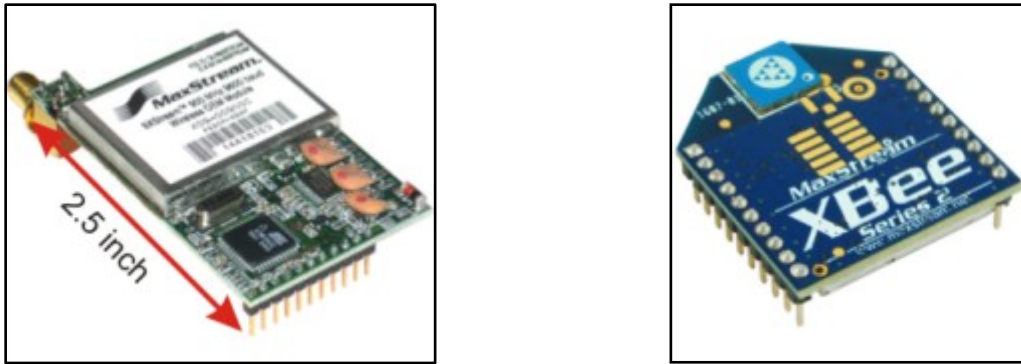


Figure 25 Shown left is the 900-MHz radio, and shown right is the 2.4 GHz radio for the underground communication link feasibility test.

I installed the CS616 TDR soil moisture probes (CS616 2010) to observe any changes in soil water content. The probes were installed at an angle to incorporate measurements in the top 15 cm of soil. The probes were installed near the surface to minimize the disruption of the soil from burying the sensors at a deeper depth. I deployed soil temperature sensors at several locations, but since this experiment was performed in late November, little fluctuation in soil temperature was observed. Figure 26 illustrates the experimental setup used to measure RSSI for radio modules at frequencies of 900 MHz and 2.4 GHz.

Campbell Scientific model CS616 probes collected soil moisture data between PVC. The CS616 is a class of probes called time-domain reflectometry Probes (TDR). Figure 27 left shows the operation. The metal rods on the CS616, shown Figure 27 right, function as a transmission line pulse *A* is launched and when reflected pulse *B* arrives, the next pulse is launched. Electronics in housing output a scaled frequency proportional to time-of-flight. Time of flight is a function of soil permittivity, which is dominated by soil water content. Soil conductivity impacts measurement, and soil permittivity is also a function of temperature. To obtain proper measurements of soil moisture, one has to calibrate the sensors to the specific soil. With the CS616, it is possible to observe trends in soil water content without precise calibration. For this

experiment, only the relative change in water content is of concern. The decision to use this sensor was based prior experience with this particular sensor.

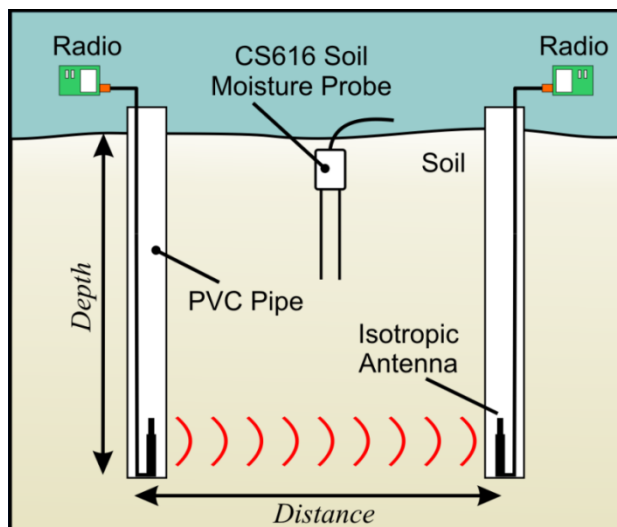


Figure 26 Experimental setup for measuring RSSI as a function of antenna depth and separation distance using XStream radio modules. Antennas were lowered in to PVC tubes that were driven in the ground. Campbell Scientific's CS616 monitored changes in soil water content.

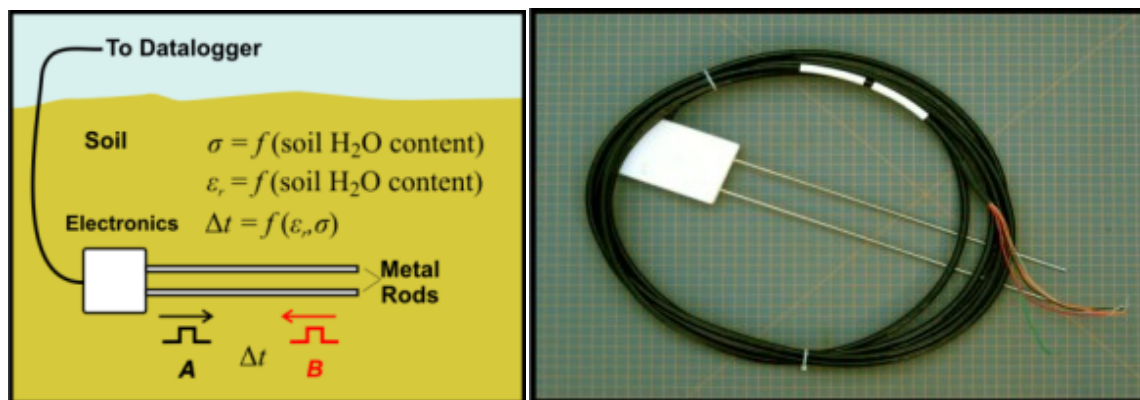


Figure 27 The left panel depicts the principle of operation of TDR-based soil moisture sensors (see text). The right panel is a photograph of CS616 water content reflectometer.

The internal circuitry of the CS616 detects the reflected pulse and triggers the next pulse. In free air the frequency of the pulses are 70 MHz. The frequency is scaled down at the output of the CS616 to allow for easier measuring. As water content increases, the propagation velocity of the pulses decreases. The probe output frequency or period is empirically related to the water content using a calibration equation. This output swings from -0.7V to 0.7V. A standard calibration equation given in the datasheet is

$$VWC = C_0 + C_1 * period + C_2 period^2$$

The outputted period is in microseconds and the result is volumetric water content on a fractional basis. Multiply by 100 to express in percent volumetric water content. Standard calibration coefficients listed in the data sheet are  $C_0 = -0.0663$ ,  $C_1 = -0.0063$  and  $C_2 = 0.0007$ .

One must be very careful when inserting the rods in the ground to maintain an equal distance between the rods. The period of the CS616 in air is approximately 14.7 microseconds, and the period in saturated soil is approximately 31 microseconds. The CS616 draws 65 mA at 12 VDC when enabled and 45  $\mu$ A quiescent. The maximum cable length is 1000 feet (305 m). The CS616 are equipped with an enable/disable line for putting the sensor in power down mode to conserve energy.

For proper soil moisture measurements the CS616 needs to be calibrated to the soil type. One possible way this can be done by taking a soil sample and weighing the sample, and then completely drying the sample and reweighing the sample with the water removed. This technique is called the gravimetric method. The difference between the weights is the weight of the water contained in the soil. I was assured by Dr. Logsdon (personal communication, 2009) at the National Laboratory for Agriculture & the Environment that it is possible to observe the percentage change in soil water content without calibrating the probe to a specific soil type.

The 2.4 GHz radio module was test first with data throughput baud rate set to 9600 bits/s. Both antennas were lowered to a depth of 0.5 meter with a separation distance of 0.33 meter. The RSSI was averaged over 120 packet transmission and recorded. The remote echo server was then

lowed into the next PVC tube located at a distance of 0.66 meter. The RSSI was again averaged over a 120 packets. This process was repeated until the communication link failed for all 120 packets. This entire process was then repeated for antennas lowered to a depth of one meter. Once all measurements were made, the same investigation process was performed for the 900 MHz modules. The soil moisture varied little between links over the time I performed the experiment, and remained around 34%.

Figure 28 shows the RSSI data collected for both 900 MHz and 2.4 GHz at antenna depths of 0.5 and one meter along with a linear approximation for the sampled data points. Markers represent an average of 120 measurements.

The top panel is RSSI data collected at 900 MHz collected for antennas buried in soil at depths of 0.5 meter in blue and depths of one meter in red for various separation distances. The model is also shown for data collected at a depth of 1 m. The bottom panel shows 2.4 GHz RSSI data collected for antennas buried in soil at depths of 0.5 and one meter for various separation distances. Lines shown are linear approximations for reference only since attenuation of collected data was high.

### A Buried Sensor Network

The next step was to construct and operate a multi-mote underground WSN. I constructed the network using so-called *EduMotes* that are used for a class in Wireless Sensor networks at The University of Iowa. The EduMotes shown in Figure 29 consist of power supply, ATmega128 microcontroller, MaxStream radio, Liquid Crystal Display (LCD) and sensor area. Figure 30 shows the design of such a network that was used for this trial.

Rather than burying all the electronics, I buried the only the antennas. I programmed the EduMotes to route the packets as indicated in the Figure 30. Node  $R_0$  originates a packet that the other nodes route to a base station located at  $R_4$  as the packet traverses the network, nodes tack

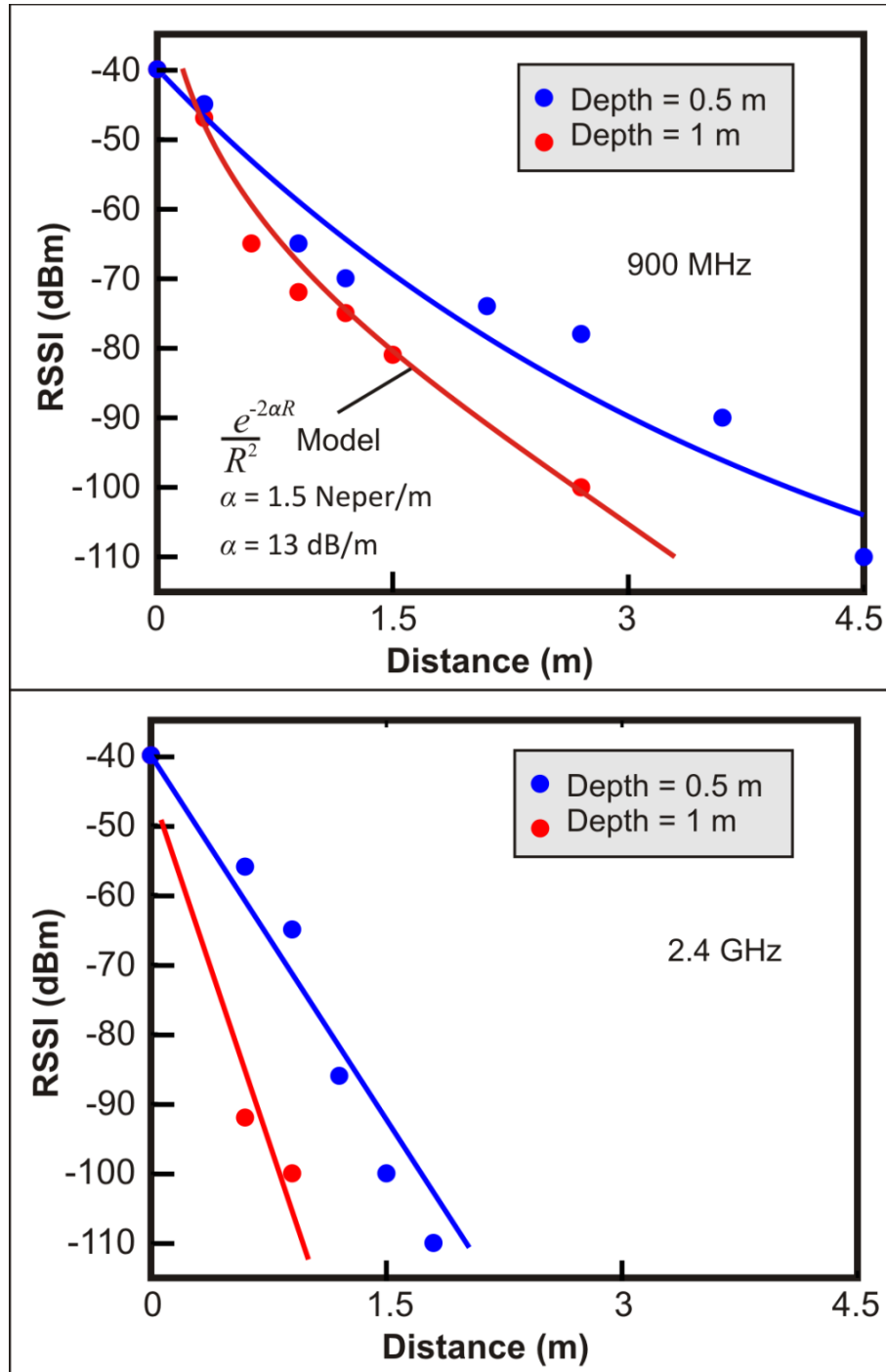


Figure 28 The top panel is RSSI data collected at 900 MHz collected for antennas buried in soil at depths of 0.5 meter in blue and depths of one meter in red for various separation distances. The model is also shown for data collected at a depth of 1 m. The bottom panel shows 2.4 GHz RSSI data collected for antennas buried in soil at depths of 0.5 and one meter for various separation distances. Lines shown are linear approximations for reference only since attenuation of collected data was high.

the RSSI between it and the previous node and record that links RSSI in the packet. The base station records time-series data of the RSSI of the various links. The TDR soil moisture probes were installed at strategic places in the WSN. This allowed me to investigate the impact of changing soil moisture on the quality of the communication links. The information about RSSI and VWC collected in this network would lead to the experiment performed in chapter V of this document.

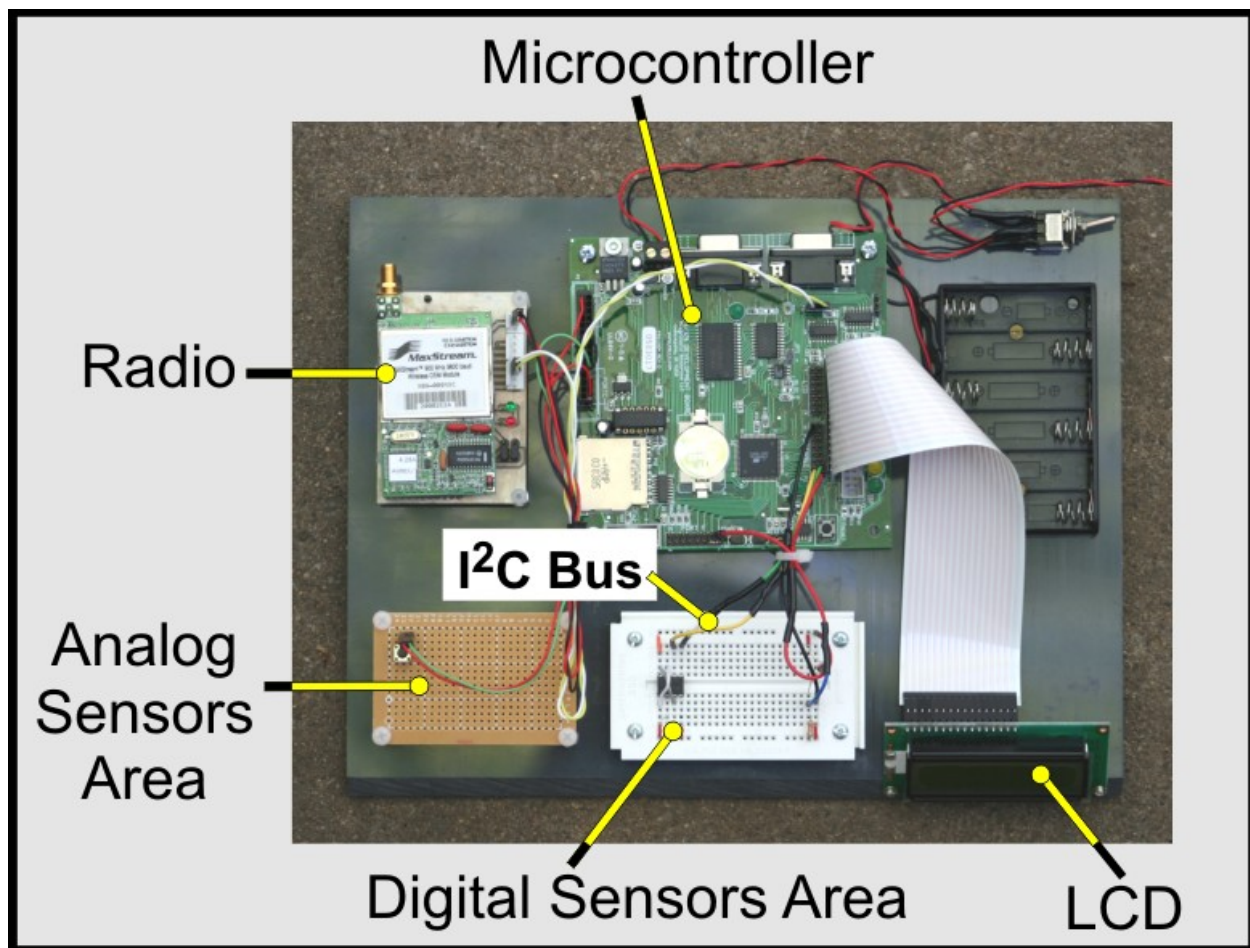


Figure 29 EduMote node used in field experiments and for teaching purposes at The University of Iowa. The EduMote consists of power supply, ATmega128 microcontroller, MaxStream radio, LCD, and sensor area.

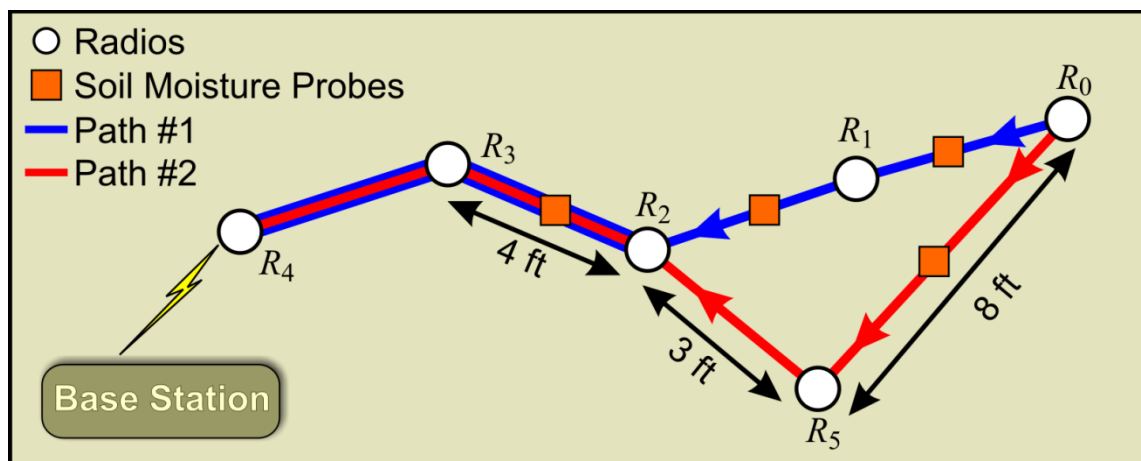


Figure 30 Schematic of proof-of-concept buried WSN. Packets are routed from  $R_0$  to  $R_4$  via Path #1 as well as Path #2. Packets' payloads are the links' RSSI measures.  $R_4$  transmits the payloads to the base station above ground.

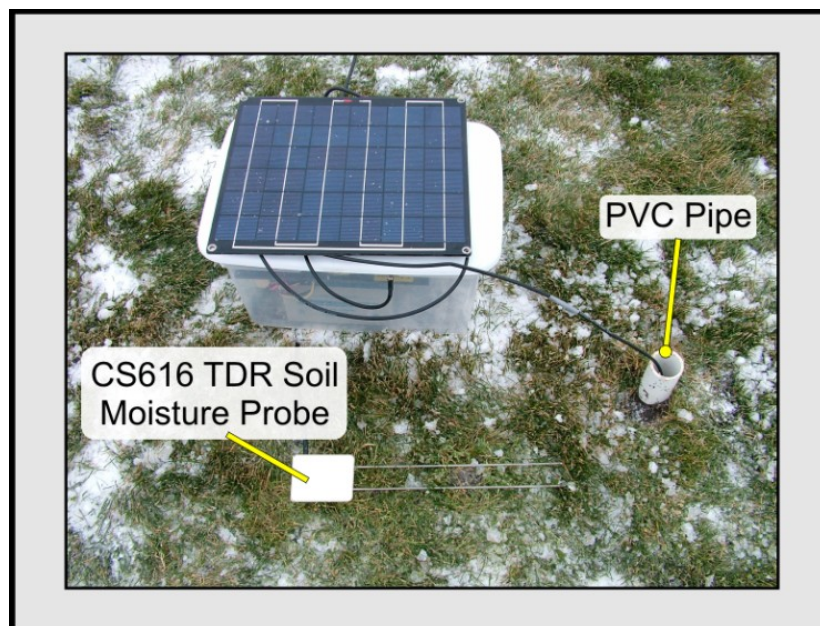


Figure 31 An EduMote, which The University of Iowa uses for laboratory exercises in WSNs, inside its enclosure. I used EduMotes to build the underground WSN. Rather than burying the whole node, we only bury the antennas. Soil moisture was also monitored in between links.

Figure 31 shows an EduMote with power supply inside of its plastic enclosure along with Campbell Scientific model CS616 soil moisture probe. The probes were installed in the top 15 cm of soil to minimize soil disruption. Figure 32 shows the entire experimental setup deployed in the field to test the feasibility of underground WSN.

### Results

Figure 33 shows a 3-day time series Time-series of RSSI data for links  $R_0 - R_1$  in Path 1, and  $R_0 - R_5$  in Path 2 of the prototype WSN (see above). When the longer link  $R_0 - R_5$  fails, the other links provide an alternate route for packet delivery (shaded area).

The RSSI, while low, is sufficient for the WSN to operate. When a marginal link fails, other nodes take over and route the packet. We were hoping to operate the WSN for several months to see the effect of soil moisture changes resulting from rainfall, but the timing was such that we could not. As an alternative, we wetted the soil at various locations, simulating a rain event. Figure 34 summarizes the results from such an experiment.



Figure 32 Experimental setup. Only the antennas were installed below the surface of the ground at a depth of 80 cm. The antennas were lowered into PVC tubes driven into the ground. Motes were sealed from the elements inside of plastic containers. CS616 soil moisture probes monitored soil conditions between links. Data consisted of RSSI and soil moisture between all links. All data was routed and stored at the base station that consisted of custom data logger designed for this experiment.

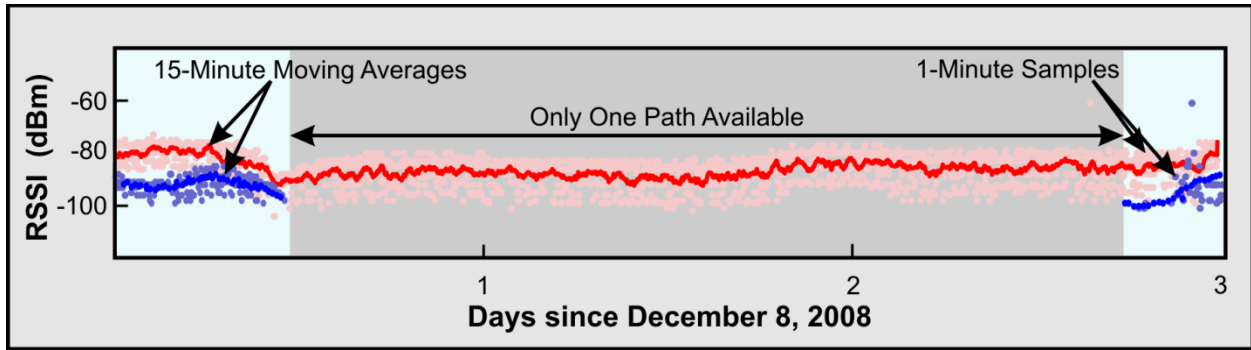


Figure 33 RSSI for a three meter link (blue) and a shorter alternative path (red) are shown for a three day period. As the soil was manually moistened, the longer link began to drop packet and only the alternative route was available for packet routing. Packets were transmitted every two minutes and the dark lines are the five minute moving average of RSSI.

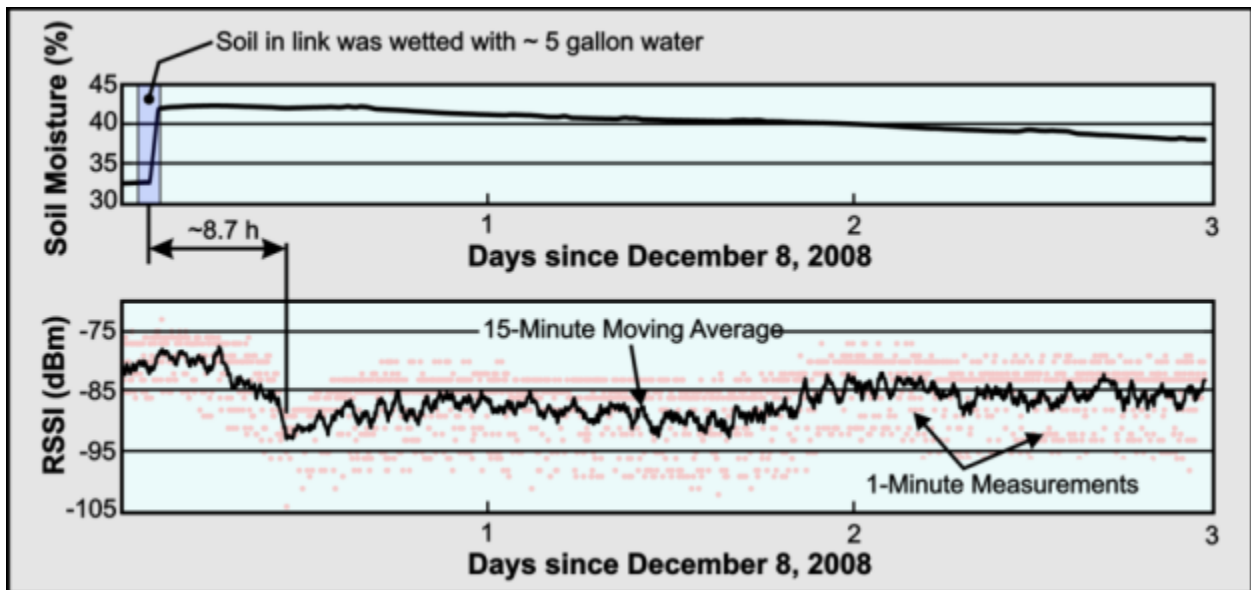


Figure 34 Time-series of RSSI data for link  $R_2 - R_3$  in Path 1 in the prototype WSN. The soil was wetted with ~5 gallons of water shortly after the start of the test. As the water seeps into the soil, the link's attenuation increases (RSSI decreases) and then slowly increases as the soil dries out.

The soil was wetted in the middle of the link at the location of the CS616 probe. The probe immediately showed an increase in VWC since it was installed in the top 15 cm of soil. After about eight hours the water began to attenuate the RF signal for that the link, the antennas for that link had been installed at a depth of one meter. The black line in the in the bottom panel of Figure 34 indicates the moving 15 minute moving average of RSSI measurements. RSSI and soil moisture for the link were sampled every minute. The RSSI measurements were obtained using the built in AT commands of the module and provide the RSSI of the previous packet. From the plot one can see that signal strength varied nearly 15 dBm between samples. Signal strength recovered as the water dispersed in the ground and is evident in the diminishing soil moisture reading from the CS616.

For a network to be feasible alternative routes will be needed longer links. Alternatively longer links can be achieved by not burying the nodes as deep in the ground. The tradeoff between sensor depth, soil moisture conditions and farming practices will all need to be taken into account when deciding maximum link distance.

### Discussion and Conclusions

The experimental results show that one can operate radios underground and create underground WSNs. In an agricultural research setting, an advantage of such buried wireless sensor networks is that, if nodes were buried deep enough, they may be left in place during agricultural field work (Niemeier et al. 2006, Niemeier et al. 2008). Links of a few meters are possible for typical soil found in eastern Iowa. Although short, these links provide the possibility for nodes to be buried enough to allow farm practices to take place without the removal of equipment. It may be possible for one to recharge node internal batteries using inductive coupling through the soil or possible through thermal gradients within the soil. This would eliminate the need to dig up nodes to replace batteries.

It is clear that from the data that water contained in the soil modulates the RF signal and that it may be possible to quantify the amount of water present in the soil by improving RSSI

measurement techniques used in this experiment (Chapter V). From this data it is also clear that one needs to take into account varying soil moisture conditions before deploying an underground network. As shown in Figure 33 link communication reliability is function of soil moisture. Long links installed in dry conditions will suffer in performance during wet conditions. The bounds on link transmission distances will be determined primarily by the soil moisture conditions and soil type that will be present over time with in the link. Modules operating at the lowest possible frequency should be selected if transmission distance is to be optimized.

Power consumption is an important issue in wireless sensor networks. This is especially true in a buried network where battery replacement is a major undertaking. Nodes will need to have a self contained power source that may need to supply power for several years. The selection of the RF modules transmission power will also need to be taken into consideration. A power selectable RF module would be preferred to provide reliable transmission under changing soil moisture conditions.

## CHAPTER V

### SOIL MOISTURE ESTIMATION

The next three chapters explore the possibilities of using unlicensed RF modules for alternative purposes than communication links. The applications shown here stem from my previous work at the Iowa Validation Site located near Ames, Iowa. The purpose of this site is in the validation of remotely sensed soil moisture measurement. Primarily a look at how remotely sensed soil moisture estimations are effected by vegetation, and moreover, the dew on vegetation. My part in this experiment was to design, build and implement a system for data collection of soil moisture and soil temperature sensors deployed in the 200 acre field used in the production of corn and soybeans. In-situ measurements were intended to validate the soil moisture measurements calculated by radiometers. The sensors were deployed at depths of 1.5, 4.5, 15, 30 and 60 cm. The measurements collected at depths of 1.5 and 4.5 cm were of primary concern, since radiometers operating at L-band frequencies can be used to calculate the soil moisture to a few centimeters of soil. NASA's Soil Moisture Active Passive (SMAP) satellite incorporates L-band radar and an L-Band radiometer that share a single feedhorn and parabolic mesh reflector. The goal is to combine attributes of both the radar and the radiometer in terms of spatial resolution and sensitivity to soil moisture, surface roughness and vegetation. Soil moisture will be estimated at a resolution of 10 km.

Also as part of my ongoing work at the Iowa Flood Center (IFC), I have been charged with incorporating soil moisture and soil temperature measurements into the existing rain gauge network. By incorporating the state of soil moisture with rain data it may be possible to better estimate river stage during flood conditions. One proposed task is to provide a distributed soil moisture measurement over a several meter area. One of the traditional techniques to accomplish this would be to install several in-situ point measurement sensors and interpolate conditions between probes. There are several drawbacks to this technique in the difficulty of routing power and data wiring to all the sensors, the cost of numerous sensors and point

measurement uncertainty. The uncertainty could come from improper installation or local anomalies within the soil. As an alternative I explored the possibilities of using RF links as a way to provide a distributed soil moisture estimation that is economical and needs little extra need equipment.

### Experimental Setup

After analyzing the data collected from the underground sensor network, there appears to be a relationship between soil moisture and signal attenuation. To explore this relationship, a network of 12 motes operating at 900 MHz was deployed evenly spaced around the perimeter of a three meter diameter circle. As in the previous experiment only the antennas would be below the surface of the ground. The antennas were lowered into 2.54 cm PVC pipes that were driven into the ground to a depth of 60 cm. Both ends of the PVC pipe were sealed to prevent water from entering the tube and distorting measurements. Seven CS616 soil moisture probes with accompanying temperature probes were installed inside of the circle to monitor changes in soil moisture and soil temperature. Figure 35 illustrates the experimental setup used for this experiment. Nodes were labeled using hexadecimal notation from 0→B. The seven soil moisture- soil temperature probes were installed in an evenly spaced grid pattern. All CS616 probes were installed vertically to provide an integrated soil moisture estimate of the top 30 cm of soil. The soil temperature probes were installed in the top 8 cm of soil. To minimize the soil disruption, no probes were buried in the soil to obtain soil moisture estimations beyond a depth of 30 cm.

The goal of this experiment was to explore the possibilities of exploiting the fact that changes in soil moisture modulates the RF signal between links. It may be possible for one to use RSSI measurements between links to create a soil moisture map of the area encompassed by the ring of motes, since RSSI provides a distributed measurement over the entire link. As opposed to interpolating between point measurements obtained by the CS616 probe.

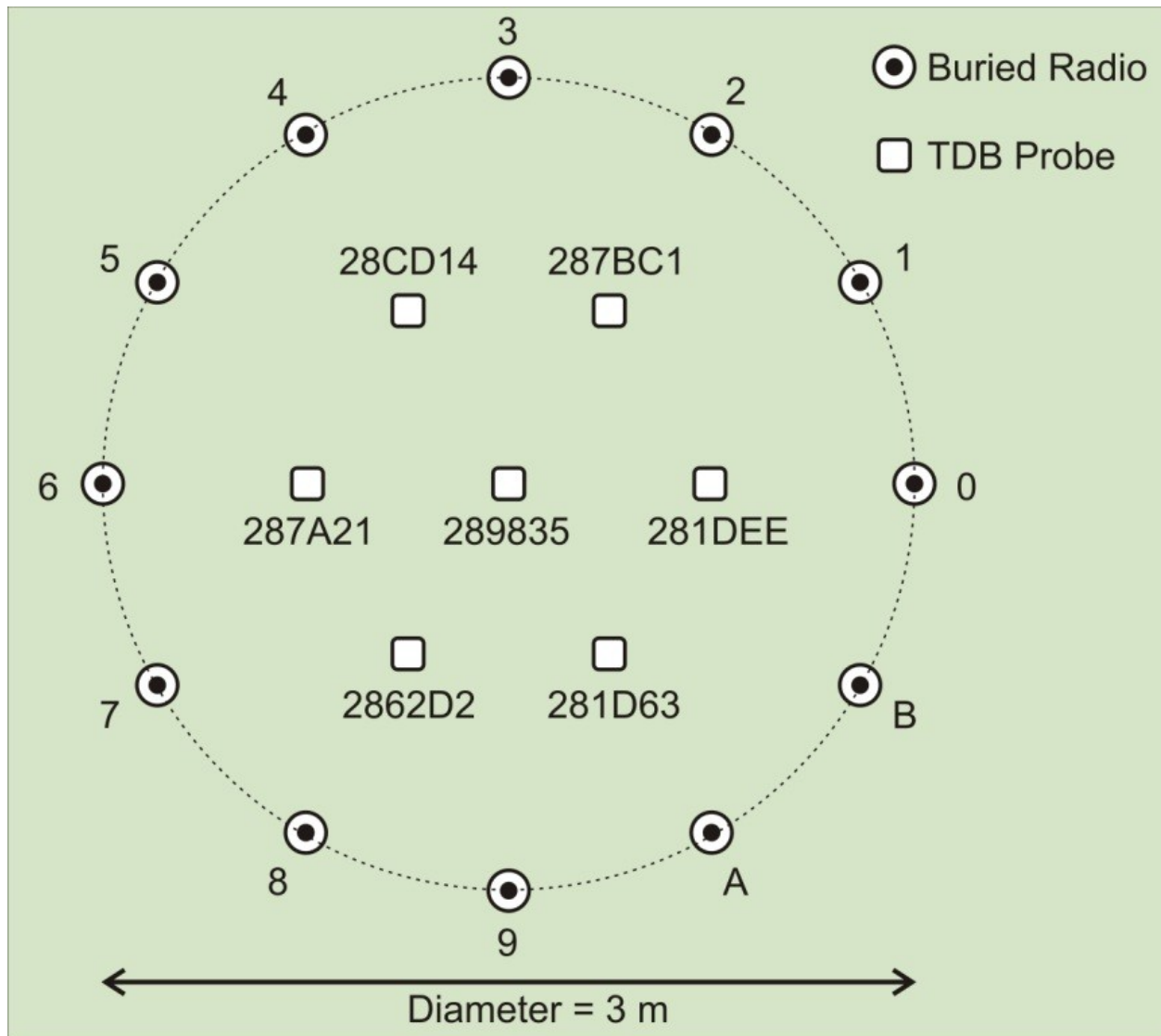


Figure 35 Layout of experimental setup for testing signal attenuation and soil moisture. The antennas for 12 motes operating at 900 MHz were lowered into the ground to a depth of 60 cm around the perimeter of a three meter diameter circle. Each mote was given a unique ID consisting of a hexadecimal value between 0→B. Seven CS616 soil moisture probe paired with temperature probes and installed inside the circle of radios. Each CS616 and accompanying temperature probe was given a unique address for identification. The CS616 sensors were installed into the top 30 cm of soil and temperature sensor in the top 8 cm of soil.

Each CS616 sensor was paired with a temperature sensor and given a unique address for identification. The soil moisture- and soil temperature data collected in fifteen minute intervals were transmitted back to The University of Iowa through a cellular modem and available in table format on a web interface specifically created for this experiment. Custom electronics sampled and transmit the output of each sensor to the database. Figure 36 shows the electronics designed to collect and transmit data to the database along with electronics needed to make RSSI measurements for one link and TDR probe with electronics used to estimate VWC.

All motes in the RSSI monitoring network were programmed identically with the exception of a unique address. The address was a hexadecimal value between zero and B. The base station orchestrates all mote transmissions, data collection and storage. All motes and base station use Maxstream's 9XStream radio modules. All radio modules were programmed with the same settings as to allow all members of the network to receive all transmissions. Unlike the motes, the base station antenna was installed above ground. Installing the base station antenna above ground improved signal strength between mote and base stations since there was approximately 60 cm of soil between the base station and any given mote. Motes use the pulse width modulated (PWM) RSSI output of the 9XStream radio module for measuring signal strength. The radio automatically outputs a pulse whose duration is proportional to the signal strength of the incoming packet. By using this functionality, the RSSI for multiple packets can be averaged as packets are received. This was a major improvement over the previous underground network experiment, where the RSSI was measured for one packet only using AT commands. In that experiment RSSI, was measured over a link every minute and the RSSI value was measured only for the previously received packet. This technique resulted in measurements that varied by up to 15 dBm between consecutive measurements, which made it difficult to clearly draw any conclusions on the relationship between RSSI and soil moisture. Figure 37 shows the experimental installation of previously described experiment in an urban setting.

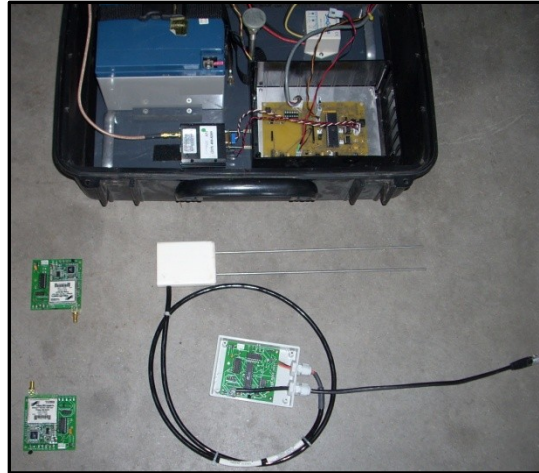


Figure 36 Components used to validate RSSI measurements in making soil moisture measurements. Top: the custom data-logger with cell modem used to collect soil moisture and soil temperature to be transmitted back to The University of Iowa. Lower left: is pair of XStream RF modules with support electronics used for measuring RSSI. Lower right: TDR probe with support electronics used in making VWC estimations.

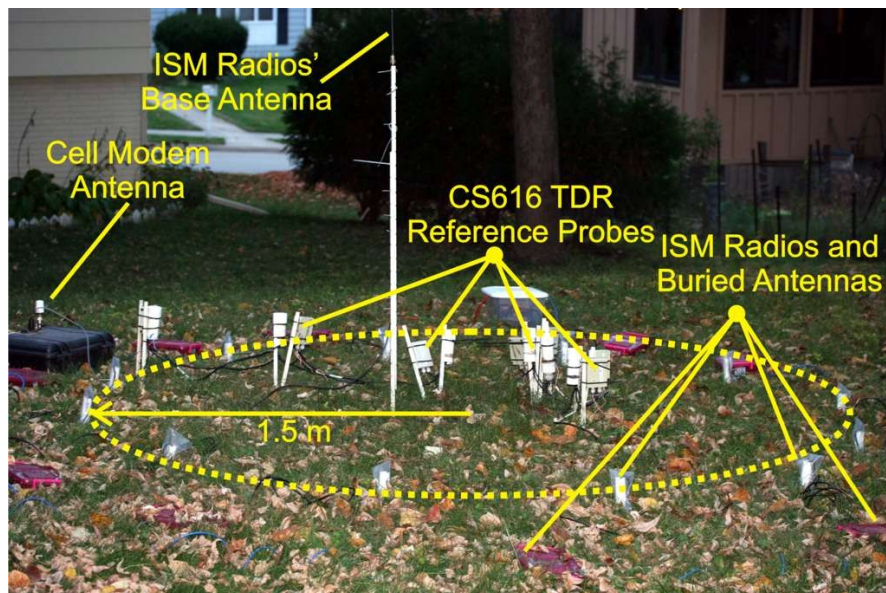


Figure 37 Experimental setup for comparing changes in soil moisture to changes in RF signal attenuation at 900 MHz as depicted in Figure 35. Seven soil moisture- soil temperature probes were installed inside a ring of 12 buried radio antennas. Data was transmitted to The University of Iowa by cellular transmission.

### Data Collection

As seen in this Figure 8, repeated RSSI measurements stabilize when measurements are averaged over more packets. To save power averages were made over 200 packets for this experiment since all equipment was run from one battery. The base station can instruct any selected mote to transmit 200 packets, followed by a series of packets that indicate to listening nodes to stop sampling the RSSI of incoming transmissions. All motes that detect transmissions, average the RSSI for incoming packets until signaled to stop sampling the RSSI. After enough time has elapsed for all 200 packets to be transmitted the base station also transmits the cue to stop sampling RSSI. This is done in case all previous cues to stop sampling RSSI may have been dropped due to poor link quality. The base station then polls the RSSI for each mote starting with zero and ending with B. The mote that transmitted the 200 packets returns the default value of -115 dBm. Any mote that didn't receive any transmissions or dropped more than 75% of the total transmissions returned the default value of -115 dBm. The default value for poor links was selected to be lower than the 9XStream's receiver sensitivity of -110 dBm. After the RSSI for all links is collected the base station records the timestamp, which mote transmitted the packets followed by the RSSI for all motes in network on a SD card. Once all values are recorded the base station sends a command for all motes to clear all internally stored RSSI values. The base station sends the request for the next mote to transmit the series of packets then repeats the process of recording the RSSI at each mote. It takes approximately four minutes to sample and record all possible RSSI measurements. Power considerations and total time of execution were also driving factors in choosing a value of 200 packets for averaging. This value allowed for the sample rate to be increased to every five minutes if deemed necessary later in the experiment. Although the total time needed to make a complete sample may seem long at nearly five minutes, the total change in soil moisture up to a depth of 60 cm may vary little in the time frame.

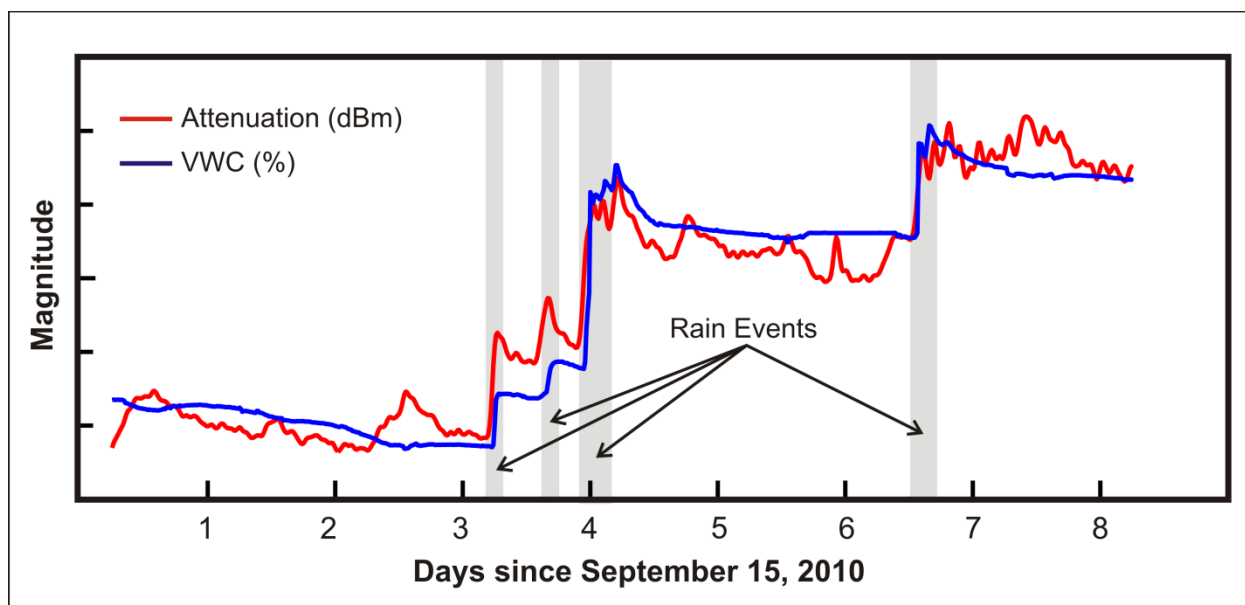


Figure 38 Normalized time series of underground link RSSI (red) and soil moisture data (blue), collected over a nine day period in mid-September 2010. Soil moisture probes were installed to measure water content in the top 30 cm of soil. Radio antennas were buried at a depth of 60 cm. During this period there were four rain events that altered soil moisture content. As the water content of soil moisture increased the attenuation of the RF signal also increased.

### Data Analysis

The real time clock (RTC) on both the soil moisture data-logger and RSSI base station provided a synchronized sample interval. Ninety six samples were collected from both systems in a twenty four hour period. The system was deployed in an urban setting in an open area with numerous surrounding trees. Little direct light fell on the sample area and the area remained shaded throughout the day. Nearly 200 mm of rainfall in the previous four weeks before installation had made the soil water content high. At deployment the volumetric water content (VWC) was observed to be about 46% using the factory provided formula. Without site specific calibration the precise value cannot be verified. Without going through the process of calibration, the CS616 can only provide the change in soil moisture over time. After installation, four rain events were observed in a one week period. Figure 38 shows data collected for RF signal attenuation for one link and VWC calculated from the soil moisture probe located within

that link over an eight day period. Both values were scaled to facilitate a visual comparison of change in attenuation compared with changes in VWC. The data shows an increase in VWC for each rain event and a corresponding increase in attenuation of the RF signal. The attenuation corresponds to the 1  $\leftrightarrow$  9 transect in Figure 35 and the VWC time series is from TDR probe 281DEE in that same figure. Outlier and dropped communication were removed from the data set and not shown.

To facilitate visual comparison the time series were manipulated as follows. First, the means for both series were subtracted. Next the RSSI values were scaled by 0.4, before plotting. The shaded areas in the figure indicate rain events which modifies the soil moisture. The figure suggest a strong correlation between VWC and link attenuation. In fact, the linear correlation coefficient, namely

$$r = \frac{\sum(x_i - \bar{x})(y_i - \bar{y})}{\sqrt{\sum(x_i - \bar{x})^2} \sqrt{\sum(y_i - \bar{y})^2}}$$

between the two time series in the figure is quite high: 0.967. Table 5 summarizes the attenuation-VWC correlation coefficient between other transect and nearest neighbor TDR probes. The correlation coefficients are generally high for all links.

Figure 39 illustrates the simple mathematical model

$$P_r = \frac{P_o e^{-\alpha R}}{R^n}$$

introduced in Chapter I of the thesis. This plot shows how RSSI changes with separation distance for underground communication. The VWC of the soil remained nearly constant during this period and varied between 52-55% for this group of data. Since the instruments were located on the perimeter of a circle there are multiple different transects of the same length. For example transects 2  $\leftrightarrow$  5, 2  $\leftrightarrow$  B and 1  $\leftrightarrow$  4 are all the same length, to name but a few possibilities. Since the soil was near saturation, not all possible links offered reliable

communication. Four distances did offer reliable communication at this VWC and are shown. Links of distance greater than 2.75 m were beyond the sensitivity of the receivers. As stated

Table 5 Correlation Coefficient for attenuation of RF transect and VMC.

<b>Transect</b>	<b>TDR Probe</b>	<b>Correlation Coefficient</b>
1 $\leftrightarrow$ B	281DEE	0.947
1 $\leftrightarrow$ B	281D63	0.939
1 $\leftrightarrow$ A	281DEE	0.854
1 $\leftrightarrow$ A	281D63	0.868
1 $\leftrightarrow$ 3	281D63	0.913
1 $\leftrightarrow$ 3	287BC1	0.927
2 $\leftrightarrow$ A	281DEE	0.923
2 $\leftrightarrow$ A	281D63	0.927
1 $\leftrightarrow$ 9	281DEE	0.967

previously the RSSI measurements were averaged over 200 packets. For each possible distance plotted, the scatter in RSSI measurements is near 6 dB and is indicative of what one would expect looking back at Figure 8 when averaging over 200 packets. The value of 6 dB is slightly higher but soil conditions also varied slightly during this period.

Since the soil was near saturation which is the worst case scenario for signal attenuation in soil, link reliability will only improve as the soil dries. The information shown in Figure 39 is also valuable for the networks depicted in Chapter IV. For underground networks operating in this type of soil, links of distance more than 2.5 m will have unreliable communication. Setting the bounds for soil conditions allows for estimation of link reliability. The data collected during this trial suggests links of distance 3 m will only have reliable communication if the VWC is

lower than 40%, while links of 1.5 m will have reliable communication under any soil conditions.

Alternatively the model can be verified by looking at the data collected over links at a single distance. Figure 40 show an interesting way of plotting the data for the model using all links at a fixed distance of 2.6 m. This plots shows all the measured RSSI for all links for distance 2.6 m for changes in VWC ranging from 46→60%. A linear fit of the data is represented by the dark line.

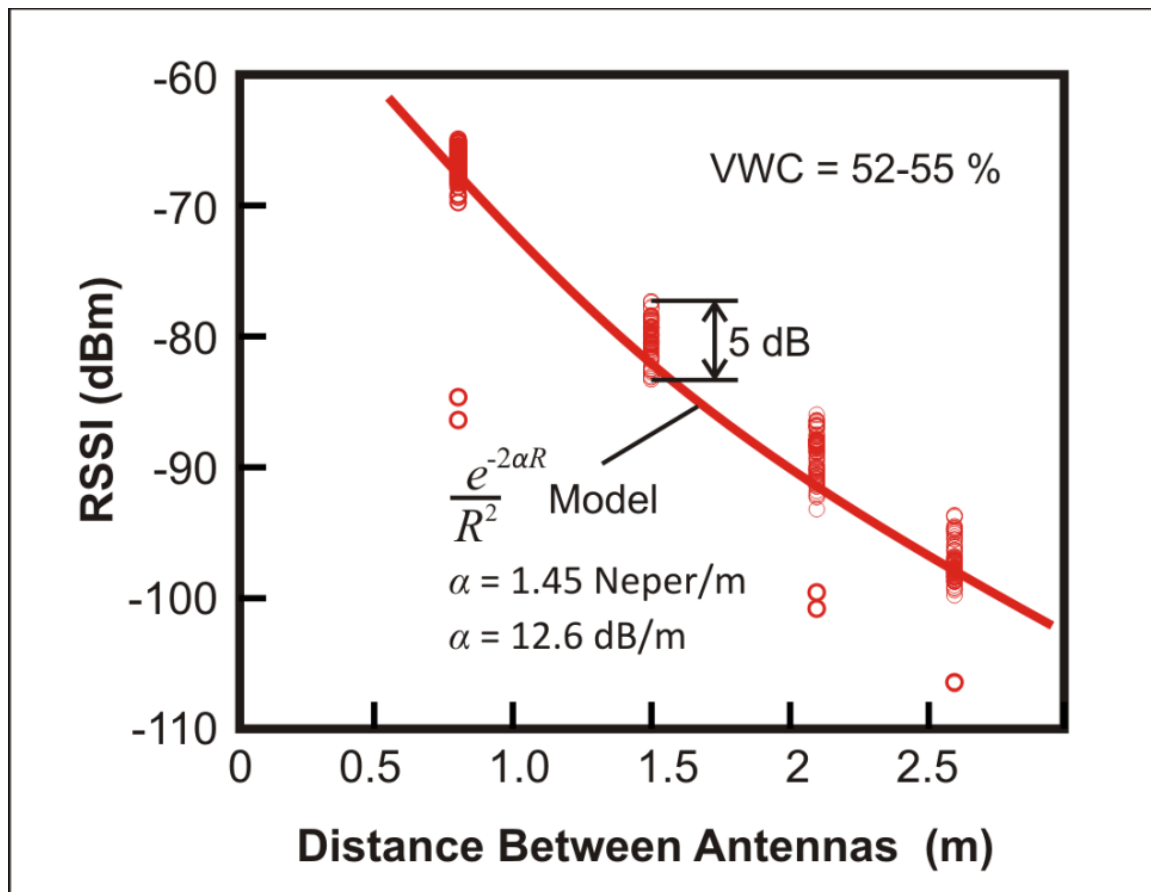


Figure 39 Measured RSSI for all possible links at four fixed distances at near a constant volumetric water content of soil of 52→55%. The data follows the simple model with  $\alpha = -18.78$  dB/m.

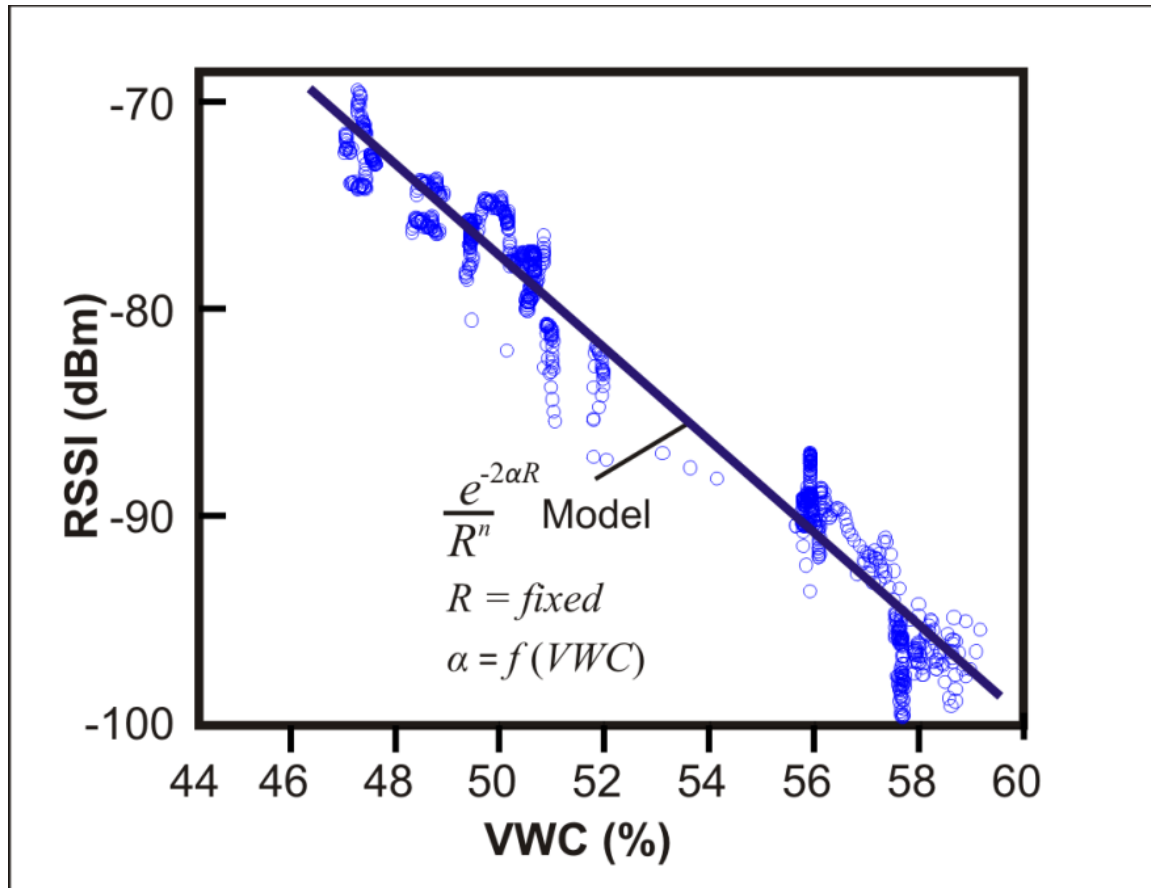


Figure 40 Measured RSSI for links of distance 2.6 m for various VWC. The data follows the model  $e^{-2\alpha R}/R^n$  for fixed distance  $R$  and  $\alpha$  is a function of VWC.

### Conclusions

It was shown in the previous chapter that it is possible to create underground networks using ISM radios. The RSSI data collected in an underground network alluded to a possible connection between signal attenuation and VWC. Attenuation of RF signals is clearly modulated by soil moisture in underground networks. This opens the door to thinking of the RF modules as a sensor capable of making distributed soil moisture measurements. An experimental underground network operating at 900 MHz was developed to validate this hypothesis. Changes in signal attenuation when compared with change in VWC followed the mathematical model

described in Chapter II of this thesis. The data showed a good correlation between attenuation and VWC.

This technique is an improvement over the existing technologies since it is low cost, straight forward to operate, easy to install and provides a distributed measurement. The cost of a single RF link is similar in price of two CS616 probes used to validate measurements. No expertise is needed to make RSSI measurements and little support electronics are needed. Installation consists of lowering antennas into PVC pipes driven into the ground. Soil moisture measurement can be made without disruptions of the area where measurements are made. This allows for the possibility to measure soil moisture around root balls of trees and other locations that were it has been traditionally difficult to measurements in the past.

Variations in soil type will effect soil moisture estimations and therefore site specific calibration will need to be preformed. This is true of many of the soil moisture sensors that are commercially available.

## CHAPTER VI

### VEGETATION WATER CONTENT

In this chapter, I describe experiments and results that strongly suggest the use of radios as sensors for measuring corn water content, and by extension, vegetation water content (Hunt et al. in press, and J. Giacomini et al. 2007). The relevance of this work is that vegetation water content can influence passive microwave remote sensing of soil moisture. This is discussed in more detail in the Conclusion section of Chapter VII.

As part of an ongoing research effort at The University of Iowa, seven rain gauge platforms are deployed in a 1×1-km cornfield near Ames, Iowa. Each site transmits its data to The University of Iowa via a cellular modem operating at 1.8 GHz, at 15 minute intervals. To monitor communications quality, the system records the received signal at each site in the field every 15 minutes. As the growing season progressed, we noticed changes in the signal strength. The signal strength data is quite noisy, yet one can clearly identify a long-term trend where the signal strength decreases as the growing season progresses and the plants progressively obscure the radios' view to the cell towers. Inspection of the data suggested a diurnal cycle. At the end of the growing season, as the plants dried out and were harvested, the signal strength recovered.

The hypothesis was that the vegetation caused these changes, and we decided to explore this possibility. This is reasonable, since it is well known that vegetation affects the propagation of radio signals (Bertoni et al. 1999). Thus, even though we did not collect signal strength data for this purpose, the data gathered between mid-May and the end of October 2007 provide an opportunity to investigate how corn affects the propagation of radio waves. One can think of this as an unplanned experiment that uses signal strength data from cellular modems in the cornfield. We were excited about the cellular-modem aspect. We performed analysis on the data (Hunt et al. in press), and the results were promising enough that we subsequently conducted a planned experiment and made high-resolution measurement of signal strength variations through a corn canopy, this experiment is discussed in detail in a later chapter. Concurrently, other researchers

are recognizing the feasibility of using the commercial cellular communication infrastructure for hydroscience research (David et al. 2009, Leijnse et al. 2007, Messer et al. 2007, Messer 2006).

### An Unplanned Experiment

As I mentioned above, the unplanned experiment refers to analysis of the signal strength data obtained from seven cellular modems deployed in a cornfield near Ames, Iowa, during 2007. The deployment was part of a NASA-funded project. Figure 41 top shows the NASA Rain Gauge (NRG) deployment in the corn field relative to the cellular tower. Figure 41 bottom shows a dual tipping bucket rain gauge platform developed by IIHR at The University of Iowa for monitoring rain fall. To monitor the health of the data collection system, the cell modems record the signal strength at the cell modem located in the field. Figure 42 illustrates the location of each rain gauge relative to the local topography. Gauges NRG01, NRG02 and NRG03 are in the flat part of the field with unobstructed views of the cell tower. Gauges NRG04, NRG05 and NRG06 were located on the opposite side of a small hill and NRG07 is located in a depression in the southeast corner of the field. The topography between the deployment field and cell tower was relatively flat.

The field north of the experimental site was planted with soybeans, whose height at maturity was shorter than the antenna height. Gauges NRG01, NRG02 and NRG03 were located along the north edge of the field and had no vegetation to block their views of the cellular tower. Gauges NRG04, NRG05 and NRG06 were all located in the middle of the corn field inside of the canopy. NRG07 was inside of the canopy approximately 20 meters from the southern bordering gravel road and approximately 20 meters from the east bordering highway. All antennas were located at a height of 0.6 meters above ground. At maturity the corn reaches a height of approximately 2.5 meters. This placed the antenna in the lower one fourth of the total canopy height. Around the second week of June the corn had overtaken the modem's antenna and the corn reached its final height around the second week of July.

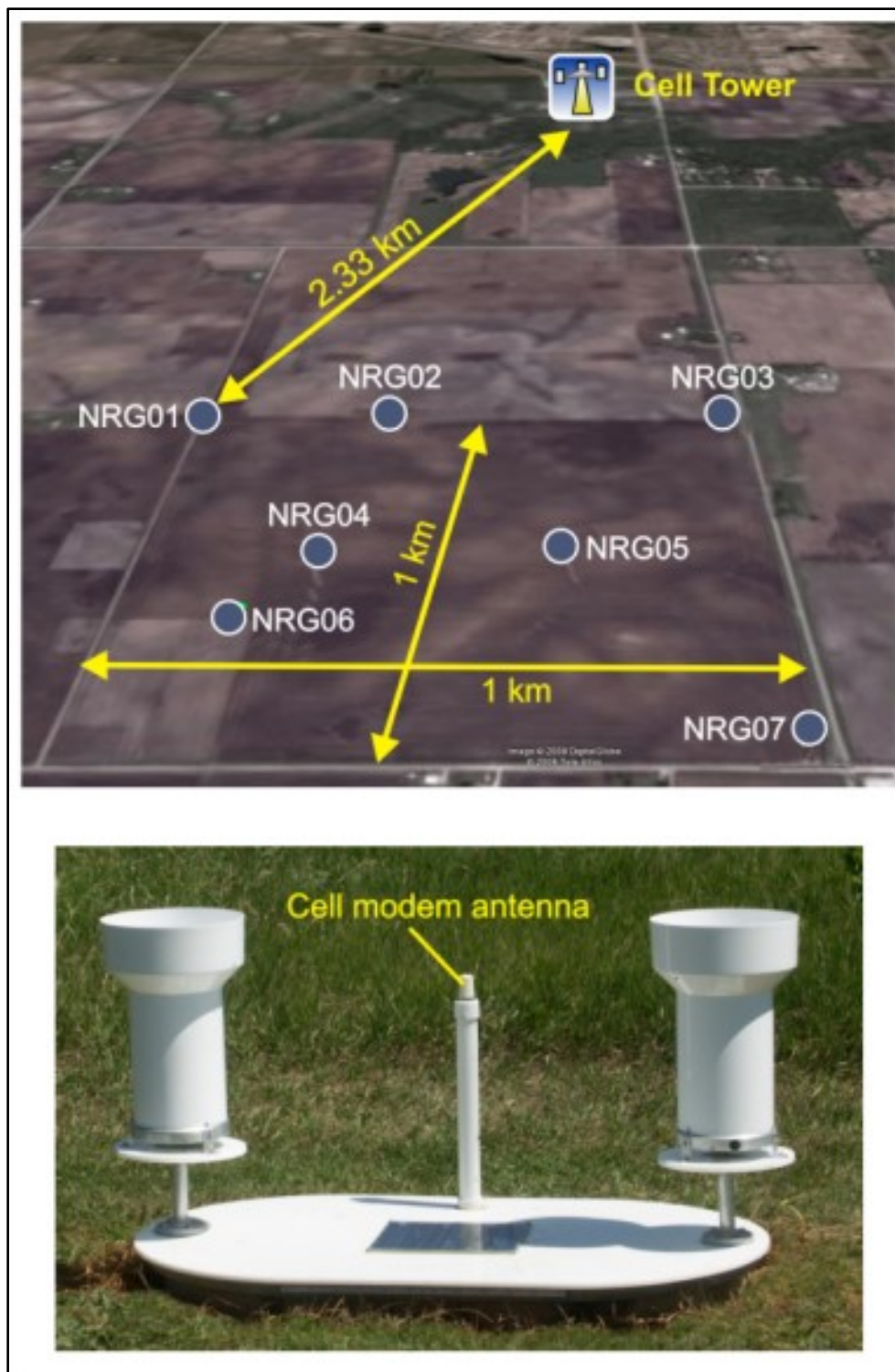


Figure 41 The top panel shows the experimental site at Ames, Iowa, and the bottom panel shows the dual tipping platform that houses a cell modem for relaying data. We observed variations in the cell modem RSSI, which inspired the techniques outlined in this chapter.

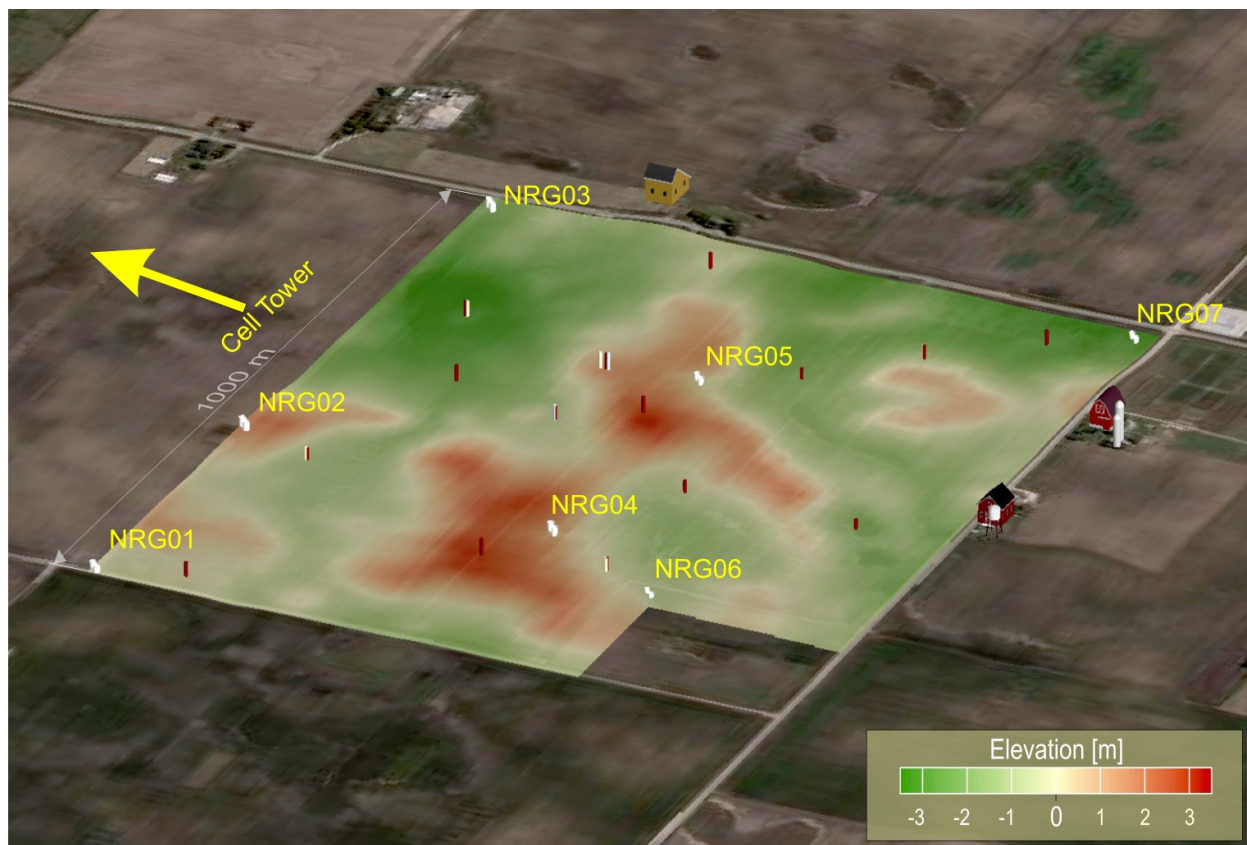


Figure 42 Gauges NRG01, NRG02 and NRG03 are in the flat part of the field with unobstructed views of the cell tower. Gauges NRG04, NRG05 and NRG06 were located on the opposite side of a hill from the tower and NRG07 is located in a depression in the southeast corner of the field. The topography between the deployment field and cell tower was relatively flat.

Figure 43 shows the RSSI time-series for one of the sites in the field. The time-series exhibits a long-term trend with decreasing RSSI as the corn grows, and a signal strength recovery as the corn senesce. There is a distinct jump in the RSSI on the day that the farm manager harvested the corn. Additionally, if one zooms into the data, the fluctuations suggest a diurnal cycle.

### Simple Propagation Model

Figure 44 depicts a simple propagation model for the radio signals from the tower to a cell modem at the cornfield. The direct transmission path from the cell tower to a modem in the

cornfield consists of a distance  $L_a$  about 2.3 km through the air, and a distance  $L_c$  that ranges from 0–1 km through the corn. Radio waves are attenuated far more by vegetation than air, and we expect the average attenuation of signals between the cell tower and a cell station in the field to be proportional to  $L_c$ . We also expect the signal attenuation to be proportional to the water content of the corn. Additionally, we expected that rain would have a big impact on the signal strength. We did not consider the effects of dew on the corn.

### Determining Corn Water Content

To investigate the relationship between RSSI and plant water content, we collected corn plant samples over a 2-month period from mid-August until mid-October. Since the original experiment looked at plant water content, samples were not collect at a consistent time of day. Some samples were collected very early in the morning while the dew was still on the plants. Other samples were collected in the afternoon when all the dew had dried off of the plants. At this point little thought was given to a possible daily cycle generated by the dew on the plant's leaves.

The sampling process consisted of collecting six sets of whole corn plants near antenna locations. The plants were selected to be of good representation for the plants in that area. Some samples collected in the morning may have contained dew on the leaves. No attempt was made to remove the dew from the plants during the collection process. We divided each plant into 4 sections, namely "top", "middle-top", "middle-bottom", and "root". We sealed the plant in bags at the field to prevent water loss. At the lab, we weighed the bags, and then dried samples by opening the bags and circulate air over them, see Figure 45. Once the plants lost most of their water, we dried the samples further in a microwave oven, taking care not to burn the samples. We then weighed the plant material again and calculated the total water content of the plant by subtracting the dried sample mass from the original sample mass.

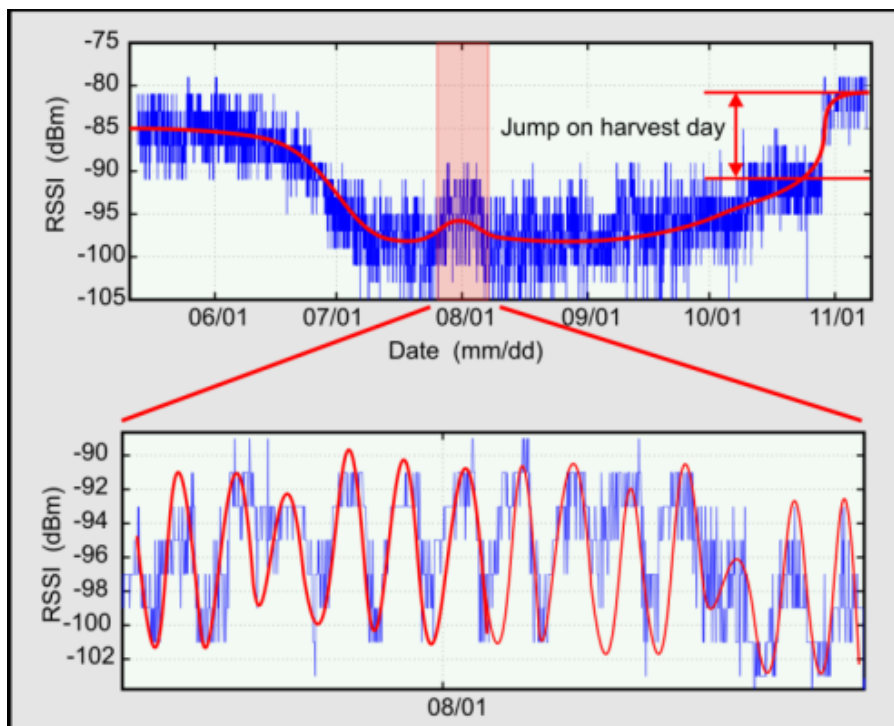


Figure 43 The top plot shows RSSI time series for Station 7. One can clearly observe a long-term decrease, and then a gradual increase in the received radio signal. On the day the corn was harvested, the average RSSI jumped 10 dBm. Other stations showed similar behavior. The bottom plot is an exploded view of time series plot that suggests that a diurnal cycle in the RSSI signal may be present as well (red line, drawn in by hand).

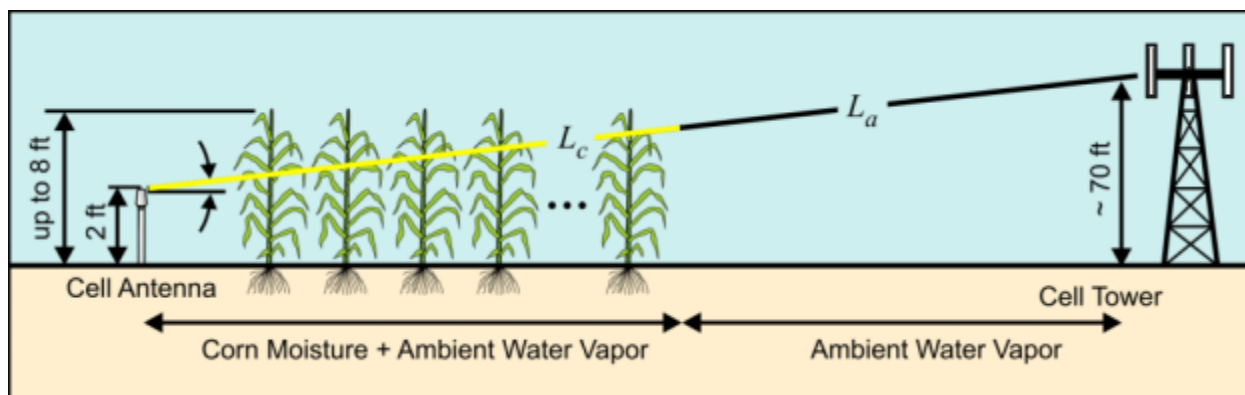


Figure 44 Cell modems in the rain gauge network at the experimental site in Ames transmitted through a combination of corn and air. Antennas are located in the lower one fourth of the mature plant height.



Figure 45 Drying corn plants to determine plant water content. Sample plants were harvested from the field, weight, dried and reweighed to calculate the water contained in the plant. We performed this 6 times over the summer of 2007.

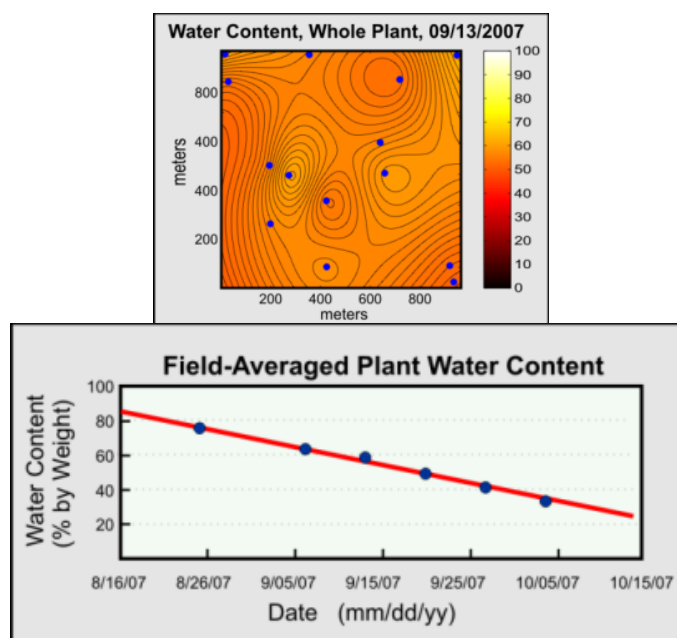


Figure 46 The top plot is a contour plot of interpolated plant water content (by weight), for the whole plant. The uniformity indicated here is representative of the water content at other times and individual parts of the plants. Dots indicate collection locations. The plant water content was uniform with respect to weight, so we averaged all values for a day. The bottom plot shows the results.

Next we analyzed the plant water contents. We were surprised (as electrical engineers) that green corn can be by weight, 80% water. Thus, from the perspective of a radio wave, a corn field appears as a matrix of straws filled with water. Second, we did not see any significant variation in plant water content with respect to height. The “top”, “middle-top”, “middle-bottom”, and “root” parts all have approximately the same amount of water. Third, on any given day, we did not observe major variations of the plant water content across the field. Figure 46 shows an interpolated contour plot of the plant water content on one day, indicating a field average of about 60%. Because plant water content was uniform with height and across the field, we averaged all values for a particular day. These values are also shown in Figure 46, indicating how the plants dried over the 2-month period.

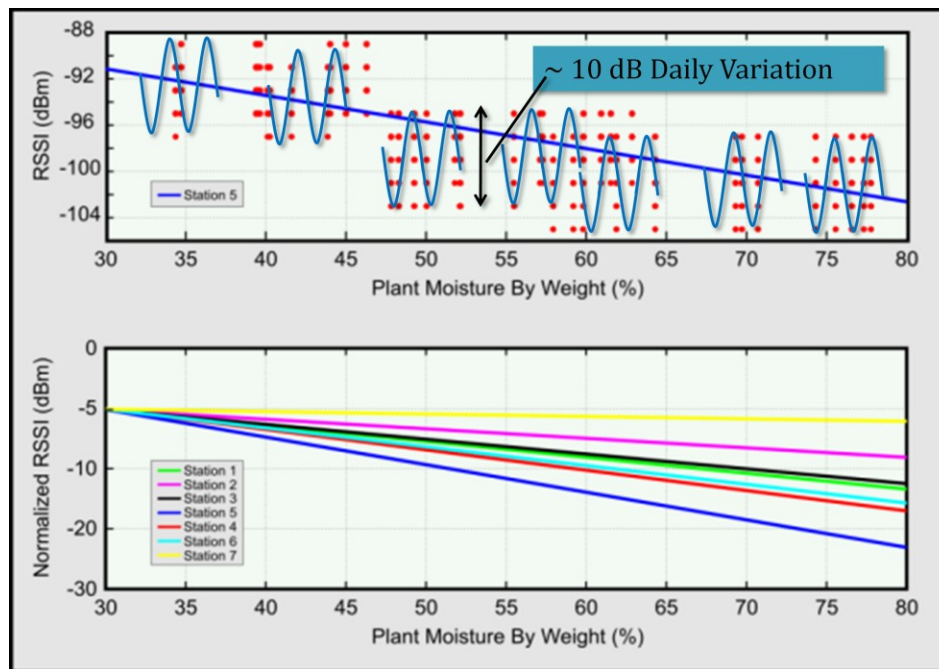


Figure 47 The top plot shows RSSI as a function of plant water content for Station 5. The bottom plot shows normalized linear fits for all stations. Surprisingly, Station 7, which transmits through the longest path of corn, shows the least variation of plant water content.

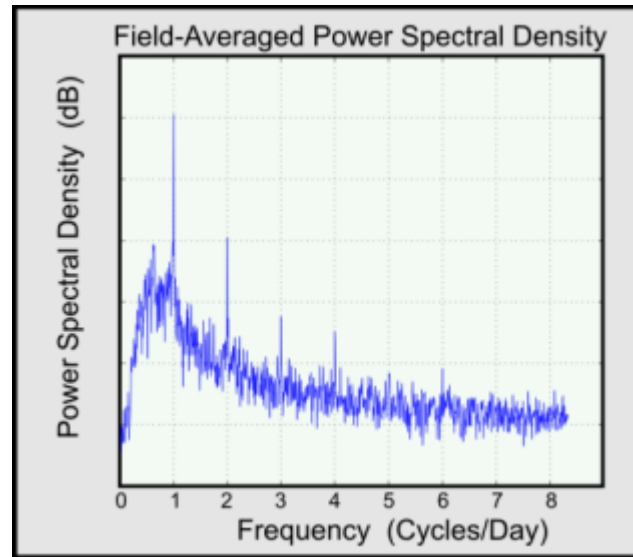


Figure 48 Average (for all stations) power spectral density of RSSI. One can clearly observe a spike at 1 cycle/day, indicating a diurnal cycle in the RSSI. This is consistent with results from Empirical Mode Decomposition (EMD) and Data Stacking, see below.

#### Corn Water Content and RSSI

Figure 47 (top plot) shows the RSSI as a function of plant moisture content for Station 5. There is significant scatter; this is due to the quantization of the RSSI measurement and the overriding daily cycle. I believe one can conclude that RSSI decreases with increasing plant moisture. Figure 47 (bottom) plots the least squares fit of daily average vs. vegetation water for all stations. To ease comparison between stations, we normalized the least squares fit so all stations have the same RSSI at the minimum water content. This graph illustrates that the attenuation of RSSI is a function of both vegetation water content and the distance the signal travels through the corn. For example, stations 1, 2 and 3 (light colored lines), which have a clear view to the cell tower, show less change in RSSI as the vegetation dries than do stations 4, 5, and 6 (dark colored lines), which transmit through the corn. An anomaly is station 7; its attenuation is the least dependent on vegetation water content despite transmitting the longest distance through the corn. A possible reason for this is an elevated area that partially obscures the transmission path between Station 7 and the cell tower.

## Diurnal Cycles

Inspection of the time series data suggested that the cell modem RSSI exhibits a diurnal cycle—see Figure 43. We confirmed a diurnal cycle using three different methods, namely Fourier-based spectral analysis, Empirical Mode Decomposition, and data stacking.

### Fourier Spectral Analysis

We performed a spectral analysis of the RSSI data to confirm a diurnal cycle. To obtain a complete set of evenly spaced data points, missing data points were interpolated by averaging the ten data points before and after the missing point. Next, we detrended the data by subtracting the three-day moving average from each data point. Next, we divided the data for each station into four sections and computed the power spectral density after applying a Hamming window (Press et al. 2007). Finally, we averaged the power spectral densities from all the stations to obtain a field-averaged power spectral density. This field-averaged power spectral density contained pronounced spikes at one cycle per day and harmonics of a cycle per day, confirming a diurnal RSSI cycle.

### Empirical Mode Decomposition

Empirical mode decomposition (EMD) is a method of breaking down a signal without leaving the time domain (Huang et al. 1998, Wu and Huang 2005). One can compare it to other analysis methods such as Fourier- and wavelet decomposition. This process is useful for analyzing natural signals, which are most often non-linear and non-stationary. EMD filters out functions that form a complete and nearly orthogonal basis for the original signal. The functions, known as *Intrinsic Mode Functions* (IMFs), are sufficient to describe the signal. Since the IMFs are in the time-domain and of the same length as the original signal, this allows for varying frequency in time. Obtaining IMFs from real world signals is important because natural processes often have multiple causes, and each of these causes may happen at specific time intervals. This type of data is evident in an EMD analysis, but hidden in the Fourier domain or in wavelet coefficients.

Figure 49 shows an EMD for the cell modem RSSI. The EMD for the other stations are very similar. Of interest to us is the daily periodic mode, which is the third plot from the top in the figure. An expanded view of the daily periodic mode is shown in Figure 50, which clearly shows a diurnal cycle.

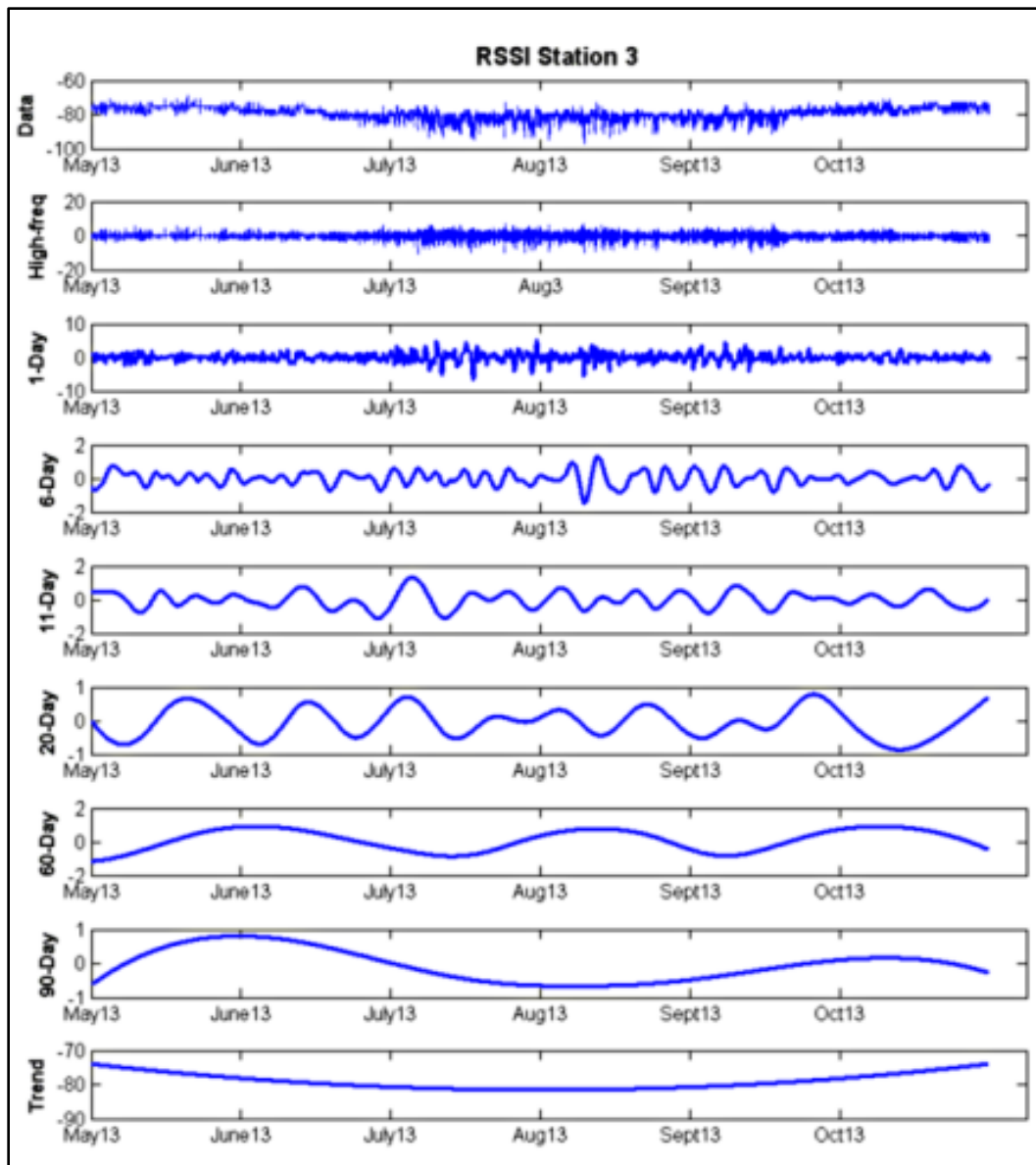


Figure 49 Empirical mode decomposition for RSSI data from Station 3. EMDs for other stations are very similar.

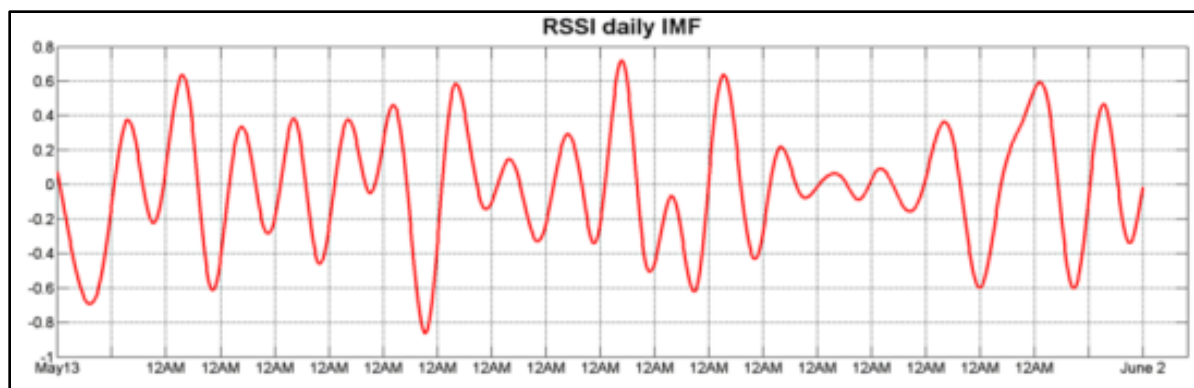


Figure 50 Zoomed in plot of the daily periodic mode, showing a clear diurnal cycle.

### Data Stacking/Averaging

We also used data stacking to explore the daily cycle of the RSSI data. The aim is to compute RSSI data for an “average day”. First, we detrend the data as we describe above. Then we divide a station’s data into runs that correspond to days. Then we stack the days on top of each other and average across days. One can think of the result, shown in Figure 51, as the signal variation with time for an average day. Referring back to the location of the cell modems in the field (see Figure 41) note that some stations transmit through the corn, while others have a clear view to the cell tower. We partitioned the data into these populations in Figure 51, and both clearly show a diurnal variation. Additionally, the peak-to-peak signal variation is larger for stations transmitting through the corn than for stations with a clear path to the cell tower. This suggests that both atmospheric conditions and the corn contribute to RSSI fluctuations.

### Effect of Rain on Signal Strength

From the previous analysis it is clear that corn water content strongly affects cell modem RSSI, but what about rain—how does that affect cell modem RSSI? Since rain gauges were deployed in the field, we were able to evaluate the effect of rain on RSSI. Comparing the RSSI time series with the time and rate of recorded rainfall showed that rain did not appear to affect

RSSI. Furthermore, a scatter plot of RSSI and rainfall (Figure 52) shows that RSSI and rain are *not* significantly correlated.

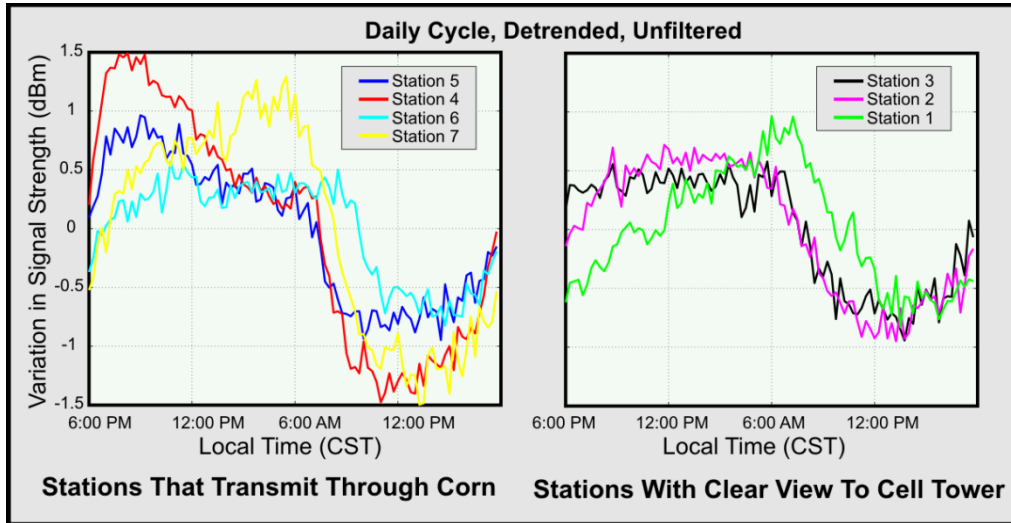


Figure 51 An “average day” RSSI obtained using data stacking. The left plot is for stations that transmit through the corn, while the right plot is for stations that have a clear view to the cell tower.

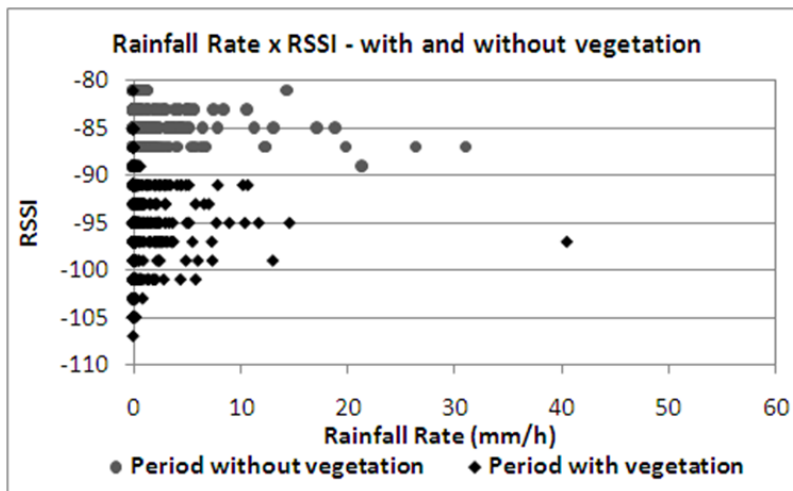


Figure 52 Scatter plot of cell modem RSSI vs. rainfall rate. The data suggests that there appears to be no correlation between rainfall and RSSI of the cell modem.

The result may be somewhat surprising to some, but one can explain this as follows. The attenuation of radio waves at 2.4 GHz by rain is small (Messer 2007). Even at high rain rates, say 150 mm/h, the attenuation at 2.4 GHz is on the order of 0.096 dBm/km (Press et al. 2007). For the approximately 2-km length between the cell tower and the modems, the attenuation of the tower/station link is on the order of 0.33 dBm. Figure 44 also shows that rain water collecting on the plants' leaves has little effect on the signal strength. The next chapter explores the effect of signal strength as rain collects on the plants' leaves.

### Conclusions

One can relate cell modem and radio module RSSI to corn water content. The presence/absence of vegetation influences signal strengths, as shown by the sudden increase in RSSI when the crop was harvested. The results from the cell modem (unplanned) experiment shows that signal strength is inversely proportional to the distance the signal propagates through the vegetation. In addition, the signal strength is also inversely proportional to vegetation water content. For both the cell modem RSSI and the RF module (Chapter VII) RSSI one can observe long-term changes in signal strength data that are similar to the annual changes in the corn. Inspection of the time-series data, Fourier spectral analysis, and Empirical Mode Decomposition (EMD) reveals clear diurnal cycles that one can relate to corn water content. There is also a diurnal cycle in RSSI, which is similar to the diurnal pattern in vegetation water content. Finally, observations indicate that rain does not affect RSSI significantly. This includes rain suspended in the air and any rainfall covering the exterior of the plants.

I conclude that the signal strength of cellular communications can be an effective tool for monitoring the state of vegetation in an area. Besides directly deploying cell modems to monitor vegetation characteristics, RSSI data from sensors deployed for other purposes or from cellular communication networks can also be analyzed to monitor vegetation. Such measurements can be made with very limited data plans for the modem. RSSI measurement can be made by "pinging" the tower without an additional need to transmit data. There is no cost involved in

making RSSI measurements at the modem but a service plan is needed to get access to make measurements.

Terrestrial satellite remote sensing often use microwave emissions, two examples are the Soil Moisture and Ocean Salinity (SMOS) mission of the European Space Agency (SMOS 2010) and the upcoming Soil Moisture Active and Passive (SMAP) mission of the National Aeronautics and Space Agency (SMAP 2010). Both use terrestrial microwave emissions to monitor soil moisture. The effect of vegetation on terrestrial microwave emissions is well known (Hornbuckle 2004), but vegetation characteristics vary in time and space. Measurements made by cellular modems potentially offer a way to quantify the state of vegetation over a large area over the entire season.

## CHAPTER VII

### LEAF WETNESS

The conclusions from the unplanned experiment were that corn water content affected the RSSI, also seen in Giacomini et al. 2007, while rain didn't have a significant effect. We hypothesize that during rain, water that accumulates on the plants attenuate the radio signal, while the rain itself causes little attenuation. Further, the RSSI has a clear diurnal cycle. Our hypothesis is that dew on plant leaves attenuates the radio signals, and by recording the received signal strength, one can detect changes in leaf wetness (Niemeier et al. 2009). Further, such measurements are distributed/volume measurements that counters sampling errors inherent in point measurements.

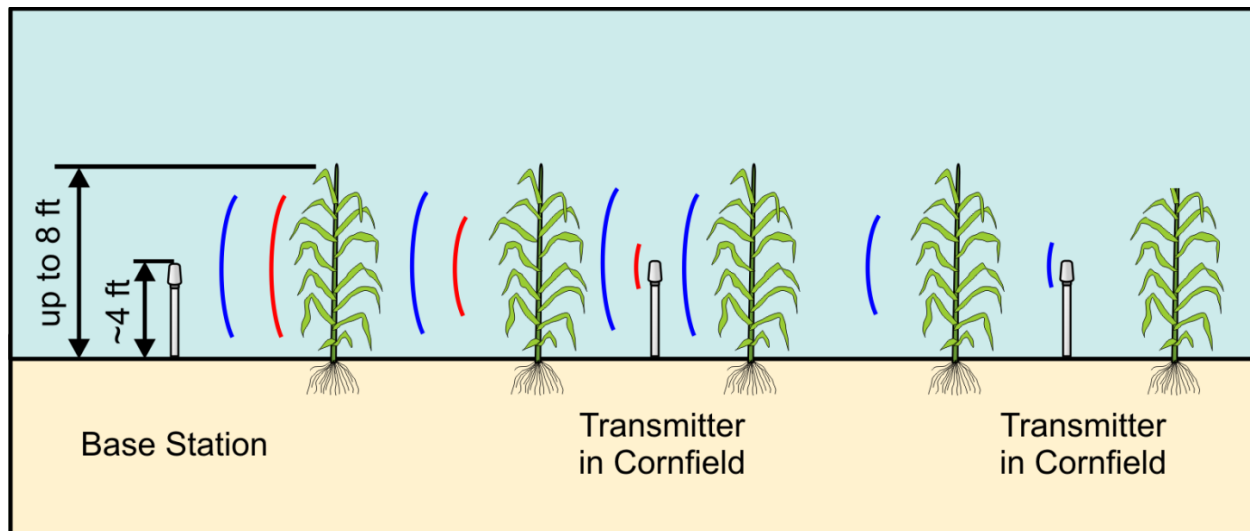


Figure 53 Schematic of experimental concept. Small, low power radios are placed inside a corn field and transmit to a base station outside of the field. Leaf wetness modulates the attenuation through the canopy. The base station records the received signal strength indicator (RSSI) and allows one to infer leaf wetness.

We devised an experiment to investigate the observed daily cycle using inexpensive radios as leaf wetness sensors. We conducted the experiment during the summer of 2009. We collaborated with other researchers who deployed leaf wetness sensors in the experimental field at the same time. This experiment used radios operating at 2.4 GHz, which has a similar wavelength to L-band radiometers. L-band radiometers operate at wavelength of 15-30 cm, corresponding to a frequency of 1–2 GHz.

Figure 53 illustrates the idea behind the experiment of how the RF modules were deployed in the field. Module antennas were located in the middle of the corn plant and all transmissions for this experiment were contained within the canopy. It was decided that a single node would be deployed with an unobstructed link for use as a control.

Figure 54 shows the experimental setup in the field near Ames. Nodes were placed on level ground, and the radio links were all contained within the canopy, except for one placed in a bare area adjacent to the corn field. This latter node provides a control link—exposed to the same rain, atmospheric conditions, but it does not transmit through the corn canopy. A control link was one of the main elements missing in the vegetation water content experiment. There were no obstructions between the control and the base station. The control was placed along an access road separating the validation field from the neighboring field. A small amount of ground vegetation did grow in the path to a height similar to the antenna heights during the time of the experiment. The control link was installed at a significantly farther distance from the base station, than nodes installed within the canopy. We chose the antenna heights to be near the middle of the corn plant. Early in the experiment, we observed that the majority of the dew accumulated on the top 2/3 of the corn plant. The rows of corn were spaced approximately 30 inches apart and were perpendicular to the communication links. Radio nodes were collocated with traditional leaf-wetness sensors operated by our collaborators. There were six radio nodes in the field. We had rain data available from and dual tipping bucket rain gauge stations in the field.

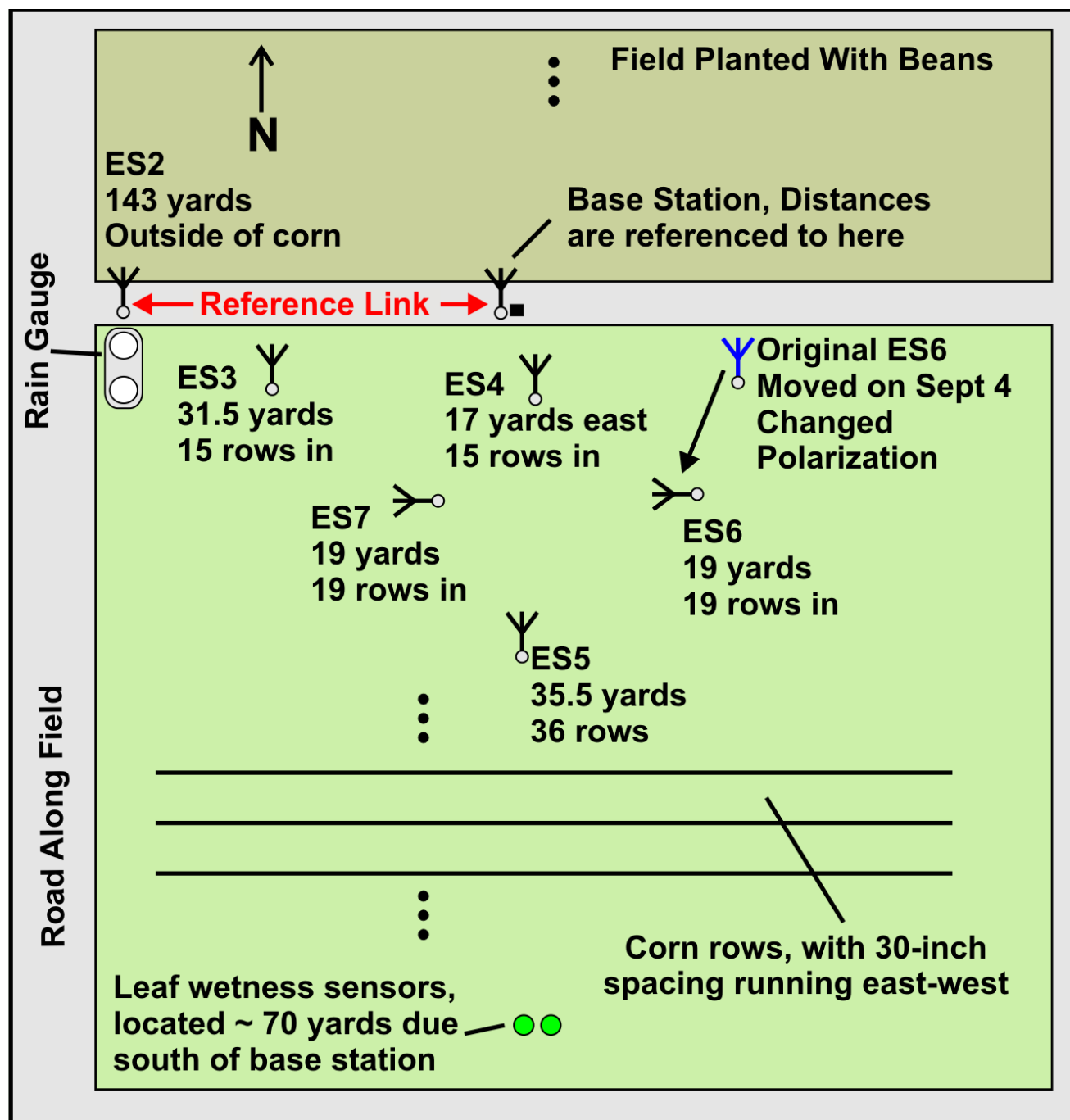


Figure 54 Locations of six RF nodes and base station collocated with rain gauge and leaf wetness sensors in the field in Ames. Node ES02 was used as a control and had an unobstructed view of the base station, all other nodes were located within the canopy.



Figure 55 The bottom panel is an example of a resistive leaf wetness sensor. In a resistive leaf wetness sensor, a change in resistance occurs at the wet-dry transition. The change in resistance is in the range of 50 k $\Omega$  to 200 k $\Omega$ . The top panel is an example of a dielectric leaf wetness sensor. A change in the dielectric constant occurs as the sensor wets and dries. The manufacturer claims the sensor can detect trace amounts of water/ice on the sensor. Both of these types of leaf wetness sensors merely model the leaf of a plant.

Figure 55 shows typical sensors used in leaf wetness measurements. In a resistive leaf wetness sensor, a change in resistance occurs at the wet-dry transition. The change in resistance is in the range of 50 k $\Omega$  to 200 k $\Omega$ . For best results, the leaf wetness sensor should be field calibrated since the transition point will vary for different areas and vegetation. The figure also shows an example of a dielectric leaf wetness sensor. A change in the dielectric constant occurs as the sensor wets and dries. The manufacturer claims the sensor can detect trace amounts of water/ice on the sensor. Both of these types of leaf wetness sensors merely model the leaf of a plant and therefore may not be indicative of the amount of dew on the plants. As is the case when the plant enters the end of its life cycle and leaves wither as they dry. Total leaf area decreases and must be taken into account when calculating the appropriate amount of water on the leaves relative to the leaf wetness measurement. The modulated RF signal through the vegetation is primarily a function of the amount of dew on the plant and amount of water in the plants. Changes in RSSI give a true indication of the change in the amount of water between the links.

The base station measured and recorded the average received signal strength of each remote node. The radios used for this experiment were Model 24XStream produced by Digi International. This radio uses frequency-hop spread spectrum techniques to combat multipath and has several different user-selectable hopping sequences. This model also has a pulse width modulated output proportional to the RSSI of the incoming packets. This allowed for quick averaging of multiple received packets. We recorded the average RSSI for each node every two minutes, which consisted of up to 120 packets. Each packet consisted of eight ASCII characters along with the additional overhead need for the 24XStream.

The 24XStream has a transmit power level of 50 mW (17 dBm) and a receiver sensitivity of -105 dBm at a throughput data rate of 9600 bps. Remote nodes consisted of a 24XStream connected to an ATmega8 microcontroller. Both radio and microcontroller were put in low power sleep mode when not transmitting data packets to the base station. The majority of the power consumption of the remote nodes could be attributed to the transmission of 120 data

packets. 26-Ah batteries provided power for remote nodes and base station. At a sample rate of two minutes, the battery life was estimated to be approximately 45 days. Since we planned for a 50 to 60-day experiment, we used solar panels to augment the batteries. Figure 56 shows some of the equipment used in the experiment. Our collaborators placed four leaf wetness sensors at several locations throughout the field, with pairs of sensors at heights of 1/3 and 2/3 of canopy height. They collected leaf wetness data every 15 minutes.

We placed the equipment in the field for a two-week period prior to August 21, 2009. We spent this two-week period altering antenna heights and node locations. By August 21, the corn plants were mature and had stopped growing. Around September 10, 2009 corn plants began drying out. By October 10, 2009 the corn was at the end of its life cycle and all equipment, except the rain gauges, was removed for field harvest.

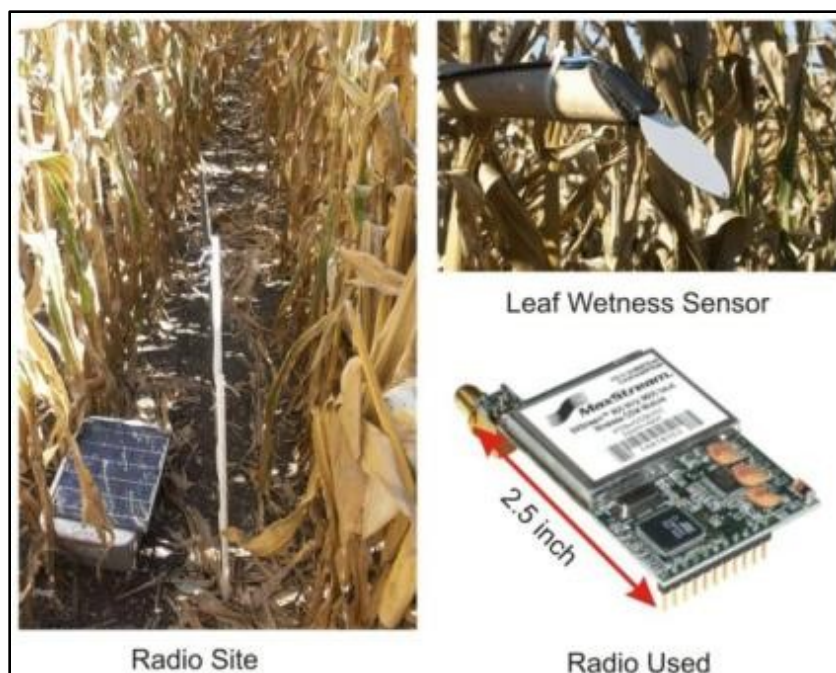


Figure 56 The radio antennas were installed in the center of the cornrows at about half of canopy height. Leaf wetness sensors were installed at one third and two-thirds canopy height. 2.4 GHz RF modules provided the links for making RSSI measurements.

### Data Analysis

Figure 57 shows a time series for all data types collected over a 50-day period from August 21 until October 10 in 2009. Data shown in red is the received signal strength of remote node ES3 (see Figure 54) located inside of the canopy. The average of all four leaf-wetness sensors located at heights of 1/3 and 2/3 canopy height is shown in green. The average of the rainfall measurements collected by the dual rain gauge tipping buckets is shown in blue.

Since the sample rates were different for the various instruments, the first step in data processing was to provide a uniform sample interval. The two-minute averages for the RSSI data were averaged to 15-minute intervals to match leaf wetness and rain data. The second step in processing the data was to eliminate the gradual long-term change in plant water content as the plant dries and fixed attenuation due to different link distances. RSSI time series were filtered using a 96-point (equivalent to 1 day) zero phase moving average digital filter. The result was subtracted from the original series and the results for remote node ES0 is shown in Figure 58.

Once all the remote node data were detrended, RSSI for links ES3, ES4, and ES5 were averaged for comparison with leaf wetness sensor data. Figure 59 shows the combined average of links ES3, ES4, and ES5 along with the data collected for the reference link. The reference link outside the corn shows much less variation, supporting the hypothesis that the plant moisture modulates RSSI.

To establish if a daily cycle was present in the system, we calculated an “average day” for the RSSI canopy nodes. The average day consist of all data point averaged at the same time every day for the entire 50 day period. Figure 60 shows the average day calculated for nodes located within the canopy (red) along with average day calculated for reference node (black) and leaf wetness sensor nodes (green). Both rain data and RSSI data was sampled using Coordinated Universal Time (UTC) and leaf wetness sensor data was collected using Central Standard Time (CST). Five hours was subtracted from the leaf wetness data to convert it to UTC time so to match the RSSI and rain data.

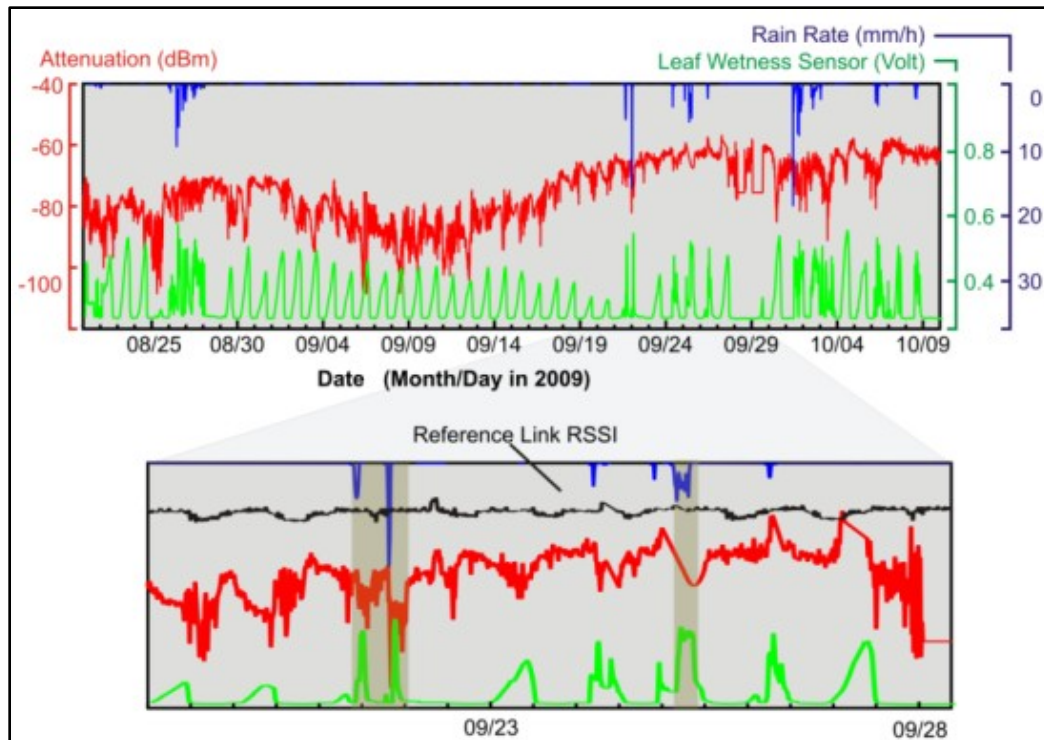


Figure 57 Time-series of RSSI from ES3 (red), voltage from leaf wetness sensor (green), and rain rate (blue). One can observe long-term increase in RSSI as the corn dries out, as well as high-frequency fluctuations. Our hypothesis is that these high frequency fluctuations are related to leaf wetness. The bottom plot is a zoomed-in section of the time-series showing how rain changes the leaf wetness and attenuation, while the RSSI of the reference link (black) is essentially unaffected by rain.

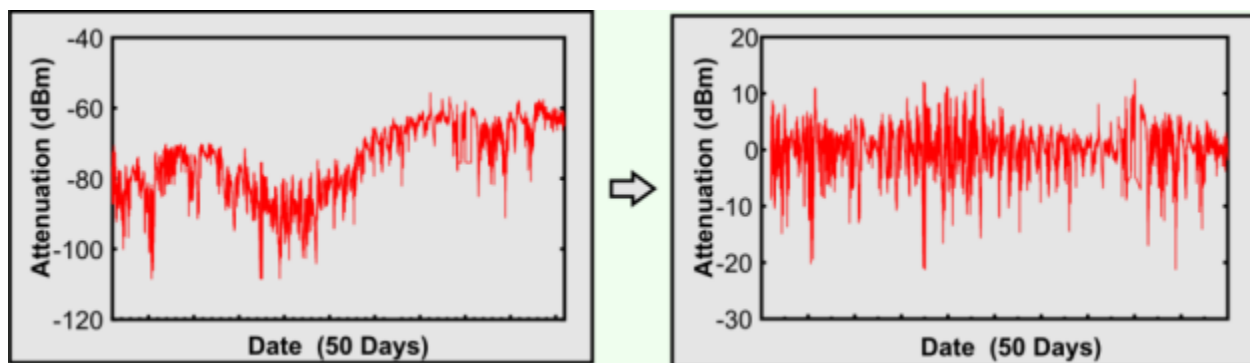


Figure 58 The left plot shows original RSSI data for site ES3 sampled at 2-minute intervals. The right plot is the detrended data averaged to 15-min intervals, and normalized to 0-dBm attenuation.

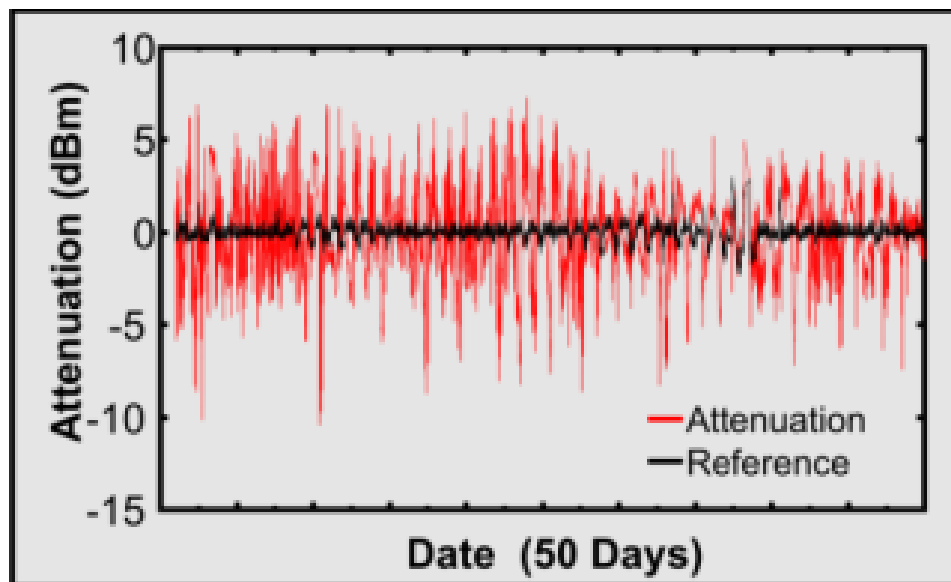


Figure 59 RSSI for links ES3, ES4, and ES5 were averaged for comparison with leaf wetness sensor data. The reference link outside the corn shows much less variation, supporting the hypothesis that the plant moisture modulates RSSI.

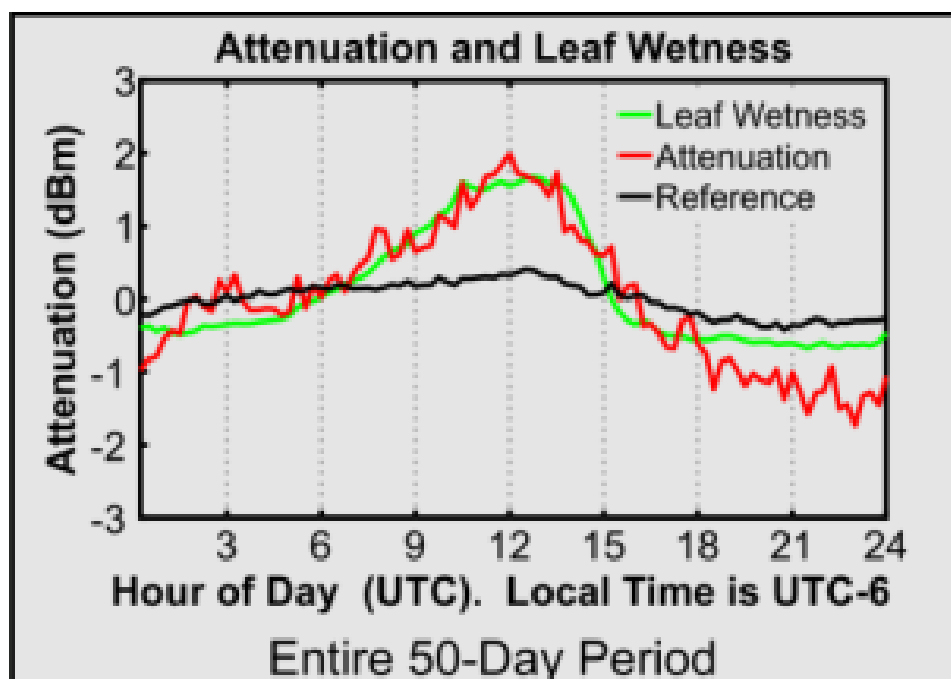


Figure 60 The plot shows an “average day” leaf wetness and RSSI for both canopy nodes and the reference link.

Results suggest a clear relationship between leaf wetness and attenuation. Significantly-smaller variation in attenuation of reference link outside of corn, despite being four times farther from base station, implies water on plants is major cause of attenuation. The variation of the reference node may be attributed to atmospheric vapor or minimal amount of vegetation that grew between the reference link and base station. This particular leaf wetness sensor has a threshold set by the user. The threshold sets the lower limit of the sensor during dry conditions and is evident in the flat minimum of Figure 61.

Leaf wetness sensors do not distinguish between rain events and dew. The effect of dew is different from the effect of rain on the signal attenuation. Rain collects primarily on the top of the leaf, and dew collects to both the top and bottom of the leaf. In fact, it collects on the whole plant. Thus, it seems reasonable, more water is present on leaves during dew periods than when raining. The average day analysis for a no-rain, three-week period in early September is shown in Figure 61. This figure shows a stronger daily cycle present when the effects of rain are not present. The correlation between leaf wetness measurement and RSSI was calculated to be  $R^2 = 0.83$  and scatter plot is shown in Figure 62.

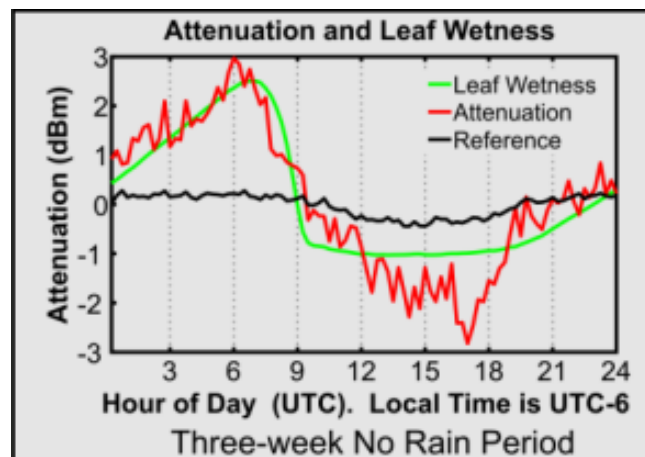


Figure 61 The plot shows an “average day” leaf wetness and RSSI for both canopy nodes and the reference link. However, rather than the whole 50-day period, this plot corresponds to a three-week no-rain period.

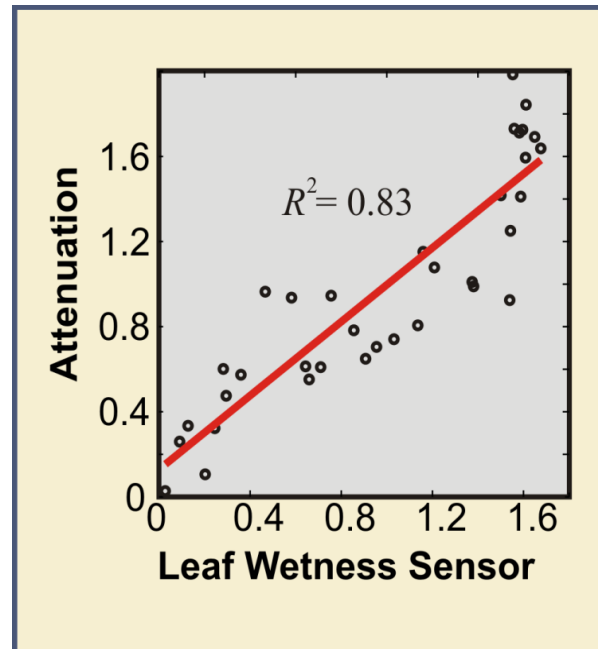


Figure 62 Scatter plot of leaf wetness sensor output voltage versus normalized attenuation of the averaged RF signal for links ES3, ES4, and ES5. A correlation coefficient of  $R^2 = 0.83$  was calculated

### Discussion and Some Conclusions

An exciting result from the planned experiment is that dew affects the RSSI, since this can have significant practical application for monitoring dew on plants at the field scale. Kabela et al. 2008, look at dew frequency, duration, amount and distribution in corn and soybean plants over a 21 day period during June and July 2005 in Central Iowa. Their finding concluded: dew was most likely to be present between 12:30 and 6:30 CST in both corn and soybean. At 1:30, 6:00, and 6:30 CST (which correspond to the overpass times of three current or planned satellite remote sensing instruments), dew was present 76%, 71%, and 57% of the days, respectively, in corn and 76%, 62%, and 38% of the days, respectively, in soybean. Dew was present until 7:00 CST on about 40% of days. In corn, the majority of dew was found on top of the leaf for the light dew event. For the moderate and heavy dew events, they found more dew on the bottom of a corn leaf than on the top in every instance. The percentage of dew in the leaf collar was lowest

during the light dew event and greatest during the heavy dew event. Soybean plants generally observed more dew on the top of a leaf than on the bottom for a light and moderate dew event, and more dew on the bottom than on the top in a heavy dew event.

The deployment of a network of RF modules in a field may assist a better understanding of dew variability. The measurement of such networks could aid in the validation of remotely sensed soil moisture estimations made by SMOS and SMAP. Such networks will also provide information about the state of the vegetation as described in Chapter VII. Measurements made by the RF module provide a true indication of the water contain on the plant, an improvement over the current technology that merely models the plant.

## CHAPTER VIII

### FUTURE WORK

#### Introduction

From Chapter II an expression for the magnitude of a time-harmonic linearly-polarized plane wave traveling in the x direction is

$$E_y = E_0 e^{-\gamma x}$$

where  $\gamma$  is the wave number or propagation constant, given by

$$\gamma^2 = j\omega\mu\sigma - \omega^2\mu(\epsilon' - \epsilon'')$$

As in Chapter II one can set  $\gamma = \alpha + j\beta$  which leads to

$$E_y = E_0 e^{-\alpha x} e^{-j\beta x}$$

Note that both  $\alpha$  and  $\beta$  depend on the dielectric permittivity, but I have only used  $\alpha$  thus far. Is it possible to use  $\beta$  to make similar and perhaps better measurements? The answer is that in principle “yes”. However, in practice this is not a simple matter, especially using the ISM radios that are the subject of discussion in this thesis.

One should distinguish between *carrier phase* and *time delay* measurements. Carrier phase measurements refer to measurement of the phase shift the radio frequency carrier undergoes as it propagates through the medium. Carrier phase measurements are used in, for example, Doppler- and polarimetric radars. They operate by sampling the outgoing pulse and measuring the phase shift of the return signal with this reference. This requires a stable time base as well as access the RF carrier. One simply does not have access to the carrier phase in the ISM radio modules used in this thesis.

The second type of “phase” measurement that comes to mind is time-of-flight measurements. Imagine that one sets up a radio link and measure the time-of-flight between the transmitter and receiver, rather than path attenuation. Changes in the intervening medium (for

example humidity) will then change to time-of-flight and one can use this to measure atmospheric vapor. This type of measurement does not require access to the radio frequency carrier, but rather to the baseband modulation/demodulation signals. Figure 63 shows the possible implementations. The implementation in the top figure uses an echo server (see Chapter II) and the implementation in the bottom figure uses a streaming server. In both implementations the transmitter transmits a low frequency (say 500-Hz) square wave that is then echoed back. The received, demodulated signal is delayed by  $2 \times$  time-of-flight as well as the latencies of the radios:

$$\Delta t = l_{tA} + t_{tof} + l_{rB} + l_{echo} + l_{tB} + t_{tof} + l_{rA}$$

Here  $l_{tA}$  is the latency associates with the transceiver  $A$  that initiates a measurement. That is, the time it takes to start transmitting after its Tx line is asserted. The time-of-flight is  $t_{tof}$  and receive latency at the echo server is  $l_{rB}$ , while the echo latency is  $l_{echo}$ . The remaining three latencies are at transceiver  $A$  when it receives the echo. Presumably the latencies are constant or one can measure quire easily. One can then lump all the latencies together

$$\Delta t = 2t_{tof} + l_{system}$$

There are a variety of techniques available to measure delays. A simple and extremely effective method for digital signals is a digital phase detector. Probably the simplex implementation consists of an exclusive-or (XOR for short) gate, followed by a simple resistor-capacitor low-pass filter. The XOR gate functions as a digital multiplier. The average value of its output is a linear function of the phase difference between its inputs. The low pass filter extracts the average value and an analog value. One can measure the analog voltage very accurately using standard laboratory digital multimeters. Multimeters with 6.5—7.5 significant digits are common place. Consequently, using a simple XOR gate, capacitor, and resistor (cost  $\sim$  \$1) along with measurement equipment found in most electronics labs, one can make very accurate delay measurements.

However, there are some real practical implementation issues. For example, one can make the filter's time constant quite large (several minutes) and remove 60-Hz mains interference and other noise. However, resistors and capacitor drift with time and temperature so one cannot make the time constant arbitrary large. Second, XOR gates have their own inherent

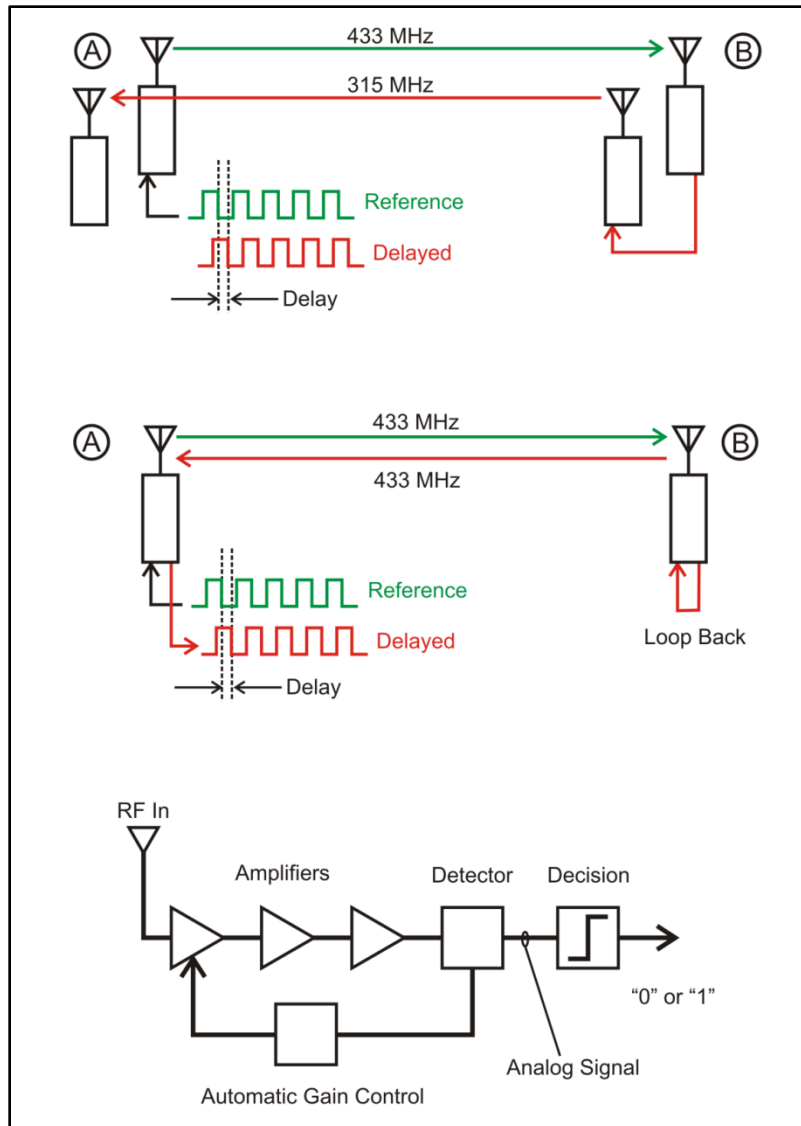


Figure 63 Top is the possible implementation of measuring TOF using a streaming server. Latency is a function of the fixed overhead of the radios and

delays that differs between parts (but one could calibrate this out) and is temperature-dependent. Still, it would seem that one could solve these problems.

It turns out that the real problem lays with the ISM radio modules. Consider the expression for the total delay

$$\Delta t = l_{tA} + t_{tof} + l_{rB} + l_{echo} + l_{tB} + t_{tof} + l_{rA}$$

We discovered experimentally there was a small, but significant, relationship between the received signal level (i.e., RSSI) and the receiver latencies, namely  $l_{rB}$  and  $l_{rA}$ . Specifically, these latencies increased when the RSSI decreased. Thus one should write

$$\Delta t = l_{tA} + t_{tof} + l_{rB}(RSSI) + l_{echo} + l_{tB} + t_{tof} + l_{rA}(RSSI)$$

Lumping the other latencies together, this becomes

$$\Delta t = 2t_{tof} + l_{system} + l_{rA}(RSSI) + l_{rB}(RSSI)$$

One could “calibrate out”  $l_{system}$ , but  $l_{rA}(RSSI) + l_{rB}(RSSI)$  poses a significant problem. Imagine one set up a link to measure changes in phase rather than amplitude. One would want the phase detector to be insensitive to changes in amplitude. However, the equation shows that the phase detector will respond to purely amplitude fluctuations.

To understand why the RSSI impacts the latencies, consider how the ISM modules work. Generally-speaking several stages of amplifiers take the incoming radio signal from microvolt to volt level. Given the tremendous dynamic range (80 dB or more) of the input signal, radios use so-called automatic gain control (AGC) to condition the signal for the detector. The detector demodulates the signal. Detection techniques depend on the modulation scheme (OOK, ASK, FSK). However, it is important to recognize that at this point, the signal process has been analog and the demodulated signal is an analog signal. The next step is to decide if a “1” or a “0” were sent. That is the analog signal is passed through the threshold-detector for signal above the threshold, the receiver outputs a “1”, otherwise it outputs a “0”. A little thought will convince

the reader that unless the AGC circuit is perfectly linear, there will be small fluctuations in the decision. In other words, the amplitude fluctuations become phase fluctuations.

Upon closer inspection of the datasheet for Radiotronix receiver model RCR-433 it becomes apparent that phase measurements will not work with this model. The datasheet states that the decision time is not linear with RF input levels. Here the central theme of this thesis, use of off-the-shelf modules, restricts this technique.

Still, the prospect of using time-of-flight measurements are appealing and below I describe some (failed) attempts to use time-of-flight measurements. My aim is to further explore this in the future.

I discuss here continuing work to use TOF measurements made with radio modules to perform water height measurements that may find use in application for measuring river stage. Briefly, one places a streaming server on the bottom of the river. Next, one transmits a signal

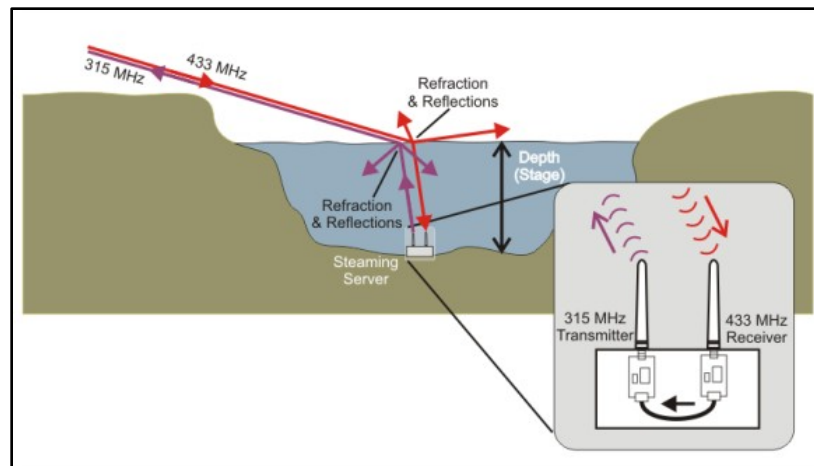


Figure 64 The figure depicts the concept behind round-trip TOF measurements to estimate river stage. A transmitter on the bank transmits on 433-MHz to a streaming server on the bottom of the river. The streaming server echoes back on 315 MHz. The river stage modulates the phase difference between the 433-MHz and 315-MHz signals on the bank. One can easily measure the phase difference and estimate the river stage.

from the riverbank to the streaming server, which echoes the signal back on a slightly different frequency. Roughly speaking, the speed of radio waves in water is about 1/9 of the speed of light, so the delay between transmission and reception (TOF) is dominated by distance the signal travels through the water. My hypothesis is that by measuring the TOF one can estimate river stage, as depicted in Figure 64.

### River Stage Measurement

When deployed as a stream gauge, pressure transducers can become plugged with debris that is washed down stream. Problems such as environmental fouling and need for atmospheric pressure compensation have long plagued pressure transducers. The USGS uses other techniques for measuring stage that have eliminated such problems, but are costly. I have also worked on developing an economical form of remote sensing to measure river stage using ultrasonic sensors (Kruger et al. 2009). The developmental ultrasonic sensor mounts to the sides of bridges and measures the air space between sensor and water. At deployment the distance from the sensor to the stream bed is recorded into the sensors memory. Stage is then calculated by subtracting the measured air space from the distance to the stream bed and transmitted back to The University of Iowa via cellular communication. The major drawback to the USGS style of stage measurement is cost of implementation. Objects such as birds and debris on the water's surface can corrupt measurements. Finally you need something to mount the sensor to above the water. The proposed RF sensor would be completely sealed and impervious to the water. Debris on the water surface or on top of the sensor would only lead to a slight error in measurement accuracy not complete loss of data. Since most debris would have a significantly smaller permittivity than water, the error generated by the debris would be small.

A radio wave takes 3.33 ns to travel 1 m in air and 33.3 ns to travel 1 m in water. By measuring the time of flight of a radio wave one can calculate the distance between two points if  $\epsilon_r$  of the medium is known.

For proof of concept testing, the change in propagation velocity as function of water, conductivity was neglected. One may be able to incorporate compensation for conductivity by measuring signal strength along with signal propagation velocity. For this test, radio wave velocity of propagation is dependent on  $\mu_r$  and  $\epsilon_r$  of the medium, ignoring for now the affect of conductivity  $\sigma$ . The dielectric permittivity of pure water is a function of water temperature, water pressure, the frequency of the radio wave, and water impurities. Changes in permittivity associated with pressure are insignificant for the water level depths that this system will be applicable. One can compensate for changes in permittivity with respect to temperature by measuring the temperature of the water, and using established correction formulas. Additionally, unless the antennas of the streaming server are properly-design for operation in water, they will be quite inefficient receivers and radiators. Despite all the losses, previous experiments in this thesis have shown that one can achieve a reliable communication link at 315/433-MHz in several meters of water, enough to make the technique I am promoting feasible.

Figure 65 depicts the experimental setup for a feasibility test I performed. It consists of a streaming server, exclusive-or digital phase detector, digital multimeter and a signal generator.

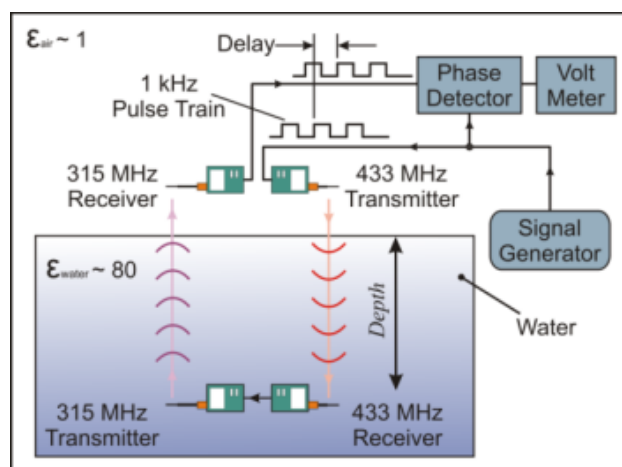


Figure 65 EM waves propagate at  $\sim 30$  ns/m in water. The delay between received- and transmitted pulse trains are  $t_1 + 30 \times \text{Depth}$  (ns), where  $t_1$  represents the latencies of the radios, time-of flight through air, electronics, etc.

### TOF Measurement

I measured the TOF delay that the water introduces using an exclusive OR (XOR) gate functioning as a digital multiplier. The output of an XOR gate is high when the inputs are different and low when the inputs are the same. If the inputs to an XOR gate are at the same frequency, but differ in phase, the output of the XOR gate will be a square wave at the input frequency. The duty cycle of the output pulses is a function of the TOF. Low-pass filtering recovers the average value. Figure 66 depicts this. A low-pass filter extracts the average value, resulting in a dc voltage that is a linear function of *Depth*. The phase delay introduced by the water is on the order of nanoseconds, and the overhead latencies of a single radio transmitter and receiver pair is on the order of 75 microseconds. The fixed overhead/latency results in a dc offset at the phase detector output.

### Experimental Results

I allowed the filter to stabilize for approximately five minutes before sampling the output and averaging for one minute. The measurements were made at depths of 0.5, 1, 2, 2.25, 3, 4, 4.25, 4.5, 5 and 6 feet below the surface of the water. At a depth of six feet the sensor was on the bottom of the flume. After a depth of four feet the measured results deviate from the expected results. This may be caused by the wave propagating through the bottom of the tank and reflecting to the receiver. The voltage output began to decrease which equate to a decrease in measured water depth as the transmitter approached the bottom of the elevated tank. The measurements at the bottom of the tank were very similar to measurements made just above the water's surface. Figure 67 shows the filtered phase detector output as a function of the water depth along with a linear fit of the data. The data shown in this figure is only to a depth of four feet were the experimental data is valid since a depth of six feet for this experiment was equal to a depth of just above the surface of the water.

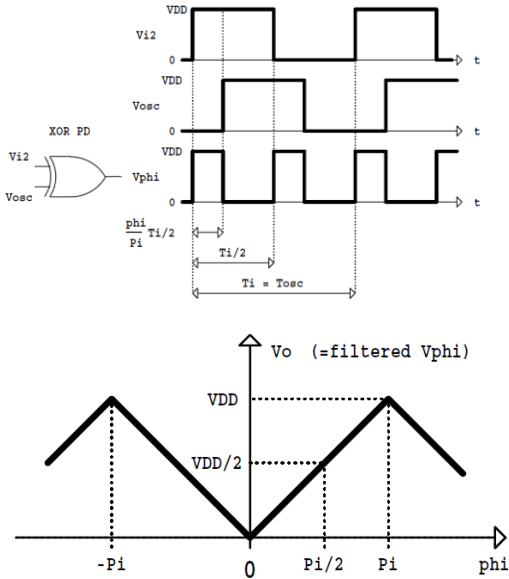


Figure 66 The top panel shows the operation of an XOR gate as a phase detector. The inputs to the XOR gate are square waves at the same frequency  $f_i$ , but not at the same phase. The output of the XOR gate is a series of pulses at frequency  $f_i$ , but the duty cycle is a function of the phase difference between inputs. Low-pass filtering the pulses extracts the average value, giving an output voltage linear with phase difference, as shown in the lower pane.

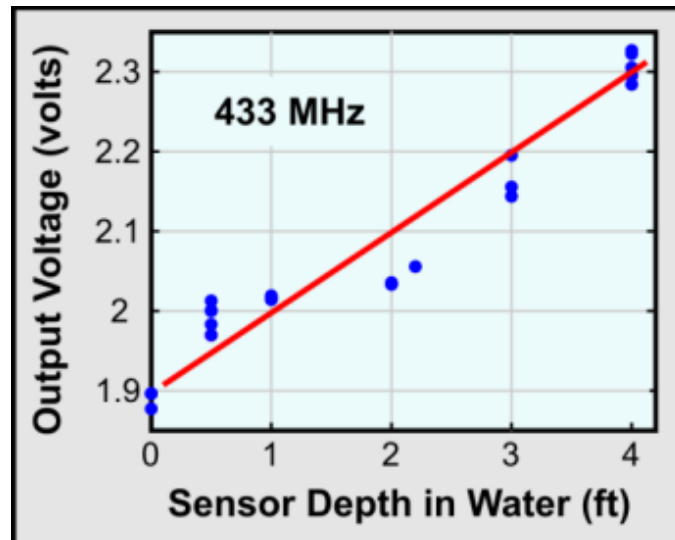


Figure 67 Results from the phase measurement experiment. The data suggest that it is possible to measure water depth by measuring the TOF. Unfortunately results were skewed by the functionality of very off-shelf modules depicted in the thesis.

At first the results looked promising since there was a clear change in output voltage with distance. It was observed that the change in output voltage compared with the change in water depth were much higher than would be expected. By doing some back of the envelope calculations, the fixed offset of 75  $\mu\text{s}$  produced a voltage of 1.9 V so a delay of 30 ns (one meter of water) should be 750  $\mu\text{V}$ . For this experiment a change in water depth of one meter produced a change in output voltage of about 350 mV. Since there was no amplification of the output voltage there was clearly other factors that added to the phase measurement.

The explanation for the increase in measurement is in the RF module design. Upon closer inspection of the datasheet for Radiotronix receiver model RCR-433 it becomes apparent that phase measurements will not work with this model. The datasheet states that the decision time is not linear with RF input levels. As stated previously in this document the attenuation of a 433MHz signal in water is 17.6 dB/m. What was truly measured for this experiment was the attenuation of the RF signal with increasing distance in water. While this sensor did succeed in measuring the depth of the water it didn't do so by measuring of phase but yet another application of using changes in signal strength to infer changes in the medium.

Several other RF modules were examined as possible candidates for phase measurements including Linx TRM-315-LT which used OOK modulation and several FM modules. To keep with the theme of using off the shelf RF modules, the difficulty now was in making precision measurements on the order of nanoseconds with equipment that has precision on the order of tens of microseconds. Since these modules operate at baud rate of less than 9600 bps variations on the order of tens of microseconds has no effect on the modules performance.

The central theme of this thesis is that one can use **off-the-shelf** radios for alternative purposes for applications in hydroscience. Here the central theme leads to difficulties in using such radios in phase measurements. While the technique seems solid, its implementation is far beyond the original planned use of the RF modules. Future work will consist of finding the proper source of RF waves to provide a consistent TOF measurement.

## CHAPTER IX

### CONCLUSION

The central assertion stated in the Introduction and repeated here is as follows. One can use unlicensed and often very inexpensive radios for unconventional communication (underwater- and underground) links. However, one can go further, and use these radios as sensors rather than communication links. The communication links and sensors can have important application in hydroscience. In this thesis, I validated this assertion through a physics-based argument, engineering considerations, and several field experiments.

Starting with Maxwell's equations, I derived the wave equation in a conductive medium. I argued that at the frequencies the proposed RF modules operate, one can view freshwater and soil as a dielectric medium. This has important implications for the use of RF modules in hydroscience applications. First, the conduction losses are so small compared to the dielectric hysteresis losses that one can ignore Ohmic/conductive coupling between antennas. Second, one can bring to bear results and intuition from radio wave propagation in air. Third, the following simple mathematical model adequately describes the received power:

$$P_r \propto \frac{P_t e^{-2\alpha R}}{R^n}$$

where  $P_r$  is the received power,  $P_t$  is the power transmitted,  $R$  is the distance between transmitter and receiver,  $n$  is the path loss exponent, and  $\alpha$  is the attenuation constant. The attenuation,  $\alpha$ , is high in water and soil, but it is still possible to get reliable communication over short (up to 2 m) distances, using widely-available radios.

By employing WSN paradigm, it is possible to build RF networks that operate underwater and underground. The application for underwater networks was in routing data collected from mussels between the water and air interface. This is possible since RF waves can transverse the boundary between the water and air easier than ultra-sonic and IR. The collected mussel data could provide a better understanding of water quality in our rivers. The second

application was in underground networks for monitoring soil moisture. Completely self-contained nodes for monitoring soil moisture would eliminate much of the tedious work of installing and removal of sensors during field work. Such networks could be left in year round if provisions are made to provide alternative data routing to accommodate changes in soil moisture conditions between long RF links. It was shown that a change in soil moisture modulates the RF signal.

After analyzing the RSSI and soil moisture data collected in the underground network, it became clear that one could stop thinking of the RF modules as a form of communication but a potentially a sensor. This revelation lends itself to thinking of these modules as inexpensive generators of RF waves at prescribed unlicensed frequencies. This is a tool that requires little expertise to operate and minimal additional equipment. Additionally, this is a tool that is readily available to everyone. To validate this new line of thinking three experiments were designed to test the usefulness of RF modules as sensors used in hydroscience. The radios allow one to easily measure the received power  $P_r$  in

$$P_r = \frac{P_o e^{-2\alpha R}}{R^n}$$

through their RSSI interrogation mechanism. For the sensors in this thesis, the distance  $R$  between transmitter and receiver remained constant. The transmit power of the module is known and the received power can be measured. Observed changes in RSSI are related to changes in  $\alpha$ , and by implication changes in the medium.

The first experiment showed that off-the-shelf RF modules operating at 900 MHz could be used to monitor soil moisture. One can relate changes in observed signal strength to changes in the amount of water contained in the soil. The RSSI measurement provides a distributed measurement over the entire link. This new sensor has the potential to fill the gap in the spatial resolution between traditional point measurements and remote sensors, such as radiometers.

Additionally, the cost is comparable to traditional point measurements, and eliminates the need to disturb the area where the measurements are taken.

The second example showed the use of cell modem networks in monitoring vegetation water content. This serendipitous experiment showed how the water contained in the vegetation modulates the RF signal throughout the plants life cycle. The presence/absence of vegetation influences signal strengths, as shown as shown by the sudden increase in RSSI when the crop was harvested. The results showed that signal strength is inversely proportional to the distance the signal propagates through the vegetation. In addition, the signal strength is also inversely proportional to vegetation water content. From the cell modem RSSI, one can observe long-term changes in signal strength data that are similar to the annual changes in the corn. The relevance of this work is that vegetation water content can influence passive microwave remote sensing of soil moisture. Growing up in a region where corn is considered “king”, this technique for monitoring the state of crop may provide better insight into yearly crop potentials by monitoring the amount of water with in the plants.

The final experiment stems from the observation of an overriding daily cycle on the long term trend seen in the vegetation water content experiment. The daily cycle of presence/absence of dew on the corn plants modulated the RF signal. This experiment validated the use of RF modules in making leaf wetness measurements. The RSSI showed a direct connection to the amount of dew on the plant. As with all the RSSI monitoring techniques mentioned, the measurement offers a distributed measurement over the entire link. While traditional leaf wetness sensors merely model a plant’s leaf, the RSSI measurements offered a true look at the amount of water that is within the RF link. This technique may also help in eliminating some of the uncertainty in passive microwave remote sensing of soil moisture. Since the presence of vegetation and more over the dew on the vegetation can affect remote soil moisture measurements made by satellites.

This thesis served to validate the use of inexpensive unlicensed RF modules as more than just communication links through air, but as links in unconventional media and more importantly as measurement instruments.

## REFERENCES

- Akyildiz, I.; Stuntebeck, E.;, "Wireless underground sensor networks: Research challenges", *Ad Hoc Networks*, vol. 4, no. 6, Pages 669-686, Nov. 2006  
doi: 10.1016/j.adhoc.2006.04.003.  
URL: <http://www.sciencedirect.com/science/article/B7576-4KCXG2V-1/2/8642adef0a093d1b0901b0793106b926>
- Ali, K.; Hassanein, H.; , "Underwater Wireless Hybrid Sensor Networks," *Computers and Communications, 2008. ISCC 2008. IEEE Symposium on* , vol., no., pp.1166-1171, 6-9 July 2008  
doi: 10.1109/ISCC.2008.4625635  
URL: <http://ieeexplore.ieee.org/stamp/stamp.jsp?tp=&arnumber=4625635&isnumber=4625572>
- Al-Shamma'a, A.I.; Shaw, A.; Saman, S.; , "Propagation of electromagnetic waves at MHz frequencies through seawater," *Antennas and Propagation, IEEE Transactions on* , vol.52, no.11, pp. 2843- 2849, Nov. 2004  
doi: 10.1109/TAP.2004.834449  
URL: <http://ieeexplore.ieee.org/stamp/stamp.jsp?tp=&arnumber=1353478&isnumber=29739>
- Anguita, D.; Brizzolara, D.; Parodi, G.; , "Optical communication for Underwater Wireless Sensor Networks: a VHDL-implementation of a Physical Layer 802.15.4 compatible," *OCEANS 2009-EUROPE, 2009. OCEANS '09.* , vol., no., pp.1-2, 11-14 May 2009  
doi: 10.1109/OCEANSE.2009.5278148  
URL: <http://ieeexplore.ieee.org/stamp/stamp.jsp?tp=&arnumber=5278148&isnumber=5278099>
- Belostotski, L.; Landecker, T.L.; Routledge, D.; , "Distance measurement with phase-stable CW radio link using the Chinese remainder theorem," *Electronics Letters* , vol.37, no.8, pp.521-522, 12 Apr 2001  
doi: 10.1049/el:20010343  
URL: <http://ieeexplore.ieee.org/stamp/stamp.jsp?tp=&arnumber=919998&isnumber=19885>
- Bertoni H.;, "Shadow Fading and the Effect of Terrain and Trees, " in *Radio Propagation for Modern Wireless Systems*. Upper Saddle River NJ: Prentice Hall PTR, 1999, pp. 201-210.
- Bin Zhang; Sukhatme, G.S.; Requicha, A.A.; , "Adaptive sampling for marine microorganism monitoring," *Intelligent Robots and Systems, 2004. (IROS 2004). Proceedings. 2004 IEEE/RSJ International Conference on* , vol.2, no., pp. 1115- 1122 vol.2, 28 Sept.-2 Oct. 2004  
doi: 10.1109/IROS.2004.1389546  
URL: <http://ieeexplore.ieee.org/stamp/stamp.jsp?tp=&arnumber=1389546&isnumber=30276>

BIRDNET 2010; [http://www.nmnh.si.edu/BIRDNET/OC/fact/Radio\\_tracking.html](http://www.nmnh.si.edu/BIRDNET/OC/fact/Radio_tracking.html), Retrieved 2010-06-09

Bluetooth;  
[http://bluetooth.org/foundry/adopters/document/Bluetooth\\_Core\\_Specification\\_v1.2](http://bluetooth.org/foundry/adopters/document/Bluetooth_Core_Specification_v1.2),  
 Bluetooth Core Specification v1.2, Retrieved June, 2010

Bril, J.; Just, C.; Loperfido, J.; Young, N.;, "2009. Upper Mississippi River Basin Envirohydrologic Observatory," ASCE Conference Proceedings, 342-323, 2009

Chesnoy, J.; Lemaire, V.; Barnes, S.R.; , "Submarine communications the new age of WDM connectivity," *Optical Communication, 1996. ECOC '96. 22nd European Conference on* , vol.3, no., pp. 57- 64 vol.3, 15-19 Sept. 1996  
 URL: <http://ieeexplore.ieee.org/stamp/stamp.jsp?tp=&arnumber=715619&isnumber=15506>

CS616 2010; <http://www.campbellsci.com/cs616-1>, Retrieved May 25, 2010

Curtis, J.O.; , "Moisture effects on the dielectric properties of soils," *Geoscience and Remote Sensing, IEEE Transactions on* , vol.39, no.1, pp.125-128, Jan 2001  
 doi: 10.1109/36.898673  
 URL: <http://ieeexplore.ieee.org/stamp/stamp.jsp?tp=&arnumber=898673&isnumber=19440>

Dal Bello, J.C.R.; Siqueira, G.L.; Bertoni, H.L.;, "Effects of vegetation on urban cellular systems," *Universal Personal Communications, 1998. ICUPC '98. IEEE 1998 International Conference on* , vol.1, no., pp.113-116 vol.1, 5-9 Oct 1998  
 doi: 10.1109/ICUPC.1998.732814  
 URL: <http://ieeexplore.ieee.org/stamp/stamp.jsp?tp=&arnumber=732814&isnumber=15797>

Daniels D.;, "*Ground Penetrating Radar* (2nd ed.), "Knoval , Institution of Engineering and Technology, pp. 1–4. , 2004 ISBN 978-0-86341-360-5

David N.; Alpert P.; Messer H.;, "Novel method for water vapour monitoring using wireless communication networks measurements, " *Atmos. Chem.and Phys.*, vol. 9, pp. 2413–2418, April 2009

Davies, J.; Niemeier J.; Kruger A.; Mantilla R; Ceynar D;, "Drifters for New Measurements Along River Networks," *Eos Trans. AGU*, **89**(53), Fall Meet. Suppl., Abstract H51H-0969, 2008

De Zwart, D.; Kramer, K.; Jenner H.; , "Practical Experiences With the Biological Early Warning System 'Mosselmonitor'," *Environ, Toxicol, Water Qual*, 10, 4 237–24, 1995  
 doi:10.1002/tox.2530100403.

Giacomin, J.C.; Vasconcelos, F.H.; da Silva, E.J.; , "Estimating Vegetation Water Content with Wireless Sensor Network Communication Signals," *Instrumentation and Measurement Technology Conference Proceedings, 2007. IMTC 2007. IEEE* , vol., no., pp.1-5, 1-3 May 2007  
 doi: 10.1109/IMTC.2007.379418

URL: <http://ieeexplore.ieee.org/stamp/stamp.jsp?tp=&arnumber=4258297&isnumber=4258012>

Gueuning, F.; Varlan, M.; Eugene, C.; Dupuis, P.; , "Accurate distance measurement by an autonomous ultrasonic system combining time-of-flight and phase-shift methods," *Instrumentation and Measurement Technology Conference, 1996. IMTC-96. Conference Proceedings. 'Quality Measurements: The Indispensable Bridge between Theory and Reality'*, *IEEE* , vol.1, no., pp.399-404 vol.1, 1996  
doi: 10.1109/IMTC.1996.507414

URL: <http://ieeexplore.ieee.org/stamp/stamp.jsp?tp=&arnumber=507414&isnumber=10914>

Hafez, H. M.; Chudobiak, Walter J.; Wight, James S.; , "The Attenuation Rate in Fresh Water at VHF Frequencies," *Instrumentation and Measurement, IEEE Transactions on* , vol.28, no.1, pp.71-74, March 1979  
doi: 10.1109/TIM.1979.4314763

URL: <http://ieeexplore.ieee.org/stamp/stamp.jsp?tp=&arnumber=4314763&isnumber=4314746>

Hashim, M.; Stavrou, S.; , "Measurements and modeling of wind influence on radiowave propagation through vegetation," *Wireless Communications, IEEE Transactions on* , vol.5, no.5, pp. 1055- 1064, May 2006  
doi: 10.1109/TWC.2006.1633358

URL: <http://ieeexplore.ieee.org/stamp/stamp.jsp?tp=&arnumber=1633358&isnumber=34245>

Heidemann, J.; Wei Ye; Wills, J.; Syed, A.; Yuan Li; , "Research challenges and applications for underwater sensor networking," *Wireless Communications and Networking Conference, 2006. WCNC 2006. IEEE* , vol.1, no., pp.228-235, 3-6 April 2006  
doi: 10.1109/WCNC.2006.1683469

URL: <http://ieeexplore.ieee.org/stamp/stamp.jsp?tp=&arnumber=1683469&isnumber=34934>

Hipp, J.E.; , "Soil electromagnetic parameters as functions of frequency, soil density, and soil moisture," *Proceedings of the IEEE* , vol.62, no.1, pp. 98- 103, Jan. 1974

URL: <http://ieeexplore.ieee.org/stamp/stamp.jsp?tp=&arnumber=1451319&isnumber=31176>

Hornbuckle B.; England A.; , "Radiometric sensitivity to soil moisture at 1.4 GHz through a corn crop at maximum biomass," *Water Resour. Res.*, vol. 40, pp. W10204, Oct.2004.

Hornbuckle, B.; England, A.W.; , "Dew: invisible at 1.4 GHz?," *Geoscience and Remote Sensing Symposium, 2003. IGARSS '03. Proceedings. 2003 IEEE International* , vol.5, no., pp. 3404- 3406 vol.5, 2003  
doi: 10.1109/IGARSS.2003.1294797

URL: <http://ieeexplore.ieee.org/stamp/stamp.jsp?tp=&arnumber=1294797&isnumber=28605>

Hunt, K.; Kruger A.; Cunha K.; , "An Investigation of the Effects of Vegetation on Radio Signal Propagation Through a Corn Field," *Eos Trans. AGU*, **89**(53), Fall Meet. Suppl., Abstract H11A-0714, 2008

Hunt, K.; Niemeier, J.; Cunha, L.; Kruger, A.; "Using Cellular Network Signal Strength to Monitor Vegetation Characteristics, " *Geoscience and Remote Sensing Letters*, Manuscript ID GRSL-00106-2010.R1, In Press

Hunt, K.; Niemeier, J.; Kruger A.; "RF Communication in Underwater Wireless Sensor Networks," *IEEE International Conference on Electro/Information Technology*, May, 2010. URL: [//www.eit-conference.org/eit2010/](http://www.eit-conference.org/eit2010/)

Jiejun Kong; Jun-hong Cui; Dapeng Wu; Gerla, M.; , "Building underwater ad-hoc networks and sensor networks for large scale real-time aquatic applications," *Military Communications Conference, 2005. MILCOM 2005. IEEE* , vol., no., pp.1535-1541 Vol. 3, 17-20 Oct. 2005

doi: 10.1109/MILCOM.2005.1605894

URL: <http://ieeexplore.ieee.org/stamp/stamp.jsp?tp=&arnumber=1605894&isnumber=33743>

Johansson, L.A.; Ramaswamy, A.; Vikash; Rodwell, M.; , "Coherent optical receiver with linear XOR phase detection and frequency down-conversion," *Microwave Symposium Digest, 2009. MTT '09. IEEE MTT-S International* , vol., no., pp.157-160, 7-12 June 2009

doi: 10.1109/MWSYM.2009.5165656

URL: <http://ieeexplore.ieee.org/stamp/stamp.jsp?tp=&arnumber=5165656&isnumber=5165586>

Kabela E.; Hornbuckle B; Cosh M.; Anderson M.; Gleason M.; "Dew frequency, duration, amount, and distribution in corn and soybean during SMEX05," *Agricultural and Forest Meteorology*, Volume 149, Issue 1, 4 January 2009, Pages 11-24, ISSN 0168-1923, DOI: 10.1016/j.agrformet.2008.07.002.

URL: <http://www.sciencedirect.com/science/article/B6V8W-4TB0TY1-1/2/0969b08c64d7e1202f59544fa5c8dad7>

Keeler R.; Serafin J.; "Meteorological Radar, " *Radar Handbook*, 3rd ed., M. I. Skolnik Ed., New York NY: McGraw Hill, pp. 19.10-19.11, 2008

Kelly, K.; "Out of Control: "The New Biology of Machines", " *Social Systems and the Economic World* Addison-Wesley, Boston, MA. 98, 1994

Kraus J.; Felisch D.;, *Electromagnetics with Applications, 5th edition*, 1999, McGraw-Hill

Kruger, A.; Niemeier J.; Krajewski W.; Ceynar D.; Wagner G.; "An Exploration of Inexpensive, Automated Methods for Measuring River Stage, " *Eos Trans. AGU*, **90**(52), Fall Meet. Suppl., Abstract H11E-0873, Dec. 2009

Leijnse H.; Uijlenhoe R.; Stricker J.;, "Rainfall measurement using radio links from cellular communication networks, " *Water Resour. Res.*, vol. 43, p. W03201, Mar. 2007

Lindsay, J.; Long, F.; Weeks, R.; , "A practical look at antenna and propagation requirements in biotelemetry systems for fresh water fish," *Antennas and Propagation Society International Symposium, 1977* , vol.15, no., pp. 132- 135, Jun 1977  
 URL: <http://ieeexplore.ieee.org/stamp/stamp.jsp?tp=&arnumber=1147790&isnumber=25852>

Meihong Sui; Xinsheng Yu; Fengli Zhang; , "The Evaluation of Modulation Techniques for Underwater Wireless Optical Communications," *Communication Software and Networks, 2009. ICCSN '09. International Conference on* , vol., no., pp.138-142, 27-28 Feb. 2009  
 doi: 10.1109/ICCSN.2009.97  
 URL: <http://ieeexplore.ieee.org/stamp/stamp.jsp?tp=&arnumber=5076827&isnumber=5076790>

Meissner, T.; Wentz, F.J.; , "The complex dielectric constant of pure and sea water from microwave satellite observations," *Geoscience and Remote Sensing, IEEE Transactions on* , vol.42, no.9, pp. 1836- 1849, Sept. 2004  
 doi: 10.1109/TGRS.2004.831888  
 URL: <http://ieeexplore.ieee.org/stamp/stamp.jsp?tp=&arnumber=1333169&isnumber=29436>

Messer H.;, Zinevich A.; Alpert P.;, "Environmental monitoring by wireless communication networks," *Science*, vol. 312, no. 5774, p. 713, May 2006.

Messer, H.; , "Rainfall Monitoring Using Cellular Networks [In the Spotlight]," *Signal Processing Magazine, IEEE* , vol.24, no.3, pp.144-142, May 2007  
 doi: 10.1109/MSP.2007.361621  
 URL: <http://ieeexplore.ieee.org/stamp/stamp.jsp?tp=&arnumber=4205108&isnumber=4202144>

Messer, H.; Goldshtein, O.; Rayitsfeld, A.; Alpert, P.; , "Recent results of rainfall mapping from cellular network measurements," *Acoustics, Speech and Signal Processing, 2008. ICASSP 2008. IEEE International Conference on* , vol., no., pp.5157-5160, March 31 2008-April 4 2008  
 doi: 10.1109/ICASSP.2008.4518820  
 URL: <http://ieeexplore.ieee.org/stamp/stamp.jsp?tp=&arnumber=4518820&isnumber=4517521>

Miller, N.; , "An Underwater Communication System," *Communications Systems, IRE Transactions on* , vol.7, no.4, pp.249-251, December 1959  
 doi: 10.1109/TCOM.1959.1097581  
 URL: <http://ieeexplore.ieee.org/stamp/stamp.jsp?tp=&arnumber=1097581&isnumber=24060>

Moore, Richard K.; , "Radio communication in the sea," *Spectrum, IEEE* , vol.4, no.11, pp.42-51, Nov. 1967  
 doi: 10.1109/MSPEC.1967.5217169  
 URL: <http://ieeexplore.ieee.org/stamp/stamp.jsp?tp=&arnumber=5217169&isnumber=5217145>

Morgan, E.; Eagleson, K.; Hermann, R.; McCollough, N.; "New Developments in Automated Biosensing from Remote Water Quality Stations and Satellite Data Retrieval for Resources Management.," *Journal of Hydrology*, 51, 1-4. 339-345, 1981  
doi:10.1016/0022-1694(81)90142-6.

Niemeier, J.; Davies, J.; Kruger, A.; "Subsurface Wireless Sensor Networks, " *Eos Trans. AGU, Fall Meet. Suppl.*, Abstract H51H-0976, 89, 53, Dec. 2008

Niemeier, J.; Kruger A.; Krajewski W.; Eichinger W.; Hornbuckle B.; Cunha L.; "A High-Temporal and Spatial Resolution Soil Moisture and Soil Temperature Network In Iowa Using Wireless Links, " *Eos Trans. AGU*, **88**(52), Fall Meet. Suppl., Abstract H13A-0970, Dec. 2007

Niemeier, J.; Rowlandson, T; Kruger , A.; Hornbuckle B.; "An Exploration of Distributed Leaf Wetness and Dew Detection Using Inexpensive Radios, " *Eos Trans. AGU*, **90**(52), Fall Meet. Suppl., Abstract H51F-0821, Dec. 2009

Nintendo, "Nintendo Wii - Hardware Information".  
<http://web.archive.org/web/20080212080618/http://wii.nintendo.com/controller.jsp>.  
Retrieved 2010-06-09.

Peplinski, N.R.; Ulaby, F.T.; Dobson, M.C.; , "Dielectric properties of soils in the 0.3-1.3-GHz range," *Geoscience and Remote Sensing, IEEE Transactions on* , vol.33, no.3, pp.803-807, May 1995  
doi: 10.1109/36.387598  
URL: <http://ieeexplore.ieee.org/stamp/stamp.jsp?tp=&arnumber=387598&isnumber=8788>

Perchet, G.; Lescure, M.; Bosch, T.; , "Magnification of the phase-shift for laser distance measurement," *Instrumentation and Measurement Technology Conference, 1997. IMTC/97. Proceedings. 'Sensing, Processing, Networking'. , IEEE* , vol.1, no., pp.617-621 vol.1, 19-21 May 1997  
doi: 10.1109/IMTC.1997.604024  
URL: <http://ieeexplore.ieee.org/stamp/stamp.jsp?tp=&arnumber=604024&isnumber=13268>

Press W.;Teukolsky S.;Vetterling W.; Flannery B.;, "Fourier and Spectral Applications, " *Numerical Recipes the Art of Scientific Computing*, 3rd ed., New York NY: Cambridge University Press, pp. 652-691. 2007

Proakis, J.; Masoud S; 2002. *Communication Systems Engineering, 2nd Edition*, Upper Saddle River, New Jersey: Prentice Hall.

Richter, J.; Al-Nuaimi, M.O.; Caldeirinha, R.; Savage, N.; Seville, A.; Rogers, N.C.; , "RET input parameter estimation for a generic model of propagation through vegetation using excess attenuation and phase function measurements," *Antennas and Propagation, 2003. (ICAP 2003). Twelfth International Conference on (Conf. Publ. No. 491)* , vol.2, no., pp. 836- 839 vol.2, 31 March-3 April 2003  
URL: <http://ieeexplore.ieee.org/stamp/stamp.jsp?tp=&arnumber=1353776&isnumber=29706>

Rivera, D.F.; , "Submarine towed communication antennas: past, present and future ," *Antennas and Propagation Society International Symposium, 2001. IEEE* , vol.2, no., pp.426-429 vol.2, 2001  
doi: 10.1109/APS.2001.959753  
URL: <http://ieeexplore.ieee.org/stamp/stamp.jsp?tp=&arnumber=959753&isnumber=20720>

Sitter, N.; Niemeier, J.; Kruger, A.; Just, C.; , "Mussel-based Biosensing for Hydrologic and Eco-biologic Processes. " *Eos Trans. AGU, Fall Meet. Suppl., Abstract H51G-0842 90 52*, Dec. 2009

SMAP 2010, Soil Moisture Active and Passive Website,  
URL [smap.jpl.nasa.gov/](http://smap.jpl.nasa.gov/)

SMOS 2100, European Space Agency Website,  
URL:<http://www.esa.int/esaLP/LPsmos.html>

Stolarczyk, L.G.; , "Emergency and operational low and medium frequency band radio communications system for underground mines," *Industry Applications, IEEE Transactions on* , vol.27, no.4, pp.780-790, Jul/Aug 1991  
doi: 10.1109/28.85496  
URL: <http://ieeexplore.ieee.org/stamp/stamp.jsp?tp=&arnumber=85496&isnumber=2795>

Stuntebeck, E.P.; Pompili, D.; Melodia, T.; , "Wireless underground sensor networks using commodity terrestrial motes," *Wireless Mesh Networks, 2006. WiMesh 2006. 2nd IEEE Workshop on* , vol., no., pp.112-114, 25-28 Sept. 2006  
doi: 10.1109/WIMESH.2006.288625  
URL: <http://ieeexplore.ieee.org/stamp/stamp.jsp?tp=&arnumber=4068263&isnumber=4053600>

Tiusanen, M.J.; , "Attenuation of a Soil Scout Radio Signal, *Biosystems Engineering*," vol. 90, no. 2, Pages 127-133, Feb. 2005  
dio: 10.1016/j.biosystemseng.2004.10.013.  
URL: <http://www.sciencedirect.com/science/article/B6WXV-4F8TK4C-6/2/c854f6ba2flacc6fdc3048c439701687>

Tiusanen, M.J.; , "Wideband Antenna for Underground Soil Scout Transmission," *Antennas and Wireless Propagation Letters, IEEE* , vol.5, no.1, pp.517-519, Dec. 2006  
doi: 10.1109/LAWP.2006.887549  
URL: <http://ieeexplore.ieee.org/stamp/stamp.jsp?tp=&arnumber=4039223&isnumber=33542>

Tiusanen, M.J.; , "Validation and results of the Soil Scout signal attenuation model, " *Biosystems Engineering*, 97, 11–17, 2007  
doi:10.1016/j.biosystemseng.2007.02.005.

Tiusanen, M.J.; , "Wirless Soil Scout prototype radio signal reception compared to the attenuation model," *Precision Agriculture*, vol. 10, no. 5 ,pp372-381, Oct 2009  
doi: 10.1007/s1119-008-9096-7  
URL: <http://www.springerlink.com/content/6340g235w4618k10/>

Trincherro, D.; Fiorelli, B.; Galardini, A.; Stefanelli, R.; , "Underground wireless sensor networks," *Wireless and Microwave Technology Conference, 2009. WAMICON '09. IEEE 10th Annual* , vol., no., pp.1-3, 20-21 April 2009  
 doi: 10.1109/WAMICON.2009.5207281  
 URL: <http://ieeexplore.ieee.org/stamp/stamp.jsp?tp=&arnumber=5207281&isnumber=520723>

Turner, R.W.; , "Submarine Communication Antenna Systems," *Proceedings of the IRE* , vol.47, no.5, pp.735-739, May 1959  
 doi: 10.1109/JRPROC.1959.287241  
 URL: <http://ieeexplore.ieee.org/stamp/stamp.jsp?tp=&arnumber=4065734&isnumber=4065721>

Wang Nan; Shen Xue-li; , "Research on Nodes Location Technology in Wireless Sensor Network Underground," *Intelligent Information Technology Application Workshops, 2009. IITAW '09. Third International Symposium on* , vol., no., pp.273-275, 21-22 Nov. 2009  
 doi: 10.1109/IITAW.2009.63  
 URL: <http://ieeexplore.ieee.org/stamp/stamp.jsp?tp=&arnumber=5419441&isnumber=5419418>

Wei Zhou; Shengfeng Zheng; Zhiqi Li; Hui Zhou; Chunxu Wang; , "A Super High Resolution Phase Difference Measurement Method," *Frequency Control Symposium, 2007 Joint with the 21st European Frequency and Time Forum. IEEE International* , vol., no., pp.811-814, May 29 2007-June 1 2007  
 doi: 10.1109/FREQ.2007.4319188  
 URL: <http://ieeexplore.ieee.org/stamp/stamp.jsp?tp=&arnumber=4319188&isnumber=4318994>

Wells, I.; Davies, A.; Xianhui Che; Kear, P.; Dickers, G.; Xiaochun Gong; Rhodes, M.; , "Node pattern simulation of an undersea sensor network using RF electromagnetic communications," *Ultra Modern Telecommunications & Workshops, 2009. ICUMT '09. International Conference on* , vol., no., pp.1-4, 12-14 Oct. 2009  
 doi: 10.1109/ICUMT.2009.5345555  
 URL: <http://ieeexplore.ieee.org/stamp/stamp.jsp?tp=&arnumber=5345555&isnumber=5345316>

Xianhui Che; Wells, I.; Dickers, G.; Kear, P.; Xiaochun Gong; Rhodes, M.; , "Failure Tolerance Analysis of a Small Scale Underwater Sensor Network with RF Electromagnetic Communications," *Sensor Technologies and Applications, 2009. SENSORCOMM '09. Third International Conference on* , vol., no., pp.671-675, 18-23 June 2009  
 doi: 10.1109/SENSORCOMM.2009.108  
 URL: <http://ieeexplore.ieee.org/stamp/stamp.jsp?tp=&arnumber=5210830&isnumber=5210828>